


Winter 2011

Spectrum Adaptation in Cognitive Radio Systems with Operating Constraints

Deepak R. Joshi
Old Dominion University

Follow this and additional works at: https://digitalcommons.odu.edu/ece_etds

 Part of the [Digital Communications and Networking Commons](#), and the [Electrical and Computer Engineering Commons](#)

Recommended Citation

Joshi, Deepak R.. "Spectrum Adaptation in Cognitive Radio Systems with Operating Constraints" (2011). Doctor of Philosophy (PhD), dissertation, Electrical/Computer Engineering, Old Dominion University, DOI: 10.25777/09mz-y971
https://digitalcommons.odu.edu/ece_etds/81

This Dissertation is brought to you for free and open access by the Electrical & Computer Engineering at ODU Digital Commons. It has been accepted for inclusion in Electrical & Computer Engineering Theses & Dissertations by an authorized administrator of ODU Digital Commons. For more information, please contact digitalcommons@odu.edu.

SPECTRUM ADAPTATION IN COGNITIVE RADIO SYSTEMS WITH OPERATING CONSTRAINTS

by

Deepak R. Joshi

B.E. October 2000, Tribhuvan University, Nepal
M.Sc. January 2007, Tribhuvan University, Nepal

A Dissertation Submitted to the Faculty of
Old Dominion University in Partial Fulfillment of the
Requirement for the Degree of

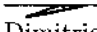
DOCTOR OF PHILOSOPHY

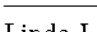
ELECTRICAL AND COMPUTER ENGINEERING

OLD DOMINION UNIVERSITY

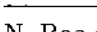
December 2011

Approved by:


Dimitrie C. Ponescu (Director)


Linda L. Vahala (Member)


Jiang Li (Member)


N. Rao Chaganty (Member)

ABSTRACT

SPECTRUM ADAPTATION IN COGNITIVE RADIO SYSTEMS WITH OPERATING CONSTRAINTS

Deepak R. Joshi

Old Dominion University, 2011

Director: Dr. Dimitrie C. Popescu

The explosion of high-data-rate-demanding wireless applications such as smartphones and wireless Internet access devices, together with growth of existing wireless services, are creating a shortage of the scarce Radio Frequency (RF) spectrum. However, several spectrum measurement campaigns revealed that current spectrum usage across time and frequency is inefficient, creating the artificial shortage of the spectrum because of the traditional exclusive “command-and-control” model of using the spectrum. Therefore, a new concept of Cognitive Radio (CR) has been emerging recently in which unlicensed users temporarily borrow spectrum from the licensed Primary Users (PU) based on the Dynamic Spectrum Access (DSA) technique that is also known as the “spectrum sharing” concept.

A CR is an intelligent radio system based on the Software Defined Radio platform with artificial intelligence capability which can learn, adapt, and reconfigure through interaction with the operating environment. A CR system will revolutionize the way people share the RF spectrum, lowering harmful interference to the licensed PU of the spectrum, fostering innovative DSA technology and giving people more choices when it comes to using the wireless-communication-dependent applications without

having any spectrum congestion problems. A key technical challenge for enabling secondary access to the licensed spectrum adaptation is to ensure that the CR does not interfere with the licensed incumbent users. However, incumbent user behavior is dynamic and requires CR systems to adapt this behavior in order to maintain smooth information transmission.

In this context, the objective of this dissertation is to explore design issues for CR systems focusing on adaptation of physical layer parameters related to spectrum sensing, spectrum shaping, and rate/power control. Specifically, this dissertation discusses dynamic threshold adaptation for energy detector spectrum sensing, spectrum allocation and power control in Orthogonal Frequency Division Multiplexing-(OFDM-)based CR with operating constraints, and adjacent band interference suppression techniques in turbo-coded OFDM-based CR systems.

To my family

ACKNOWLEDGMENTS

First, I would like to express my gratitude to my advisor Prof. Dimitrie C. Popescu for his guidance during the of course my degree, his perseverance in pushing me to improve and achieve the best result, as well as his knowledge that has allowed me to go a step ahead in this exciting world of research. I would also like to thank Prof. Octavia A. Dobre, with whom I had the privilege of co-authoring some of the papers in this dissertation, for her contributions and comments that have been extremely important for improving the quality of my work.

I would like to thank Prof. Linda L. Vahala, Prof. Jiang Li, and Prof. N. Rao Chaganty for agreeing to be on my committee. I would also like to thank Electrical and Computer Engineering Department Chair Prof. Shirshak K. Dhali, Graduate Program Directors Prof. Oscar R. González and Prof. Sacharia Albin, and Chief Departmental Advisor Prof. Vishnu K. Lakdawala for their support of my study at Old Dominion University. During my stay at ODU, I met numerous students, faculty, and staff at the Electrical and Computer Engineering Department, and Old Dominion University in general, who have made my Ph.D. experience all the more rewarding and to them I owe my thanks. In particular, I would like to thank Danda B. Rawat, Shiny Abraham, as well as Linda Marshal and Romina Samson who have directly or indirectly helped me complete my studies successfully.

I owe a special thanks to my wife Kamala for her patience, love, and encouragement throughout this journey. She definitely made me a better and stronger person. I am truly grateful for her commitment and unconditional support during writing.

this dissertation. I thank my son Sujal for the countless moments of joy and happiness he made possible since his birth, as well as for providing me with the main motivation for my work.

Finally, and most importantly, I would like to express gratitude to my parents, my parents-in-laws, my brother-in-law Dr. Tilak R. Joshi, sister-in-law Kabita P. Joshi, sister-in-law Dr. Tara J. Adhikari, and brother-in-law Dr. Sudhir Adhikari. Even thousands of miles apart, they have been present through every step of my life, providing support in difficult times, and enjoying every one of my accomplishments. Their endless love and belief in me have been a constant source of inspiration, and this dissertation is dedicated to them.

TABLE OF CONTENTS

	Page
LIST OF FIGURES	xi
Chapter	
I INTRODUCTION	1
I.1 RESEARCH MOTIVATION	1
I.2 COGNITIVE RADIO SYSTEM ARCHITECTURE	4
I.3 DISSERTATION CONTRIBUTIONS	17
I.4 DISSERTATION ORGANIZATION	18
II THRESHOLD ADAPTATION FOR DYNAMIC SPECTRUM SENSING	21
II.1 ENERGY DETECTOR	22
II.2 VARIANCE ESTIMATION	24
II.3 DYNAMIC THRESHOLD ADAPTATION	25
II.4 SIMULATION RESULTS	28
II.5 EXTENSION TO WIDE BAND SPECTRUM SENSING	30
II.6 CHAPTER SUMMARY	35
III SPECTRAL SHAPING FOR DYNAMIC SCENARIOS	37
III.1 PRECODED OFDM FOR DATA TRANSMISSION	38
III.1.1 THE LTE-A SIGNAL FRAME	40
III.2 SPECTRAL SHAPING BY PRECODER ADAPTATION	42
III.3 SIMULATION RESULTS	43
III.4 CHAPTER SUMMARY	47
IV JOINT SPECTRAL SHAPING AND POWER CONTROL FOR CR SYSTEMS WITH OPERATING CONSTRAINTS	48
IV.1 OFDM WITH LINEAR PRECODERS	49
IV.2 ADAPTIVE CR SYSTEMS WITH MF RECEIVERS	52
IV.2.1 MF-BASED CR SYSTEMS ADAPTATION ALGORITHM	58
IV.3 ADAPTIVE CR SYSTEMS WITH MMSE RECEIVERS	61
IV.3.1 MMSE-BASED CR SYSTEMS ADAPTATION ALGORITHM	70
IV.4 SIMULATION RESULTS	73
IV.5 CHAPTER SUMMARY	87
V ADJACENT BAND INTERFERENCE SUPPRESSION	88
V.1 TURBO-CODED OFDM-BASED CR SYSTEMS	89
V.2 MCS GENERATION AND SELECTION ALGORITHMS	93
V.2.1 PSEUDO RANDOM BASED MCS GENERATION	94
V.2.2 INTERLEAVER BASED MCS GENERATION	94
V.2.3 COMBINED MCS GENERATION	97
V.3 SIMULATION RESULTS	97
V.4 CHAPTER SUMMARY	100
VI CONCLUSIONS AND FUTURE RESEARCH	101
VI.1 RESEARCH CONTRIBUTION	101

VI.2 FUTURE WORK	103
BIBLIOGRAPHY	104
VITA	122

LIST OF FIGURES

Figure	Page
1 Overlay spectrum sharing	4
2 Cognitive radio system architecture	5
3 Block diagram of traditional OFDM system	9
4 Block diagram of energy detector	14
5 Dissertation Road Map and Introductions	19
6 Block diagram of energy detector system for spectrum sensing with threshold adaptation.	22
7 Sensing error versus threshold	28
8 Dynamic threshold adaptation.	30
9 Convergence dependence upon step size μ	31
10 Block diagram of DFB system for spectrum sensing.	32
11 Block diagram of the precoded LTE-Advanced CR system.	39
12 LTE frame structure.	41
13 PSD of an LTE-A system with and without spectral shaping.	45
14 Application of spectral shaping in a dynamic scenario	46
15 Block diagram of the precoded OFDM-based CR system.	50
16 Cost function convergence for varying number of sub-carriers N and number of data symbols M for a CR system.	75
17 SINR adaptation for numbers of sub-carrier $N=52$ and $M=52$ for a precoded OFDM-based CR system.	77
18 Power adaptation for numbers of sub-carrier $N=52$ and $M=52$ for a precoded OFDM-based CR system.	78
19 Average number of ensemble iterations for convergence to a fixed point for different number of sub-carriers, N and M , for varying μ and fixed $\beta=0.15$ and $\epsilon = 0.001$	80

20	Average number of ensemble iterations for convergence to a fixed point for different number of sub-carriers, N and M , for varying β and fixed $\mu=0.15$ and $\epsilon = 0.001$	81
21	Average number of ensemble iterations for convergence to a fixed point for different number of sub-carriers, N and M , for varying tolerance ϵ and fixed $\mu=0.15$ and $\beta = 0.15$	83
22	Average number of ensemble iterations for convergence to a fixed point for different number of sub-carriers, N and M , and fixed $\mu=0.15$ and $\beta = 0.15$ and increasing N and M for tolerance $\epsilon = 0.001$	85
23	A BER comparison for a precoded OFDM-based CR system receiver with varying N and M	86
24	Block diagram of the turbo-coded OFDM-based CR system.	90
25	Exampe of power spectral density for the original and MCS sequences	92
26	Sidelobe suppression with respect to the length of the MCS set $\{\mathcal{A}\}$ and for different MCS methods; QPSK; $N = 48$	98
27	Probability that average sidelobe power of the chosen MCS exceeds the threshold β ; QPSK; $N = 48$	99

Chapter I

INTRODUCTION

Cognitive Radio (CR) is an emerging concept designed to improve the use of a scarce natural resource, the Radio Frequency (RF) spectrum, which is becoming congested due to proliferating wireless communication devices. The main idea behind CR systems is the reuse of licensed frequencies under the specific condition that no harmful interference be caused to the licensed users of the spectrum. Dynamic Spectrum Access (DSA) becomes a promising approach to increase the efficiency of the RF spectrum usage with the development of the CR technologies, which allows unlicensed Secondary Users (SU) to dynamically access the licensed bands from legacy spectrum holders (Primary Users (PU)) on a negotiated or an opportunistic basis.

In this chapter, a brief background on CR Systems is provided. The research motivation and an overview of related literature is also presented. The main contributions of the dissertation along with its overall organization are also highlighted at the end of this chapter.

I.1 RESEARCH MOTIVATION

The RF spectrum is a valuable natural resource which is used in various scientific, commercial, military application, broadband wireless networks, as well as in cell phones, aviation radar, Global Positioning System (GPS), radio and television broadcasting, emergency communications, and consumer applications. The RF spectrum has a direct impact not just on science or engineering but also the national and

international economy. The recent data shows that the mobile data traffic is growing explosively [1], with current Universal Mobile Telecommunications System (UMTS) mobile subscriber base having reached 5 billion users [1].

The applications of wireless communication devices in different forms such as smartphones, wireless Internet subscription, patient monitoring system, GPS, emergency communication have been increasing continuously. In all types of the wireless communication application the RF spectrum is used to transmit information by electromagnetic wave radiation. On one hand the demand on RF spectrum is rapidly increasing, creating spectrum-jam and becoming nearly impossible to fulfill ever increasing demand completely, while on the other hand the recent measurements taken by different agencies revealed that the RF spectrum is not efficiently utilized, artificially increasing the scarcity of the spectrum [3]. Recent frequency measurements [4, 5] in various places around the world show that the use of the RF spectrum is not consistent, but rather varies spatially and temporally, creating spectrum “white spaces” which can be opportunistically utilized without interfering with the PU upon development of the proper technology.

The revolutionary wireless communications technology which is based on the Software Defined Radio (SDR) with artificial intelligence capability called CR has begun to overcome the spectrum-jam by using the DSA technology. The paradigm is shifting from traditional “command-and-control” spectrum uses policy to the novel “spectrum sharing” model. Hence, CR systems will revolutionize the way people share the RF spectrum, lowering harmful interference to the PU, fostering innovative DSA technology and giving people more choices when it comes to using the

wireless communications-dependent applications without feeling any spectrum congestion problem. A key technical challenge for enabling secondary access to the licensed spectrum adaptation is to ensure that the CR does not interfere with the licensed incumbent users. However, incumbent users' behavior is dynamic and requires CR systems to adapt to this behavior in order to maintain smooth information transmission.

Spectrum Sharing

In order to enable the sharing of the RF spectrum between licensed PU and unlicensed SU, the radio transmit power that causes no or affordable interference to PU must be chosen. A transmit power constraint cannot be globally set so that it meets interference requirements at any location and time for arbitrary PU. Two different approaches are used for spectrum sharing. One strategy would be to use the underlay approach. In this case, an upper limit of the transmit power constraints is set and both PU and SU share the same frequency spectrum.

In order to overcome the transmit power limitations, systems are allowed to use very large bandwidth so that they can trade off the data rate for robustness. This strategy is suitable for noise-like channels where Signal-to-Noise Ratio (SNR) can be improved by spreading or coding. However, spreading transmission power equally across a wide bandwidth could be largely sub-optimal in case of strong in-band interference.

The alternative is Overlay spectrum sharing in which a CR does not necessarily limit the transmission power, but rather attempts to share the spectra through a dynamic interference avoidance strategy and would use higher transmit power in "white

spaces” to maximize coverage and capacity. In the overlay approach, the requirement is to sense the wide spectrum to find the vacant spectrum for transmission. CR using the overlay approach are allowed to transmit increased transmit power levels without interfering with PU and other SU. Fig. 1 illustrates the transmitter power spectrum density profiles in the cognitive radio overlay spectrum sharing approach.

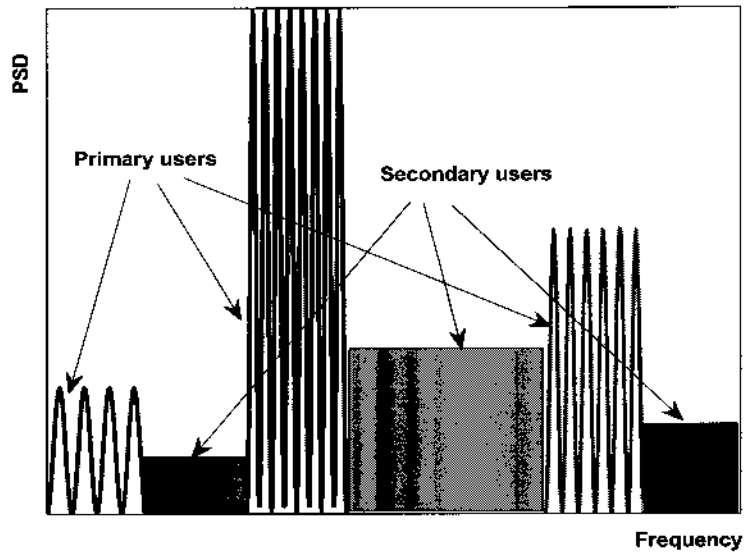


FIG. 1: Overlay spectrum sharing

I.2 COGNITIVE RADIO SYSTEM ARCHITECTURE

The design and implementation of CR [6–9] technology require the specifications of a system architecture. Traditional communications system architectures are based on the seven layered International Organization for Standardization /Open Systems Interconnection (ISO/OSI) standards. Even though CR systems is quite different from traditional wireless communication systems and still to find the suitable layered

standards, it is reasonable to study CR systems on traditional ISO/OSI standard.

Fig. 2 shows the simple architecture of a CR system.

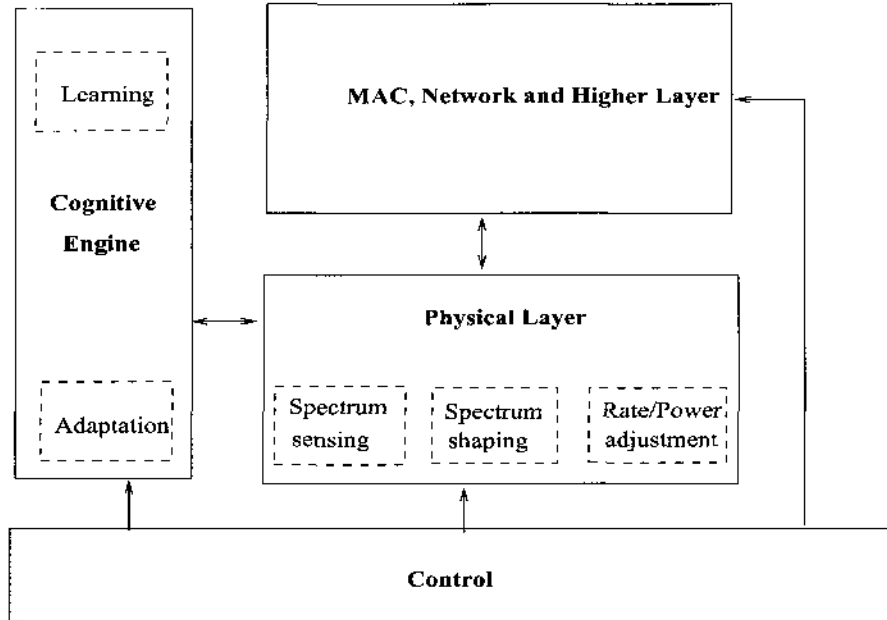


FIG. 2: Cognitive radio system architecture

Physical Layer Technologies

Multicarrier communication has been considered as a suitable technology at the physical layer of a CR system. Multicarrier modulations attract a lot of attention in both from wired and wireless communications compared to single carrier modulation because of their capability to efficiently cope with frequency selective fading channels. In the CR system context, multicarrier communication has been suggested as a candidate for a CR system due to its flexibility to fill the spectrum “white space” [10,11]. Much of the attention in the present literature emphasizes the use of conventional Orthogonal Frequency Division Multiplexing (OFDM), which is able to avoid both

Inter-symbol Interference (ISI) and Inter-Channel Interference (ICI) making use of a suitable Cyclic Prefix (CP). Though OFDM has been considered as a candidate for CR systems, it suffers from limitations such as being very sensitive to fast time variations of the wireless channel or being affected by timing offset due to imperfect synchronization. In addition, an OFDM-based CR is spectrum inefficient because of the insertion of CP. Another suitable physical layer candidate may be the Filter Bank Multi Carrier (FBMC) modulation [12–14] which does not require CP extension and shows higher robustness to residual frequency offsets than OFDM by taking advantage of the spectral containment of its modulation prototype filters. The Filter bank based multicarrier system is already considered as a physical layer candidate for CR [10]. Moreover, filter banks can be also used as a tool for spectrum sensing in CR systems. In [15,16], the application of filter banks to spectrum sensing is proved to be more promising than Fast Fourier Transform (FFT) and Thomson’s multitaper (MT) methods because of its high performance and low cost. However, FBMC is computationally more demanding. In the literature, some system performance comparisons between OFDM and FBMC can be found in [17–22]. The concept of OFDM and FBMC are briefly described as follows:

- OFDM:

Over the past several years, OFDM has emerged as the preferred choice for the physical layer of a CR due to many attractive features such as simplicity of implementation and scalability, or its ability to transmit over non-contiguous frequency bands that can be easily adapted to use idle licensed spectrum [11,23,24]. When it is desired to shape the spectrum of a transmitted

signal to meet specified constraints, OFDM provides straightforward spectral shaping abilities through notching out sub-carriers that may not be used for transmission at a given moment, and other various spectral shaping procedures have been recently proposed [25, 26]. Another advantage of the OFDM scheme is its suitability for broadcast transmissions. In case of having synchronized transmitting stations, the interference from neighboring cells is experienced as an artificial multipath [27, 28]. This has led to the Single Frequency Network (SFN) concept where the signals transmitted by the different stations are exactly the same irrespective of the transmitter location. In such a case, the active users at the cell border are those more benefited from SFN, since the signals coming from the different stations have experienced same order delay and are received with similar power level. Hence, very high frequency and time diversity may be achieved. Among others, we may emphasize the use of OFDM in the Wireless Local Area Networks (WLAN) [29], the IEEE 802.16a standard for Wireless Metropolitan Area Networks (WMAN) [30], the Digital Audio and Video Broadcasting (DAB, DVB) [31, 32], or the Asynchronous Digital Subscriber Line (ADSL) [33]. Due to its great success and broad recognition, it's also considered as a physical layer technology for Long Term Evolution (LTE) and LTE Advance (LTE-A) [34].

The basic idea behind the OFDM is the use of a large number of parallel narrow-band sub-carriers instead of a single wide-band carrier to transport information from source to destination. The requirement for higher data rates implies that the symbol duration is reduced. When a symbol is transmitted through a

multipath channel, different copies of the same symbol may span over intervals larger than one symbol period. These copies can affect several symbols, causing high inter-symbol interference and, consequently, the equalization of the signal becomes extremely challenging.

In order to implement the OFDM modulation, the FFT is used due to its very low complexity and is applied in most of the OFDM system transmission schemes [35]. Furthermore, if a guard interval is added at the beginning of each symbol the ISI can be completely avoided even if a decrease of the spectral efficiency is experienced. Usually, this guard interval lasts for 5-25% of the OFDM symbol and, in order to keep the sub-carriers' orthogonality, a copy of the symbol tail is appended at the beginning of the symbol. This operation is known as CP extension.

In the OFDM scheme, the sub-carriers over which each sub-stream is transmitted are orthogonal, being the minimum separation between consecutive sub-carriers

$$\Delta f = \frac{1}{T_s}, \quad (\text{I.2.1})$$

where T_s is the OFDM symbol duration delimited by a rectangular pulse shape. If the number of sub-carriers is N , then the transmitted OFDM symbol takes the following forms in time, $x(t)$, and in frequency domain, $X(f)$, respectively

$$x(t) = \frac{1}{\sqrt{N}} \sum_{k=0}^{N-1} b[k] \cdot \exp(j2\pi f_n t), \quad 0 \leq t \leq T_s \quad (\text{I.2.2})$$

$$X(f) = \frac{1}{\sqrt{N}} \sum_{k=0}^{N-1} b[k] \cdot \frac{\sin(\pi(T_s f - k))}{(\pi(T_s f - k))}, \quad (\text{I.2.3})$$

where $b[k]$ are the complex baseband modulated symbols (i.e. phase and amplitude modulated). The basic block diagram of the OFDM system is shown in Fig. 3. The discrete version of the OFDM signal can be written as follows,

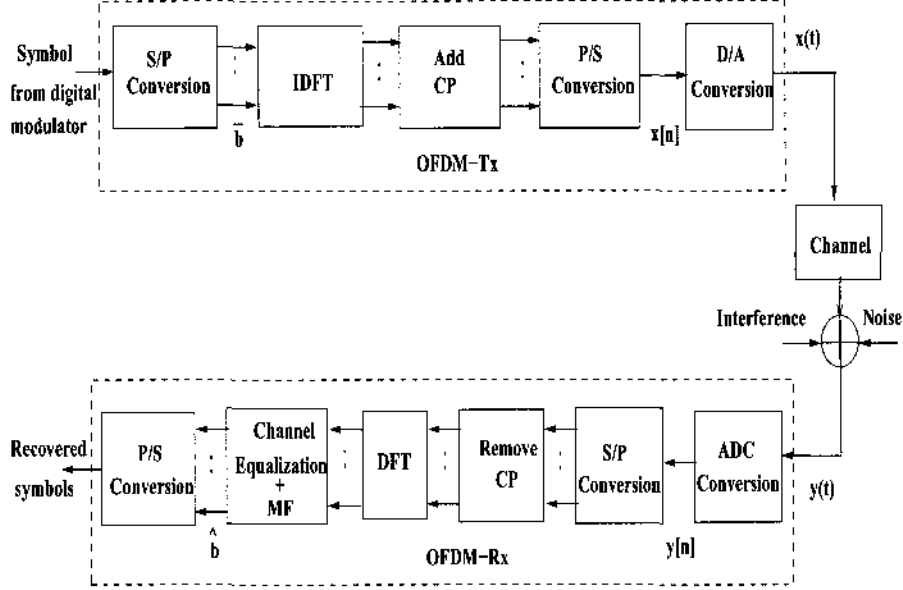


FIG. 3: Block diagram of traditional OFDM system

$$x[n] = \frac{1}{\sqrt{N}} \sum_{k=0}^{N-1} b[k].exp(j2\pi nk/N), \quad 0 \leq n \leq N-1 \quad (\text{I.2.4})$$

where the minimum sampling period that fulfills Nyquist rate is $T_r = T_s/N$.

Moreover, whether we increase N while the occupied bandwidth remains constant, the OFDM symbol duration T_s becomes larger compared to the delay spread and the amount of ISI gets reduced. Furthermore, to minimize the effects of the ISI, a guard interval can be inserted between the symbols. To maintain orthogonality between sub-carriers instead of inserting a silence period, a cyclic extension of each OFDM symbol is copied at the guard interval.

This CP is then a replica of the last part of each OFDM symbol. More details about the CP extension process, benefits, and drawbacks of this process can be found in [36].

- FBMC

The OFDM modulation with a CP as a guard interval is well known for its robustness in multipath time varying channel propagations, and for its wide use in several wireless communications standards as mentioned in previous section. To remove this guard interval, the prototype function modulating (or filtering) each sub-carrier must be very well localized in the time and in the frequency domain to limit the inter-symbol and the inter-carrier interferences. This function must also guarantee the orthogonality between the sub-carriers. An alternative to the OFDM is the OFDM with Offset Quadrature Amplitude Modulation (OFDM-OQAM) which has the advantage of not requiring the use of a guard interval, which leads to a gain in the spectral efficiency. However, the OFDM-OQAM requires independent prefiltering over each sub-carrier, thus large filter banks are required slightly increasing the system complexity. The latest detail study related to FBMC can be found in [37–50]. FBMC has the potential to fulfill the requirements of CR systems physical layer technology, but a major research effort is necessary for full exploitation and optimization in all aspects of the radio context. The physical layer is the basis on which the higher layers are built and, with the numerous scenarios and environments, a complex and coherent set of techniques and algorithms has to be found out before utilizing FBMC at a physical layer of the CR systems.

The OFDM exhibits large ripples due to the rectangular time pulse shape. The amplitudes of these ripples are null at the sub-carrier frequencies. In a filter bank multicarrier system, the frequency response has negligible amplitudes beyond the center frequency of the adjacent sub-carriers. Thus, the FBMC scheme offers high spectrum resolution and provides independent sub-channels, while it maintains or enhances the high data-rate capability. Furthermore, this high spectral resolution can be exploited by cognitive systems where the level of interference in adjacent sub-channels must be kept to a minimum.

One of the key issues regarding the FBMC is the design of the proper filter bank. Normally, uniform filter banks are considered where all the sub-carriers have the same bandwidth. Efficient uniform filter banks can be implemented using various structures such as lapped transforms, lattice structures or polyphase structures [51]. All of these structures consist of a prototype filter design with a section which modulates the data going through the filter bank. The prototype filter must control the phase and amplitude distortions in the sub-carriers as well as the interference between them. The phase distortion is eliminated when the prototype filter has a linear phase. The amplitude distortion may produce inter symbol interference.

Spectrum Sensing

In order to coexist with the PU and other SUs, CR systems must have the capability to sense the spectrum and be aware of the surrounding environment. PUs have priority and thus SUs must backoff as soon as they sense PUs commencing communications. Physical layer parameters such as modulation type, rate, and carrier

frequency should be adapted while simultaneously altering the behavior at higher layers as needed. So, spectrum sensing [52–55] is one of the important functions of CR systems by which it discovers the existence of the PU in the network.

Spectrum sensing is accomplished by performing measurements in distinct frequency bands followed by making a decision related to spectrum usage based upon the measured data. In recent years, service providers are faced with a situation where they require a larger amount of spectrum to satisfy the increasing Quality of Service (QoS) requirements of the users. This has raised interest in unlicensed spectrum access, and spectrum sensing is seen as an important enabler for this. In a scenario in which a PU exists, any SU needs to ensure that the PU is not interfered with. Spectrum sensing can be used to detect the presence (or absence) of a primary user. Spectrum sensing is an application of decision theory or detection theory. The final decisions may be binary, i.e., either the spectrum is occupied, or the spectrum is not occupied. One important observation is that it is usually the transmitter that can be detected by spectrum sensing, while, in fact, it is the receiver that needs to be protected. Thus, when a licensed user is transmitting in a specific frequency band, that band could, in principle also be used by a SU, if the SU was certain that there were no primary receivers listening. However, in most applications, the secondary user can not reliably detect primary receivers, and the focus is thus usually on transmitter detection. Of course, the secondary usage of the spectrum could be done in principle when appropriate agreements have been set up between the license owner of the spectrum, i.e. PUs, and SUs.

Various methods have been proposed for spectrum sensing in the CR system, such as, multitaper method [56], the use of pilot signals and matched filtering [57],

cyclostationarity-based methods [56–58], and the use of polyphase filter banks [15,59]. A few completely blind sensing methods that do not consider any prior knowledge about the transmitted signal have been derived in the literature, but all of them suffer from noise uncertainty and fading channels variations. Some of the spectrum sensing techniques are discussed as below:

1. **Matched Filter:** when the information about the signal to be detected e.g., signals occurring in communications applications are synchronization words for Global System for Mobile (GSM), preambles for Worldwide Interoperability for Microwave Access (WiMAX), Pseudo-Noise (PN) sequences in Advanced Television Systems Committee (ATSC), and spreading sequences for UMTS is known a priori, a Matched Filter (MF) detector is used to detect the signal. The MF detector is optimal since it maximizes the Signal-to-Noise Ratio (SNR) of a received signal in Additive White Gaussian Noise (AWGN). A MF detector works by correlating the received signal with the pattern one wishes to detect. Thus, the amplitude and the phase of the signal are extracted. If this magnitude is above a threshold value, a detection decision is made. Though MF detection has very good detection capabilities, it requires a priori information which may not be available for all applications. Hence, it is not universal choice for CR systems.
2. **Energy Detector:** Energy Detector (ED) [60] is a popular spectrum sensing method which is most useful when the CR has no knowledge about the active PU signals. Hence, it is the least demanding approach from an a priori information point of view. An energy detector measures the energy in a radio

resource and compares the value against a threshold. Generally, if and only if the measured energy is below the threshold, the received signal is declared as not occupied, i.e., it is available for opportunistic use. Energy detection is a non-specific detection method in the sense that no particular knowledge of the signal properties is used. In this sense, energy detection can be used for declaring whether a frequency band of interest is occupied or not, but it can not be used to identify the type of system or user that is occupying the spectrum. Also, an ED needs to have an idea of the noise level to adjust the detection threshold. Despite its easy implementation and low complexity, it does not perform well in low SNR and can not even differentiate between noise and signals.

The ED techniques can be broadly classified as “Transmitter Detection (TD)” and “Receiver Detection (RD)”. In the first category, the PU is assumed to be transmitting and in the latter, the PU is receiving. It is also worth noting that the main problem of ED is detecting a “low” energy signal. The basic block diagram of an ED is shown in Fig. 4.

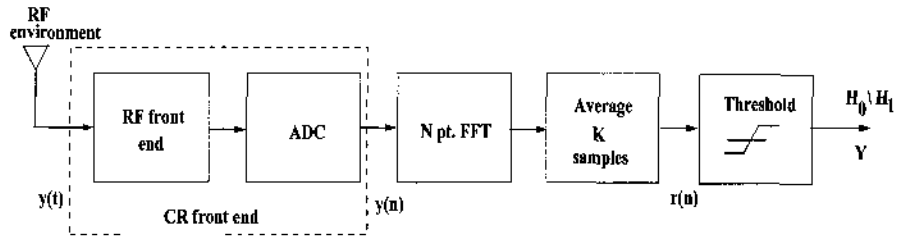


FIG. 4: Block diagram of energy detector

3. Feature Detector: The cyclostationary method is used to identify the different air interfaces of the received signal assuming that all communications signal show cyclostationarity [58,61–63] with unique cyclic signature. A cyclostationary process has statistical properties which vary periodically over time. A wide sense cyclostationary process has an autocorrelation function which is cyclic with a certain periodicity T , i.e., $R_{yy}(t, \tau) = R_{yy}(t + T, \tau)$ for all time indices τ and t . Communication signals are typically cyclostationary with multiple periodicities, e.g., the symbol frequency. Other periodicities may be related to coding and guard periods. Cyclostationary detection is typically a statistical test based on the estimated autocorrelation function of one or several known cyclic frequencies. Cyclostationary detection exploits more knowledge (i.e., the cyclic frequencies) about the process one wishes to detect than energy detection does. Hence, cyclostationary detection will only be able to detect a limited amount of systems for which the communication signals possess known cyclostationary properties, but, on the other hand, these systems can be explicitly identified by the cyclostationary detector.

4. Cooperative Sensing: When spectrum sensing is performed independently using a single unit, that unit may not detect the presence of the PU, giving the wrong information because of the received signal from the deep fading path, (e.g., it may be shadowed) relative to the transmitter one wishes to detect. This is known as the Hidden Node Problem (HNP). Because of this possibility, a SU can not use the spectrum based on its decisions on single unit sensing unless it is certain that the detected opportunities are really exists, i.e., it must

be able to detect a transmitter even as it experiences deep fading.

An approach that does not possess the above disadvantages, but requires some coordination, is cooperative sensing, in which multiple sensing radios are utilized.

- 5. Compressed Sensing:** Wide band spectrum sensing [64–69] can be described as a complex topic not only because of its technical difficulty, but also due to the large number of problems that appear at each of the steps of the detection/estimation procedure. In fact, research efforts in multichannel monitoring range from low-level physical sensing to higher-level resource allocation problems.

Compressive sensing theory has also been considered in wide band spectrum sensing techniques. An analog-to-digital converter has been used to transform the analog received signal into a digital signal by sampling at the Nyquist rate. Next, compressive sampling is applied to the sampled vector to compress it into a smaller vector and then the spectrum is reconstructed by solving an l_1 norm minimization problem. The received analog signal is sampled at the information rate of the signal using an analog-to-information converter (AIC). Here, the compressive sensing is embedded in the AIC. The same l_1 norm minimization method is used to estimate the original spectrum. The wavelet edge detector has been used to detect the channel borders in the estimated spectrum.

I.3 DISSERTATION CONTRIBUTIONS

CR systems have been proposed to enable the flexible use of the RF spectrum in future generations of wireless communications systems. Optimal allocation of power and spectrum in a multicarrier CR context with power and mutual interference constraints is still an open topic. In [70–72], downlink power allocation problems in multicarrier based CR systems are investigated. In [71], maximization of the capacity with per sub-channel power constraints is considered, but the influence of side lobes of neighboring sub-carriers is omitted. Conversely, the authors in [72] propose an optimal scheme with the interference induced to PU, but the total power constraint is not considered. In addition, CR systems are expected to both detect spectrum bands that are not actively used by PU and provide SU access to these bands. An important aspect in detecting the spectrum used by a CR is to adapt their spectrum sensing constraints to the agile patterns of the spectrum use of the PU by learning from past behavior. This motivates the work presented in this dissertation, which studies the following problems:

- **Dynamic threshold adaptation of energy detector spectrum sensing technique:**

This dissertation presents and analyzes the adaptation of the sensing threshold for energy-based spectrum sensing in dynamic scenarios. An algorithm for *energy detector spectrum sensing threshold adaptation* which *minimizes the spectrum sensing error* is presented. The concept of threshold adaptation is also extended for the wide band received signal using the filter bank approach.

- **Spectral shaping for linearly precoded OFDM-based CR system:**

This dissertation presents an algorithm for spectrum shaping in the SU signal to avoid active PU signals. LTE-A based CR systems are considered to show the “carrier aggregation” concept.

- **Power control with predetermined QoS constraints:**

This dissertation augments the spectral shaping procedure with a power control mechanism that enables dynamic spectrum access for SU without interfering with the PU.

- **Adjacent band interference reduction:**

This dissertation proposes the sidelobe reduction methods to reduce out-of-band interference. Adjacent band interference suppression using Multiple Choice Sequences (MCS) in a turbo-coded OFDM-based CR system is also investigated.

I.4 DISSERTATION ORGANIZATION

The organization of the dissertation is shown in Fig. 5. Chapter II discusses the spectrum sensing errors, i.e, probability of false alarm and probability of missed detection. This chapter also explores a threshold adaptation method for energy detector spectrum sensing.

Chapter III introduces the concept of spectrum shaping in dynamic scenarios and discusses techniques involving the notching out the spectrum actively used by the PU in multicarrier OFDM systems.

Chapter IV studies transmitter adaptation for a precoded OFDM-based CR with predefined QoS constraints. This chapter also contains the necessary and sufficient

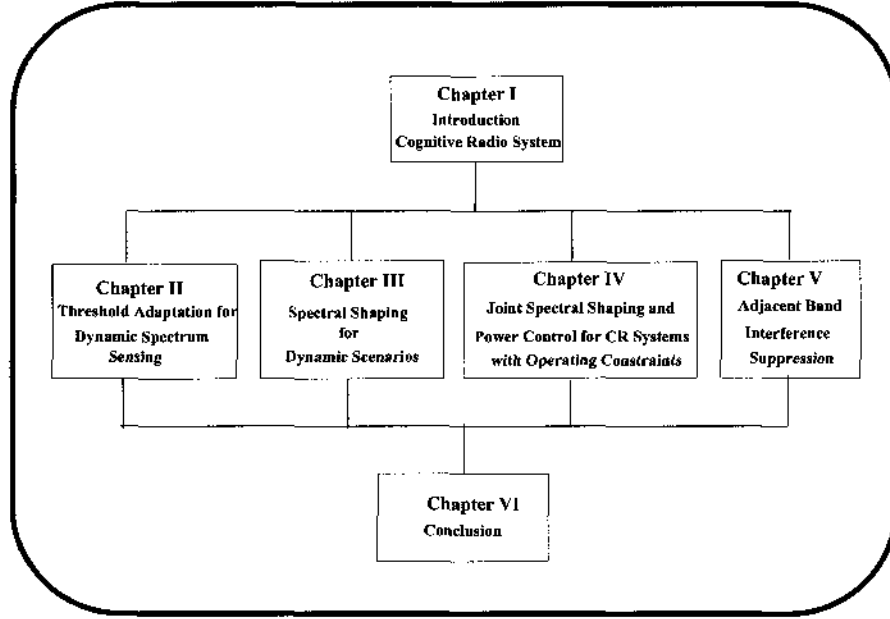


FIG. 5: Dissertation Road Map and Introductions

conditions for the optimization problem to find the optimum value of the transmitted power satisfying the predefined QoS parameter specified in terms of the SINR. Two types of receiver processing techniques, i.e., MF- and Minimum Mean Square Error- (MMSE-) based are also investigated in this chapter.

Chapter V provides an analysis of sidelobe reduction for turbo coded OFDM-based CR systems. Different ways of reducing the sidelobe power are proposed based on MCS in turbo-coded OFDM-based CR.

Chapter VI concludes this work and proposes some directions for future research.

Most of the results in this dissertation have been presented previously. The work on spectrum sensing threshold adaptation in Chapter II was presented in part at the

IEEE Radio and Wireless Symposium (RWS) [73], the 44th Conference on Information Sciences and Systems [74], and IEEE Communications Letter [75]. The work of dynamic spectral shaping in Chapter III was presented at the 43rd Annual Asilomar Conference on Signals, Systems, and Computers [76]. The joint spectral shaping and power control with operating constraints in Chapter IV was presented in part at the 44th Annual Asilomar Conference on Signals, Systems, and Computers [77]. The work on adjacent band interference reduction in Chapter V will be presented at the IEEE Global Telecommunications Conference [78].

Chapter II

THRESHOLD ADAPTATION FOR DYNAMIC SPECTRUM SENSING

CR system has been proposed to enable flexible use of the frequency spectrum in future generations of wireless networks. They are expected to detect spectrum bands that are not actively used by PU and provide SU access to these bands. An important aspect in detecting the spectrum for a CR system is to react to changes in the operating environment and to adapt its spectrum sensing constraints to the changing patterns of the spectrum use of the PU. In this chapter, an algorithm for spectrum sensing threshold adaptation for energy detector-based spectrum sensing is presented, which minimizes the spectrum sensing errors. The algorithm is also illustrated with numerical examples obtained from simulations. Extension of the threshold adaptation for wide band signal using filter bank is also presented in this chapter.

The rest of the chapter is organized as follows: Section II.1 presents the system model, along with the problem solved in this chapter. Section II.2 describes the noise variance estimation from the received noisy signal, modeling the signal as a Auto Regressive (AR) model. Dynamic Threshold Adaptation (DTA) is discussed in Section II.3. Section II.4 provides the results obtained from the simulations. The extension of the threshold adaptation for wide band signal is presented in II.5. Finally, Section II.6 summarizes the chapter.

II.1 ENERGY DETECTOR

Energy detector based spectrum sensing is described schematically in Fig. 6. After performing the front end processing along with the analog to digital conversion

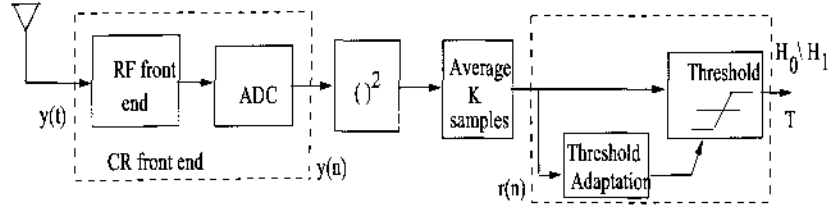


FIG. 6: Block diagram of energy detector system for spectrum sensing with threshold adaptation.

(ADC), the received signal in the band of the interest is expressed as,

$$y(n) = s(n) + v(n), \quad (\text{II.1.1})$$

with $s(n)$ being the active radio signal at the location of the CR system, and $v(n)$ the AWGN corrupting the active signal with zero mean and variance σ_v^2 . Under the assumption of non-coherent detection, the samples of the active radio signal $s(n)$ may also be modeled as a Gaussian random process with variance σ_s^2 [57]. It is also worth noting that both σ_s^2 and σ_v^2 are estimated from the received signal $y(n)$ as will be described in Section II.2. The output of the energy detector is expressed as the time average

$$r(n) = \frac{1}{K} \sum_{i=n-K}^n |y(i)|^2. \quad (\text{II.1.2})$$

This provides information on the active signal spectrum at a given moment and may be used for detecting the presence of active PUs in the tested spectrum band.

A binary hypothesis testing is performed to identify the presence of the active PU. At a given time instant n , the tested band is considered to be vacant if only noise is detected, while the band is considered to be occupied by an active PU if a PU signal and noise are detected. Thus, the following binary hypothesis testing is performed at time instant n for the band of interest to determine its occupancy by an active PU at that moment:

$$\begin{aligned}\mathcal{H}_0 : y(n) &= v(n) \\ \mathcal{H}_1 : y(n) &= s(n) + v(n),\end{aligned}\tag{II.1.3}$$

where, the hypotheses \mathcal{H}_0 and \mathcal{H}_1 respectively indicate the absence and presence of the PU signal in the received signal at that moment in the tested frequency band.

The decision rule is given by

$$y(n) \underset{\mathcal{H}_0}{\overset{\mathcal{H}_1}{\gtrless}} \gamma(n),\tag{II.1.4}$$

where $\gamma(n)$ is the sensing threshold value. The probability of detecting an active PU signal expressed in terms of the complementary error function $\text{erfc}(x)$ is [57]

$$\begin{aligned}P_d(\gamma(n)) &= \Pr[r(n) > \gamma(n) | \mathcal{H}_1] \\ &= \frac{1}{2} \text{erfc} \left[\frac{\gamma(n) - K\sigma_s^2}{2\sigma_1^2\sqrt{K}} \right],\end{aligned}\tag{II.1.5}$$

where $\sigma_1^2 = \sigma_s^2 + \sigma_v^2$ and $\text{erfc}(x)$ is related to the standard Q -function as

$\text{erfc}(x) = 2Q(x)(\sqrt{2}x)$. The probability of missed detection of an active PU signal is

$$P_{md}(\gamma(n)) = 1 - P_d(\gamma(n)).\tag{II.1.6}$$

Similarly, the probability of false alarm is [57]

$$\begin{aligned}P_{fa}(\gamma(n)) &= \Pr[r(n) > \gamma(n) | \mathcal{H}_0] \\ &= \frac{1}{2} \text{erfc} \left[\frac{\gamma(n) - K\sigma_v^2}{2\sigma_v^2\sqrt{K}} \right].\end{aligned}\tag{II.1.7}$$

The performance of the spectrum sensing at any time instant n for the tested spectrum band depends on the values of these probabilities, which are functions of the threshold value $\gamma(n)$. A large probability of missed detection implies a higher chance that the CR will not detect the presence of a PU transmission at that moment, whereas a low probability of false alarm implies better chances for the CR system to occupy at that moment in the band of the interest.

This chapter studies the optimization and adaptation of the detection threshold $\gamma(n)$ in dynamic scenarios, where the variances of the active signal σ_s^2 and/or noise σ_v^2 change in time and are estimated from the received signal $y(n)$ by modeling it as an AR process.

II.2 VARIANCE ESTIMATION

The noise variance is estimated from the received contaminated noisy signal as discussed in [79]. The uncontaminated PU signal $s(n)$ follows a p -th order AR model with transfer function

$$H(z) = \frac{1}{\left[1 + \sum_{j=1}^p a_j z^{-j}\right]}. \quad (\text{II.2.1})$$

The coefficients a_j satisfy the set of Yule-Walker equations

$$\sum_{i=1}^p a_i \mathbf{R}_s(|j-i|) = -\mathbf{R}_s(j), \quad j > 0, \quad (\text{II.2.2})$$

where, $\mathbf{R}_s(j)$ are the autocorrelation coefficients of the uncontaminated signal $s(n)$.

These are related with the autocorrelation coefficients $\mathbf{R}_y(j)$ of the noisy signal

$y(n)$ as [80]

$$\begin{aligned} \mathbf{R}_s(0) &= \mathbf{R}_y(0) - \sigma_v^2 \\ \mathbf{R}_s(j) &= \mathbf{R}_y(j), \quad j > 0, \end{aligned} \quad (\text{II.2.3})$$

with the estimate of noise variance, $\hat{\sigma}_v^2$, given by

$$\hat{\sigma}_v^2 = \frac{\left[\sum_{j=1}^p a_j \{ \hat{\mathbf{R}}_y(j) + \sum_{i=1}^p a_i \hat{\mathbf{R}}_y(|j-i|) \} \right]}{\sum_{j=1}^p a_j^2}, \quad (\text{II.2.4})$$

where, $\hat{\mathbf{R}}_y(j)$ are the estimates of the autocorrelation coefficients of the noisy signal $y(n)$. The PU signal, $s(n)$, and the noise, $v(n)$, are the uncorrelated random processes. Once the noise variance is estimated from the received noisy signal, the variance of the PU signal is calculated by subtracting estimated noise variance from the variance of the received noisy signal, i.e., $\sigma_s^2 = \sigma_1^2 - \sigma_v^2$.

II.3 DYNAMIC THRESHOLD ADAPTATION

Since both the probability of missed detection and the probability of false alarm are important for accurate spectrum sensing, the optimum value of the threshold level for the test statistic is chosen to minimize the spectrum sensing error defined as

$$\mathcal{E}(\gamma(n)) = (1 - \delta)P_{md}(\gamma(n)) + \delta P_{fa}(\gamma(n)), \quad (\text{II.3.1})$$

where $0 < \delta < 1$ is a given constant weighting the probability of missed detection relative to that of false alarm probability.

The optimum threshold for a band of interest at a given moment is found by

solving the constrained optimization problem

$$\begin{aligned} \min_{\gamma(n)} \mathcal{E}(\gamma(n)) \text{ subject to} \\ P_{md}(\gamma(n)) \leq \alpha, \text{ and } P_{fa}(\gamma(n)) \leq \beta, \end{aligned} \quad (\text{II.3.2})$$

where, α and β are the maximum values allowed for the probabilities of false alarm and missed detection. The constrained optimization problem (II.3.2) can be solved using the Lagrange multipliers method. The Lagrangian function can be written as,

$$\mathcal{L}(\gamma, \lambda_1, \lambda_2) = \mathcal{E}(\gamma(n)) - \lambda_1 [P_{md}(\gamma(n)) - \alpha] - \lambda_2 [P_{fa}(\gamma(n)) - \beta], \quad (\text{II.3.3})$$

where, λ_1 and λ_2 are the Lagrangian multipliers. In order to find the necessary conditions for the constrained optimization problem (II.3.2), the partial derivatives of the Lagrange function (II.3.3) is found with respect to γ , λ_1 , and λ_2 , respectively, and after some algebraic manipulation we obtain

$$\frac{\lambda_1 + \delta - 1}{\lambda_2 - \delta} - \frac{\exp \left[- \left(\frac{\gamma(n) - K\sigma_v^2}{2\sigma_v^2\sqrt{K}} \right)^2 \right]}{\exp \left[- \left(\frac{\gamma(n) - K\sigma_1^2}{2\sigma_1^2\sqrt{K}} \right)^2 \right]} = 0, \quad (\text{II.3.4})$$

$$1 - \alpha - \frac{1}{2} \text{erfc} \left[\frac{\gamma(n) - K\sigma_1^2}{2\sigma_1^2\sqrt{K}} \right] = 0, \quad (\text{II.3.5})$$

$$\frac{1}{2} \text{erfc} \left[\frac{\gamma(n) - K\sigma_v^2}{2\sigma_v^2\sqrt{K}} \right] - \beta = 0. \quad (\text{II.3.6})$$

The optimal value of γ , λ_1 , and λ_2 is found solving (II.3.4), (II.3.5) and (II.3.6) simultaneously. Since these equations are transcendental and have no closed-form solutions they may be solved numerically through iterative methods, such as the Newton's method.

In dynamic scenarios the optimal value of the threshold γ can be adapted by using a gradient-based update

$$\gamma(n+1) = \gamma(n) - \mu \nabla \mathcal{E}(n), \quad (\text{II.3.7})$$

where, $\mathcal{E}(n)$ is given by equation (II.3.1), μ is a suitably chosen step size, and the gradient $\nabla\mathcal{E}(n)$ is calculated as [81]

$$\begin{aligned} \nabla\mathcal{E}(n) &= \frac{-\delta}{2\sigma_v^2\sqrt{\pi K}} \exp\left[-\left(\frac{\gamma(n) - K\sigma_v^2}{2\sigma_v^2\sqrt{K}}\right)^2\right] \\ &+ \left[(1-\delta) + \frac{(1-\delta)}{2\sigma_1^2\sqrt{\pi K}}\right] \exp\left[-\left(\frac{\gamma(n) - K\sigma_1^2}{2\sigma_1^2\sqrt{K}}\right)^2\right]. \end{aligned} \quad (\text{II.3.8})$$

The proposed algorithm for sensing threshold adaptation combines the gradient based updates of the sensing threshold with the estimation of noise variance. The algorithm is formally stated in Algorithm 1. It is worth noting that, in order to estimate the

Algorithm 1 Threshold Adaptation for Energy Detector-based Spectrum Sensing

1: Input parameters:

- Step size μ and tolerance ϵ , random initialization of threshold value ($\gamma(0)$).

2: Calculate the average energy using equation (II.1.2).

3: Calculate unbiased estimate of the autocorrelation coefficients $\{\hat{\mathbf{R}}_y(j)\}$ from observed noisy signal,

4: compute the AR parameters using a least squares procedure [80],

5: calculate the noise variance using equation (II.2.4),

6: **while** $(\gamma(n+1) - \gamma(n)) > \epsilon$ **do**

7: update $\nabla E(n)$ using (II.3.8)

8: update $\gamma(n)$ using (II.3.7)

9: check the constraints conditions.

10: **end while**

noise variance, the received signal is modeled using an AR model whose parameters

are computed from an overdetermined set of $q > p$ high order Yule-Walker equations using a least squares procedure [80]. Using the estimated noise variance, the gradient-based update is then applied to adapt the sensing threshold incrementally in the direction of the optimal value which minimized the sensing error (II.3.1).

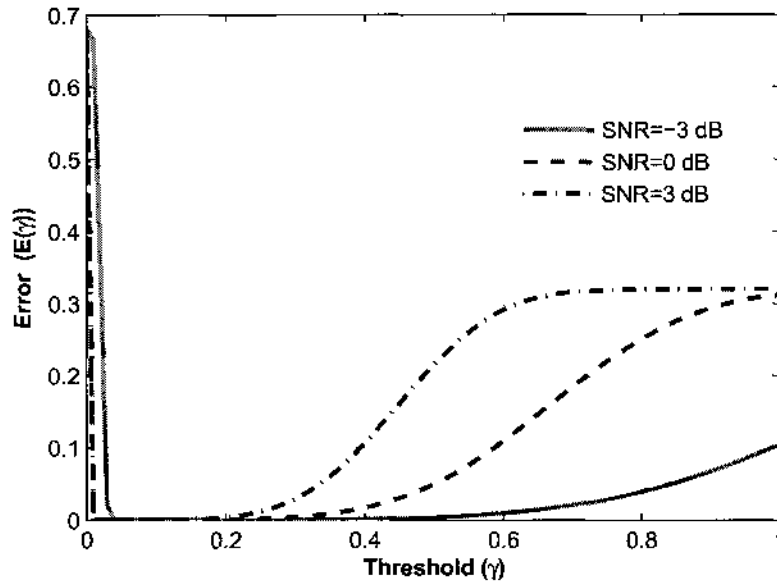


FIG. 7: Sensing error versus threshold

II.4 SIMULATION RESULTS

In order to illustrate the proposed algorithm, extensive simulations are performed for an energy detector in a dynamic scenario with noise variance that changes in time. The simulation parameters are: the threshold/probability constraints $\alpha = 0.1$ and $\beta = 0.2$, the gradient constant $\mu = 0.5$, and the algorithm tolerance $\epsilon = 10^{-3}$.

Experiment I: Sensing Error Minimization

The performance of the spectrum sensing for the tested spectrum band depends on the values of spectrum sensing errors, i.e. false alarm and missed detections, which are functions of the sensing threshold value. A large probability of missed detection implies a higher chance that the CR will not detect the presence of a PU transmission at that moment, whereas a low probability of false alarm implies better chances for the CR system to occupy at that moment in the band of the interest. In this simulation experiment, the dependence of the spectrum sensing error with the threshold value for -3, 0, and 3 dB SNR has been studied. The results of this experiment are shown in Fig. 7. From this figure, it is worth to noting that the spectrum sensing error has a minimum value for specific threshold.

Experiment II: Threshold Adaptation

In the second simulation experiment, the threshold adaptation performed by the proposed algorithm when the noise variance changes in time has been studied. Results of this experiment are illustrated in Fig. 8. This experiment starts with the SNR = 3 dB (Scenario 1), for which the algorithm adjusts the threshold to the optimal value. Once this is reached, the noise variance changes such that the SNR = 0 dB (Scenario 2). After the threshold is adapted to the new optimal value corresponding to scenario 2, the noise variance changes again such that in Scenario 3 in which the SNR = -3 dB. Once again, it is noticed that the algorithm adapts the sensing threshold to its new optimal value for the new scenario.

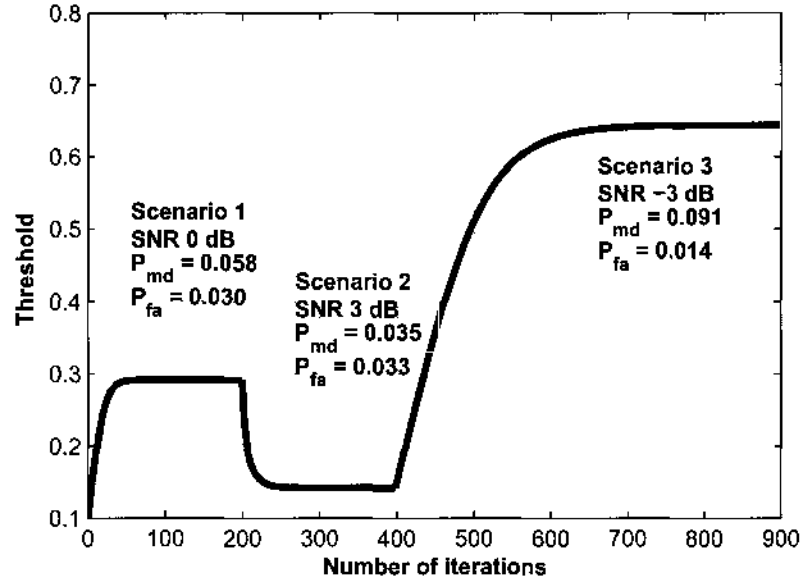


FIG. 8: Dynamic threshold adaptation.

Experiment III: Convergence Speed

Fig. 9 illustrates the convergence of the proposed algorithm for dynamic threshold adaptation for various values of the step size μ . The plot shows that the higher the values of step size the faster the convergence speed and vice versa. It is noticed that for very high value of step size (e. g. $\mu = 0.90$), there is a ripple before it comes to the steady state value.

II.5 EXTENSION TO WIDE BAND SPECTRUM SENSING

The filter bank spectrum sensing system, described schematically in Fig. 10, where the wide band received signal $\{Y(n)\}$ at some time instant n is given by:

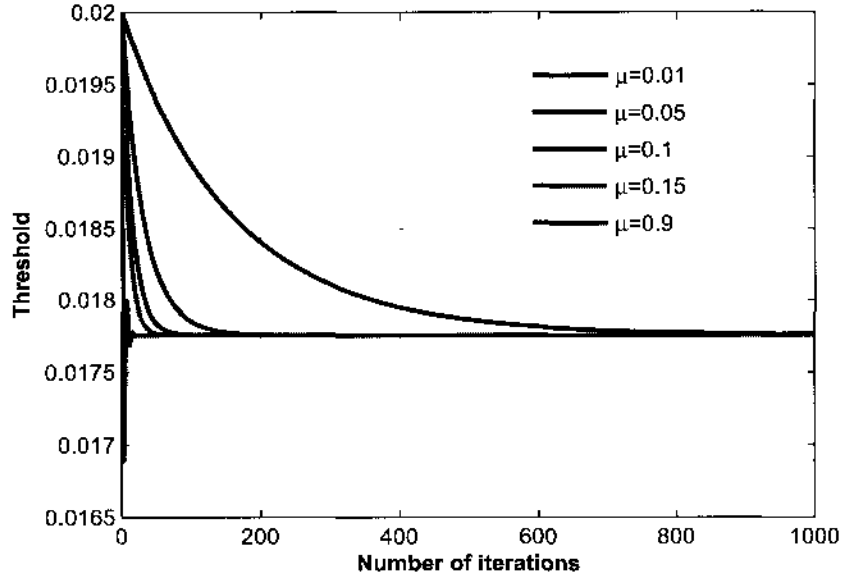


FIG. 9: Convergence dependence upon step size μ .

$$Y(n) = S(n) + V(n), \quad (\text{II.5.1})$$

with $S(n)$ being the active radio signal at the location of the CR system, and $V(n)$ the additive white Gaussian noise (AWGN) corrupting the active signal with zero mean and variance σ_V^2 . The received signal is passed through a polyphase Digital Filter Bank (DFB) whose output is used for spectrum sensing. The computational complexity is reduced by using the polyphase property of the filter banks, which yields a decrease in the sampling rate by a factor of L (the number of subbands) [59]. The basic building block of the DFB is the prototype (or zero-th band) low pass filter. Other band filters are realized by shifting the prototype filter in frequency. The prototype filter is designed to minimize the spectrum leakage and its length is chosen as the smallest multiple of L that can satisfy some desired stop-band attenuation

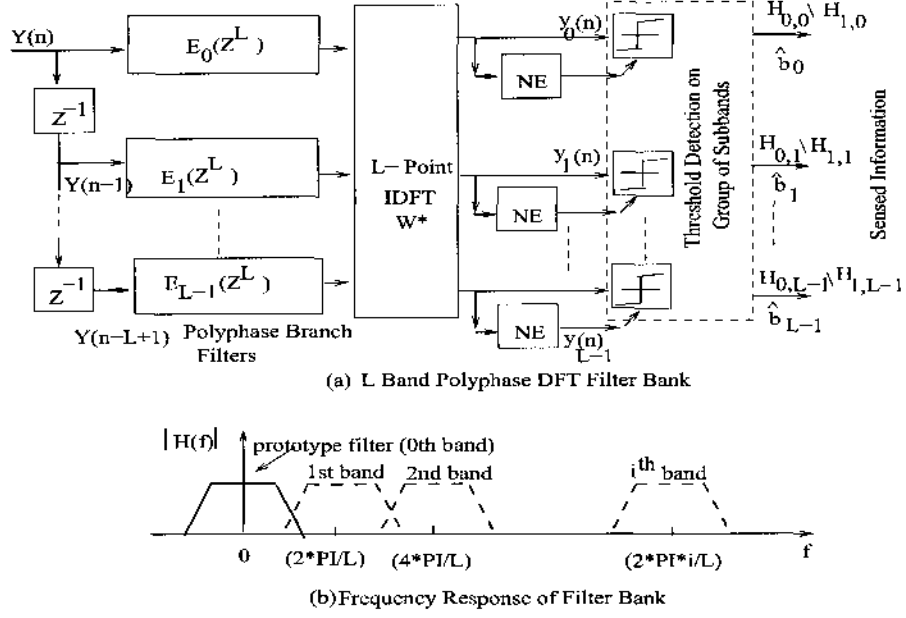


FIG. 10: Block diagram of DFB system for spectrum sensing.

requirements. The frequency response of the filter bank is written as [51],

$$H(z) = \sum_{n=-\infty}^{\infty} h(n)z^{-n}. \quad (\text{II.5.2})$$

This can be separated into even and odd numbered coefficients as,

$$\begin{aligned} H(z) &= E_o(z^2) + z^{-1}E_e(z^2) \\ &= \sum_{n=-\infty}^{\infty} h(2n)z^{-2n} + z^{-1} \sum_{n=-\infty}^{\infty} h(2n+1)z^{-2n}. \end{aligned} \quad (\text{II.5.3})$$

Applying a similar approach to represent $H(z)$ into L^{th} polyphase filter bank,

$$\begin{aligned} H(z) &= \sum_{n=-\infty}^{\infty} h(nL)z^{-nL} + z^{-1} \sum_{n=-\infty}^{\infty} h(nL+1)z^{-nL} + \\ &\quad \dots + z^{-(L-1)} \sum_{n=-\infty}^{\infty} h(nL+L-1)z^{-nL}, \end{aligned} \quad (\text{II.5.4})$$

where L is any integer. Thus, the filter bank system can be represented using polyphase components as

$$H(z) = \sum_{i=0}^{L-1} z^{-i} E_i(z^L), \quad (\text{II.5.5})$$

where

$$E_i(z) = \sum_{n=-\infty}^{\infty} e_i(n) z^{-n} \quad (\text{II.5.6})$$

and $e_i(n)$ is defined as

$$e_i(n) = h(nL + i), \quad 0 \leq i \leq L - 1. \quad (\text{II.5.7})$$

The polyphase can be efficiently implemented using DFT filter bank as [51],

$$H_l(z) = H_0(zW^l), \quad (\text{II.5.8})$$

where $W = \exp(-j2\pi/L)$ and $H_0(z)$ corresponds to the prototype filter and is expressed as

$$\begin{aligned} H(z) &= 1 + z^{-1} + z^{-2} + \dots + z^{-(L-1)} \\ &= \sum_{i=0}^{L-1} z^{-i} E_i(z^L). \end{aligned} \quad (\text{II.5.9})$$

From equations (II.5.8) and (II.5.9)

$$\begin{aligned} H_l(z) &= H_0(zW^l) \\ &= \sum_{i=0}^{L-1} (z^{-1}W^{-l})^i E_i(z^L) \end{aligned} \quad (\text{II.5.10})$$

and thus,

$$\begin{aligned} Y_l(z) &= H_l(z)Y(z) \\ &= \sum_{i=0}^{L-1} W^{-il} (z^{-i} E_i(z^L) S(z)) + \sum_{i=0}^{L-1} W^{-il} (z^{-i} E_i(z^L) V(z)), \end{aligned} \quad (\text{II.5.11})$$

where $S(z)$ and $V(z)$ are the Z-transforms of the signal $S(n)$ and AWGN $V(n)$ respectively. When L is power of two, i.e. $L = 2^j$ with j a positive integer, the DFT can be calculated efficiently using the Fast Fourier Transform (FFT). Because the output bandwidth of the DFT filter bank is approximately L times narrower than that of $X(n)$, usually decimated uniform DFT banks are used. The output of the l -th subband of the DFB can be expressed as the time average

$$Y_l(n) = \frac{1}{K} \sum_{i=n-K}^n |y_l(i)|^2. \quad (\text{II.5.12})$$

This provides information on the active signal spectrum in the l -th subband and may be used for detecting PU spectrum. The computational complexity of the system is equivalent to that of the realization of the prototype filter and one IDFT since the L bands of filter bank share the same structure.

Multi-channel detection for DFB spectrum sensing can be done by extending the energy detection results obtained for a single channel. A given spectrum band is considered to be vacant if there is only noise and the subband is considered to be occupied by the PU if there is a PU signal and noise present. Thus, the following binary hypothesis testing is performed at any given time instant n to find the occupancy of the l -th subband:

$$\begin{aligned} \mathcal{H}_{0,l} : Y_l(n) &= v_l(n) \\ \mathcal{H}_{1,l} : Y_l(n) &= y_l(n) + v_l(n) \end{aligned} \quad l = 0, 1, \dots, L-1, \quad (\text{II.5.13})$$

where the hypotheses $\mathcal{H}_{0,l}$ and $\mathcal{H}_{1,l}$ respectively indicate the absence and presence of the primary user signal in the l -th subband, and $v_l(n)$ is a Gaussian random process with zero mean and variance $(\sigma_v^{(l)})^2$. Under the assumption of absence of coherent detection, signal samples may also be modeled as a Gaussian random process with

variance $(\sigma_y^{(l)})^2$. The decision rule corresponding to the l -th subband is given by

$$Y_l(n) \underset{\mathcal{H}_{0,l}}{\overset{\mathcal{H}_{1,l}}{>}} \gamma_l(n), \quad l = 0, 1, \dots, L-1, \quad (\text{II.5.14})$$

where $\gamma_l(n)$ is the threshold. By using (II.1.4), the probability of detecting a PU signal in subband l is [57]

$$\begin{aligned} P_d^{(l)}(\gamma_l(n)) &= \Pr[Y_l(n) > \gamma_l(n) | \mathcal{H}_{1,l}] \\ &= \frac{1}{2} \operatorname{erfc} \left[\frac{\gamma_l(n) - K((\sigma_v^{(l)})^2 + (\sigma_y^{(l)})^2)}{2\sqrt{K}((\sigma_v^{(l)})^2 + (\sigma_y^{(l)})^2)} \right], \end{aligned} \quad (\text{II.5.15})$$

and, thus, the probability of missed detection of a PU signal in subband l is

$$P_{md}^{(l)}(\gamma_l(n)) = 1 - P_d^{(l)}(\gamma_l(n)). \quad (\text{II.5.16})$$

Similarly, the probability of false alarm for subband l is [57]

$$\begin{aligned} P_{fa}^{(l)}(\gamma_l(n)) &= \Pr[Y_l(n) > \gamma_l(n) | \mathcal{H}_{0,l}] \\ &= \frac{1}{2} \operatorname{erfc} \left[\frac{\gamma_l(n) - K(\sigma_v^{(l)})^2}{2\sqrt{K}(\sigma_v^{(l)})^2} \right]. \end{aligned} \quad (\text{II.5.17})$$

The performance of the spectrum sensing at any time instant n depends mainly upon the values of these probabilities, which are functions of the thresholds $\gamma_l(n)$. It is worth noting that a large probability of missed detection implies a higher chance that a CR system will not detect the presence of a PU transmission in subband l , whereas a low probability of false alarm implies better chances for a CR systems to occupy subband l .

II.6 CHAPTER SUMMARY

In this chapter a novel algorithm for adaptation of the detection threshold in an energy-detector based spectrum sensing for a CR is presented. Spectrum sensing

uses an energy detector approach and the proposed algorithm adapts the threshold to minimize the spectrum sensing errors using gradient-based updates. For accurate adaptation in dynamic scenarios, an estimate of the noise variance is used in the threshold calculation. The proposed algorithm is illustrated with numerical examples obtained from simulations, which confirm its effectiveness in optimizing the sensing threshold as well as in adapting it in dynamic scenarios. The extension of the proposed algorithms for multiband system is also described in this chapter.

Chapter III

SPECTRAL SHAPING FOR DYNAMIC SCENARIOS

Spectral shaping enables dynamic access to the RF spectrum for CR systems and in this chapter, how spectral shaping is accomplished in LTE-A based CR systems will be discussed.

LTE-A is a new standard developed by the 3rd Generation Partnership Project (3GPP) [34] to enable efficient use of the RF spectrum in future generations of wireless communication systems (4G and beyond). The radio access technology in LTE-A systems is based on OFDM modulation which offers attractive features such as simplicity of implementation or scalability. The OFDM is a mature technology which was introduced in the early 1970s [82], successfully used in implementing modems for high-speed data transmission over telephone and Digital Subscriber Lines (DSL) in the 1990s [83], and present in current wireless standards such as the IEEE 802.11 Wireless Local Area Network (WLAN) standard or 802.15 standard for Wireless Personal Area Networks (WPAN).

Due to its abilities to shape the spectrum of transmitted signals, OFDM has also been proposed for use in CR systems to take advantage of unused/underused spectrum and to enable secondary access to licensed spectrum by unlicensed users. It is worth noting that shaping the spectrum of an OFDM signal is accomplished by notching out those sub-carriers which are currently used for transmission, and various spectral shaping approaches have been proposed recently for CR systems [11, 26, 84, 85].

In this chapter, a CR system using the LTE-A standard at the physical layer [86] in conjunction with a precoded OFDM scheme for mapping digitally modulated data symbols on the available sub-carriers, is considered, and a method for dynamic spectral shaping based on precoder adaptation is presented. The LTE-A is expected to offer many attractive features such as high spectral efficiency (30 bps/Hz downlink and 15 bps/Hz uplink), low latency (user plane 10 ms), high peak-data rate (1 Gbps in downlink and 500 Mbps in uplink in scenarios with low mobility), and flexible transmission bandwidths of up to 100 MHz.

The rest of the chapter is organized as follows: Section III.1 describes the problem statement of spectrum shaping with the system model utilized in this chapter. Section III.2 shows the spectrum shaping methods in detail. Numerical results are presented in III.3. Finally, Section III.4 summarizes the chapter.

III.1 PRECODED OFDM FOR DATA TRANSMISSION

The block diagram of a LTE-A system using precoded OFDM transmission is sketched in Fig. 11, which covers both downlink and uplink scenarios. In the downlink of a LTE-A system, OFDMA is used to enable multiple access and transmission to multiple users, while in the uplink of a LTE-A system, Single Carrier Frequency Division Multiple Access (SC-FDMA) is used for multiple access to allow reception from multiple users. Accordingly, the white blocks in Fig. 11 are common to the two scenarios, while the shaded blocks are present only in the uplink scenario.

As seen on the block diagram in Fig. 11, a linear precoder described by matrices \mathbf{S} and \mathbf{P} is used to map frames of incoming symbols from the digital modulator into

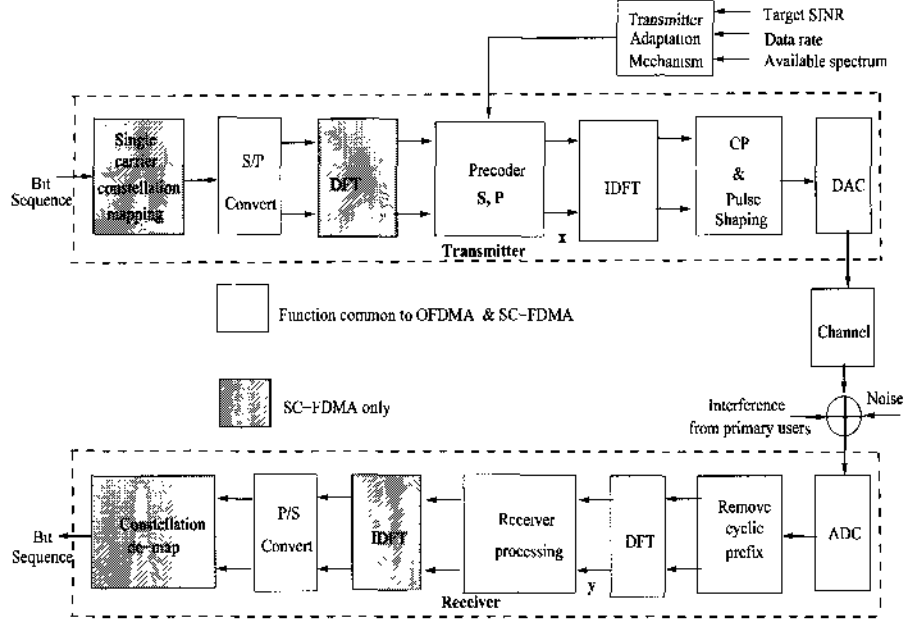


FIG. 11: Block diagram of the precoded LTE-Advanced CR system.

coded information data symbols. The $N \times M$ precoder matrix \mathbf{S} , where N is the length of the OFDM symbol and is equal to the number of sub-carriers used for transmission, and M is the length of the block of information symbols transmitted as one OFDM symbol, is represented in terms of its M columns of dimension N as

$$\mathbf{S} = \begin{bmatrix} \vdots & \vdots & \vdots \\ \mathbf{s}_1 & \mathbf{s}_m & \mathbf{s}_M \\ \vdots & \vdots & \vdots \end{bmatrix}_{N \times M}, \quad (\text{III.1.1})$$

while $\mathbf{P} = \text{diag}\{p_1, \dots, p_m, \dots, p_M\}$ is an $M \times M$ diagonal matrix containing the power values at which information symbols are transmitted by the CR transmitter. Thus, the N -dimensional OFDM symbol is written in terms of the M -dimensional

block of information symbols $\mathbf{b} = [b_1, \dots, b_m, \dots, b_M]^T$ to be transmitted as one OFDM symbol as

$$\mathbf{x} = \sum_{m=1}^M s_m p_m^{1/2} b_m = \mathbf{S}\mathbf{P}^{1/2}\mathbf{b}. \quad (\text{III.1.2})$$

In order to decode the transmitted information, the received signal distorted by the channel and corrupted by background noise and interference is processed at the receiver in the usual OFDM way through analog-to-digital and serial-to-parallel conversions, removal of the cyclic prefix, and DFT processing, such that the received signal vector after all these operations is

$$\mathbf{y} = \mathbf{A}\mathbf{x} + \mathbf{n} + \mathbf{i} = \mathbf{A}\mathbf{S}\mathbf{P}^{1/2}\mathbf{b} + \mathbf{n} + \mathbf{i}, \quad (\text{III.1.3})$$

where \mathbf{A} is the $N \times N$ diagonal matrix containing the N -point DFT of the channel impulse response, \mathbf{n} is the additive Gaussian noise that corrupts the signal at the receiver with scaled identity covariance matrix $\mathbf{R}_n = E[\mathbf{nn}^T] = \sigma^2\mathbf{I}_N$, and \mathbf{i} is the interference from licensed transmitters with correlation matrix $\mathbf{R}_i = E[\mathbf{ii}^T]$. It is assumed that matrices \mathbf{R}_n and \mathbf{R}_i are identified by the CR systems in a preliminary spectrum sensing operation and are known, and the transmitted signal spectrum will be shaped to avoid the sub-carriers actively used by PUs.

III.1.1 THE LTE-A SIGNAL FRAME

The structure of a generic LTE frame is shown in Fig. 12 [34], from where it is worth noting that the transmitted LTE signal is segmented into frames of 10 msec

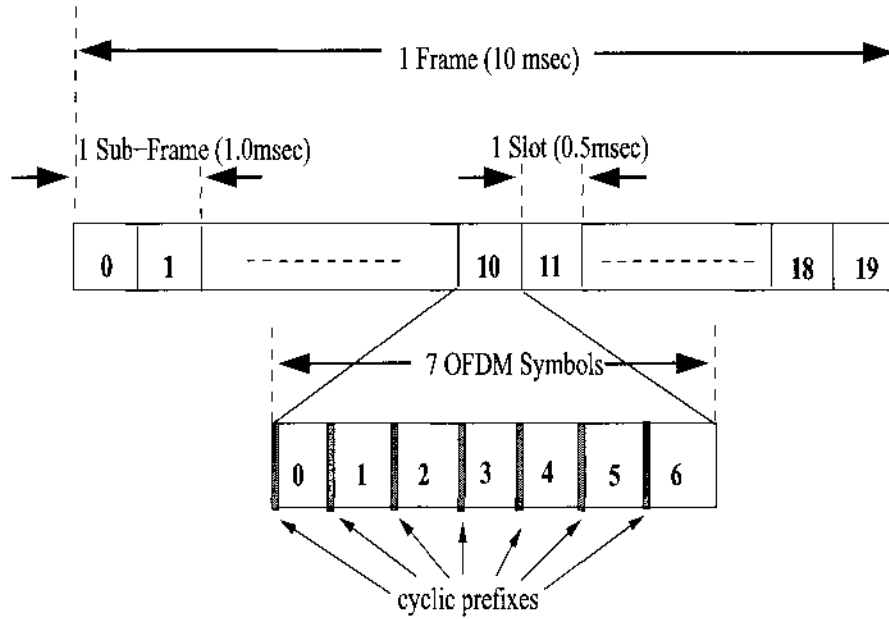


FIG. 12: LTE frame structure.

duration. Each frame consists of 20 slots of 0.5 msec duration. Two adjacent slots constitute a subframe of length 1 ms. Each slot consists of either 6 or 7 OFDM symbols for long and short CP respectively. The uses of long and short CP depends upon the fading environment, such that for longer delay spreads, longer CP is desired and vice-versa.

Multiple modulation schemes such as Quadrature Phase Shift Keying (QPSK), 16 QAM, and 64 QAM can be supported. The available bandwidth for the transmission varies up to 100 MHz with a variable number of sub-carriers while sub-carrier spacing is fixed. To meet the target peak data rate (up to 1 Gbps in downlink and 500 Mbps in uplink) a “carrier aggregation” scheme is utilized in the LTE-A system. “Carrier aggregation” represents the grouping of several LTE “component carriers” (CCs)

having up to 20 MHz bandwidth and enables the LTE-A systems to be backward compatible with LTE while providing flexibility on spectrum utilization. Carrier aggregation may be contiguous or non-contiguous component carriers. In the non-contiguous carrier aggregation, contiguous or non-contiguous spectrum band can be aggregated.

III.2 SPECTRAL SHAPING BY PRECODER ADAPTATION

The idea behind spectral shaping is to enable secondary access to the licensed spectrum for the LTE-A CR systems without interfering with the active PUs. This is accomplished by deactivating the sub-carriers used by the licensed PU at the LTE-A CR transmitter, and it is worth to note that in the precoded OFDM scheme, the frequencies over which a specific information symbol b_m in the frame \mathbf{b} is transmitted, are determined by elements of the m -th column \mathbf{s}_m of the precoder matrix \mathbf{S} . Specifically, a given element n of this column, s_m^n , determines the fraction of total power p_m of symbol m that is transmitted over sub-carrier n . Thus, when $s_m^n = 0$ symbol m does not use for transmission the n -th sub-carrier, and this property can be used to dynamically shape the spectrum of the signal transmitted by the CR in response to the spectrum patterns of the active licensed users. In this context, precoder based spectrum shaping is formally defined as follows:

Definition 1: Spectral Shaping in Precoded OFDM Systems. *The CR system avoids the spectrum actively used by the licensed PU system by deactivating the corresponding OFDM sub-carriers n through zeroing out the corresponding precoder elements $s_m^n = 0$, $m = 1, \dots, M$, $\forall n$ actively used by the PU.*

The sub-carriers actively used by the PU system can be easily identified by looking at the eigenvalues of \mathbf{R}_s , the correlation matrix of the PU signal, which is identified by a spectrum sensing operation.

Based on Definition 1, we formally state the dynamic spectral shaping algorithm 2.

This section concludes by noting that, after the corresponding precoder rows are

Algorithm 2 Dynamic Spectral Shaping

1: **Input data:**

- Precoder matrix \mathbf{S} , power matrix \mathbf{P} , and channel matrix \mathbf{A} .
 - Spectrum sensing information: noise & PU correlation matrices \mathbf{R}_n & \mathbf{R}_s .
- 2: Identify the sub-carriers actively used by PU by finding the non-zero eigenvalues of matrix \mathbf{R}_s .
 - 3: Notch out the sub-carriers identified in Step 2 by putting zeros in the corresponding rows of the precoder matrix \mathbf{S} .
-

zeroed out to notch the sub-carriers actively used by licensed PUs, the precoder may be further adapted to ensure that specified signal-to-noise-plus-interference ratios (SINRs) are met at the receiver [77], to reduce the peak-to-average power ratio (PAPR), or perform beam forming in the case of multiple antenna systems [87, 88]. The details of the precoder adaptation for power control and to satisfy the specified SINR are described in Chapter IV.

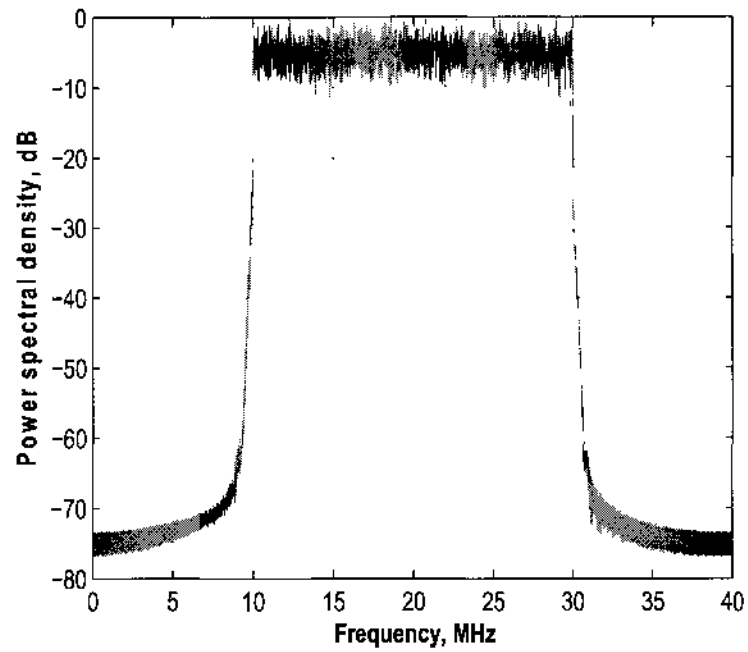
III.3 SIMULATION RESULTS

In this section, simulation results are presented which are obtained from application of the proposed algorithm for specific LTE-A system parameters summarized in Table 1. The first experiment illustrates the spectral shaping by looking at the power

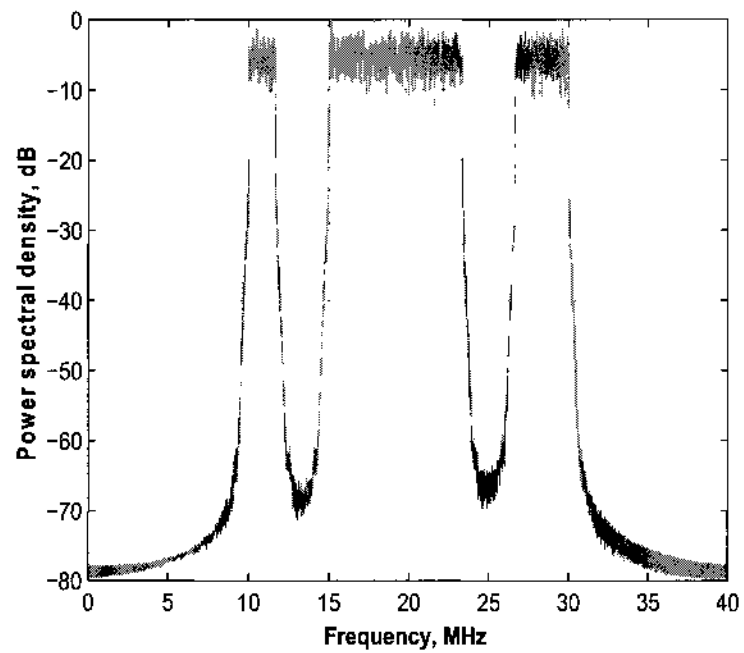
TABLE 1: System simulation parameters

Parameter		Value
Occupied bandwidth per component carrier		18.015 MHz
Number of sub-carriers per component carrier		1201
Sub-carrier spacing		15 KHz
Subframe length		1 msec (14 OFDM symbols)
Symbol duration	Useful data	66.67 μ sec
	Cyclic prefix	4.7 μ sec
Data modulation scheme		16 QAM

spectral density (PSD) of the transmitted signal when all sub-carriers are available for transmission, and when a subset of sub-carriers are deactivated in the transmitted signal. It is assumed that the frame of information symbols has length $M = 70$ such that the precoder matrix is of dimension 1201×70 , and results of this experiment are shown in Fig. 13. By taking the columns of the precoder matrix to be equal to the first M columns of the identity matrix of order N , the spectrum of the resulting precoded LTE-A signal is shown in Fig. 13(a). Next, assuming that two LTE PU are active using 3 MHz bandwidth of a component carrier from 11.75 to 14.75 MHz and 23.25 to 26.25 MHz respectively, deactivating the corresponding sub-carriers in the signal transmitted by the LTE-A CR system by zeroing out rows $200 \div 400$ and $700 \div 900$ of the precoder matrix, which results in the PSD plot in Fig. 13(b). The second experiment illustrates the application of the proposed algorithm in a dynamic scenario where the number of active PUs in the system as well as their bandwidths change. It is assumed that there are four LTE PUs along with one LTE-A CR system with component aggregation capability which takes advantage of the spectrum that



(a) All sub-carriers used for transmission.



(b) Specific sub-carriers are notched out.

FIG. 13: PSD of an LTE-A system with and without spectral shaping.

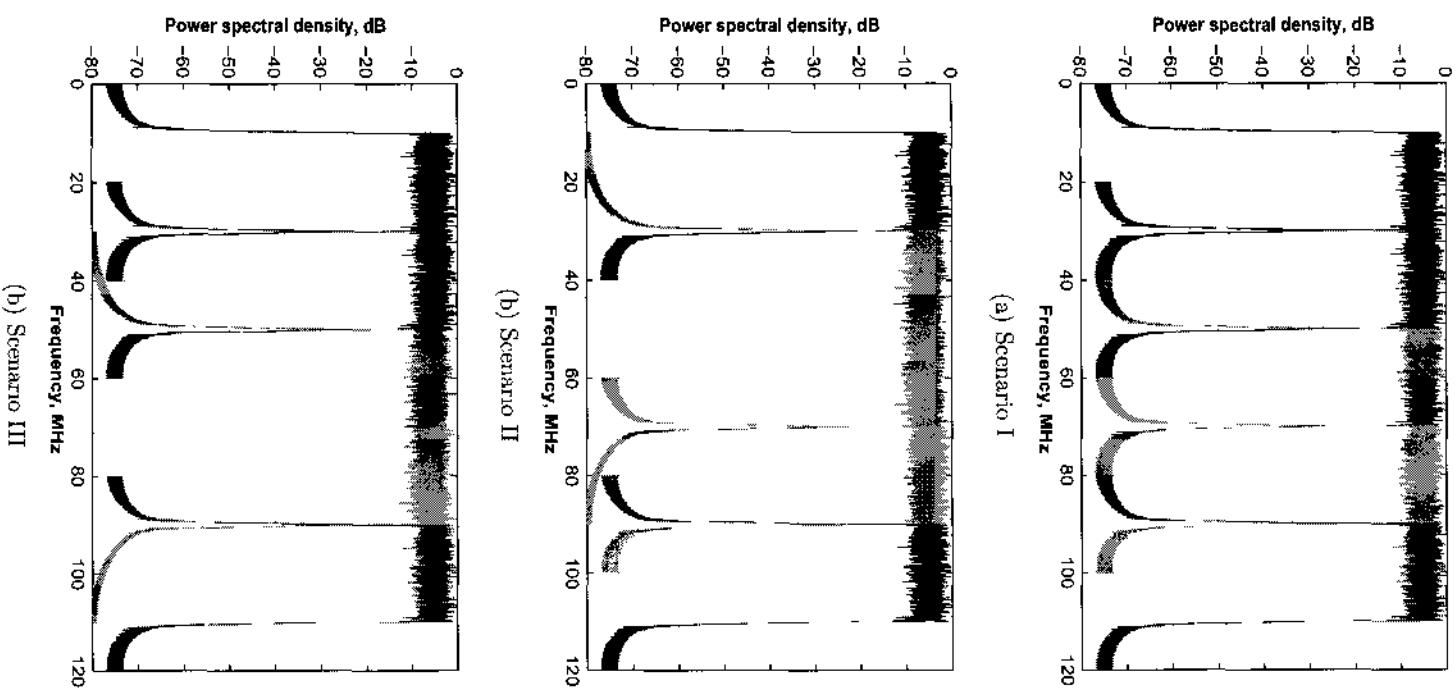


FIG. 14: Application of spectral shaping in a dynamic scenario

is not actively used by the PU. In Scenario I, shown in Fig. 14(a), each of the PU and the CR system are using single 20 MHz component carrier with non overlapping frequency bands for information transmission. At some time instant, one of the PU stops transmitting and the LTE-A CR is able to take advantage of the spectrum vacated by it by aggregating two component carriers as shown in Fig. 14(b) corresponding to Scenario II. The LTE-A CR system can utilize 40 MHz bandwidth by aggregating the two currently vacant component carriers. At a later time instant the spectrum usage of the PU changes again (Scenario III): a PU which stopped transmitting earlier becomes active again while one of the active PU stops transmitting. In this case, the LTE-A CR system must vacate the spectrum required by the first PU while taking advantage of the spectrum released by the second PU as shown in Fig. 14(c). It is worth noting that, by assuming that the LTE-A CR system has the ability to aggregate carrier components, it can use up to 100 MHz of bandwidth for its transmission depending on its availability.

III.4 CHAPTER SUMMARY

This chapter considered a LTE-A CR systems using precoded OFDM and presented an algorithm for dynamic spectral shaping algorithm. The proposed algorithm deactivates sub-carriers that are actively used by PU by zeroing out the corresponding rows of the OFDM precoder. The proposed algorithm is illustrated with simulation results in which the concept of contiguous “carrier aggregation” is also shown.

Chapter IV

JOINT SPECTRAL SHAPING AND POWER CONTROL FOR CR SYSTEMS WITH OPERATING CONSTRAINTS

Dynamic resource allocation for CR systems becomes crucial, when the transmit power, data-rate, and frequency of the CR are dynamically changed based upon the sensing information available at the CR transmitter. In such a scenario, it is desirable for the SU to dynamically adapt its transmission to conform the new spectral requirements imposed by the PU rather than dropping out of the system to update it. The CR has been attracting the extensive attention of wireless communication communities for its optimum resource allocation [89–93] using transmitter adaptation techniques. Though resource allocation represents the broad meaning in the CR context, most of the work focused into the spectrum uses maximization, total transmitted power minimization, and transmission rate maximization. Dynamic power control is an important function of CR systems because it plays a crucial role in minimizing the interference with the PU and other CRs while it is also necessary to transmit with a certain amount of power to meet the target SINR [94–96]. This chapter presents algorithms for joint adaptation of the precoder \mathbf{S} and power \mathbf{P} matrices subject to the total transmitted power and specified target SINR γ^* constraints.

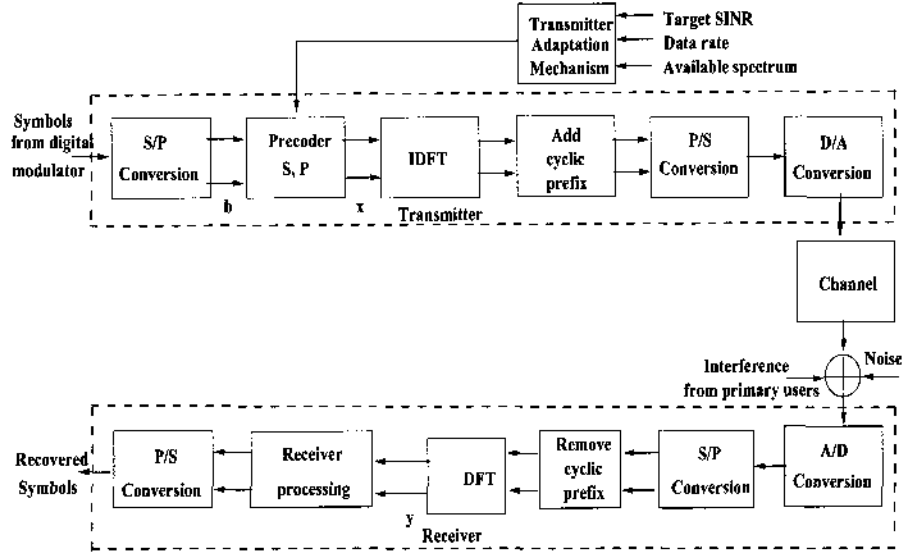
The SINR is broadly defined as the ratio of the desired signal power to the noise plus interference power and has been used as a standard measure of received signal quality in communication system. SINR is used as a measure of received signal quality in a physical layer of a communication system equivalent to Bit Error Rate

(BER) in higher layers. SINR depends on the active receiver structure and two different types of receiver structures, i.e., MF and MMSE are studied in this chapter.

The rest of this chapter is organized as follows: Section IV.1 presents the precoded OFDM-based system with a formal definition of the problem presented in this chapter. Section IV.2 presents the system model with a formal problem statement for MF-based CR systems. This section also provides the MF-based dynamic transmitter adaptation, with precoder and power adaptation procedure, followed by a formal statement of the MF-based transmitter adaptation algorithm. Similarly, Section IV.3 presents the system model with a formal statement of the problem for MMSE-based CR systems. The MMSE-based dynamic transmitter adaptation, with precoder and power adaptation procedure, and formal statement of the MMSE-based transmitter adaptation algorithm are also provided in this section. Section IV.4 presents the simulation results that illustrate the proposed algorithms. Final discussions are given in Section IV.5.

IV.1 OFDM WITH LINEAR PRECODERS

The block diagram of the CR system is sketched in Fig. 15, which employs a linearly precoded OFDM system similar to the one considered in [87, 88] where a precoding matrix is used to map frames of incoming symbols from the digital modulator into coded information data symbols. However, unlike [87, 88] the precoding matrix is no longer fixed and restricted to an orthogonal matrix, but may be adjusted to obtain desired spectral characteristics for the signal transmitted by the CR, as well as to meet specific target SINR at the CR receiver.



(a) General block diagram



(b) MF-based receiver processing.

(c) MMSE-based receiver processing.

FIG. 15: Block diagram of the precoded OFDM-based CR system.

The N -dimensional coded information data block symbol is expressed as

$$\mathbf{x} = \sum_{m=1}^M b_m \mathbf{s}_m \sqrt{p_m} = \mathbf{S} \mathbf{P}^{1/2} \mathbf{b}, \quad (\text{IV.1.1})$$

where \mathbf{S} is the $N \times M$ transmit precoder matrix with M unit norm columns each of dimension N which is represented as,

$$\mathbf{S} = \begin{bmatrix} \vdots & \vdots & \vdots \\ \mathbf{s}_1 & \mathbf{s}_m & \mathbf{s}_M \\ \vdots & \vdots & \vdots \end{bmatrix}_{N \times M}, \quad (\text{IV.1.2})$$

$\mathbf{P} = \text{diag}\{p_1, \dots, p_m, \dots, p_M\}$ is an $M \times M$ diagonal matrix containing the power values at which information symbols are transmitted by the CR transmitter, and $\mathbf{b} = [b_1, \dots, b_M]^T$ is the M -dimensional vector representing the block of uncorrelated information symbols (that is $E[\mathbf{b}\mathbf{b}^H] = \mathbf{I}_M$) to be transmitted as one OFDM block symbol. We note that the batteries are used for the hand held and mobile terminal, so the transmitted power for the CR is limited such that

$$\text{Trace}[\mathbf{P}] \leq P_{T,\max}, \quad (\text{IV.1.3})$$

where $P_{T,\max}$ is the maximum transmit power of the CR. After the analog-to-digital and serial-to-parallel conversions, removal of the cyclic prefix, and FFT processing, the received signal is given by

$$\mathbf{y} = \mathbf{A}\mathbf{x} + \mathbf{v} + \mathbf{i} = \mathbf{A}\mathbf{S}\mathbf{P}^{1/2}\mathbf{b} + \mathbf{v} + \mathbf{i}, \quad (\text{IV.1.4})$$

where \mathbf{A} is the $N \times N$ diagonal matrix containing the N -point DFT of the channel impulse response, \mathbf{v} is the additive Gaussian noise that corrupts the signal at the receiver with covariance matrix $\mathbf{R}_v = E[\mathbf{v}\mathbf{v}^T] = \sigma_v^2\mathbf{I}_N$ (σ_v^2 is a noise variance and \mathbf{I}_N is a N -dimensional identity matrix), and \mathbf{i} is the interference from licensed transmitters with correlation matrix $\mathbf{R}_i = E[\mathbf{i}\mathbf{i}^T]$. It is assumed that matrices \mathbf{R}_v and \mathbf{R}_i are identified by the CR system in a preliminary spectrum sensing operation and are known. Based on the sensing information the CR notches out the currently used sub-carriers of the PU.

There is a general receiver processing block in Fig. 15 which might be matched filter based or MMSE based processing. For MF and MMSE receiver processing the corresponding symbols are represented by using superscript *MF* and *ME* respectively in the following sections. It is also noted that the transmitter gets the

feedback from the receiver about the data rate, SINR requirement, and available spectrum through the feedback channel [97].

IV.2 ADAPTIVE CR SYSTEMS WITH MF RECEIVERS

For MF-based receiver processing (see Fig. 15 (a) and (b)), the received signal is first equalized by multiplying it with the inverse channel matrix to obtain

$$\tilde{\mathbf{y}} = \mathbf{\Lambda}^{-1}\mathbf{y} = \mathbf{S}^{(\text{MF})}(\mathbf{P}^{(\text{MF})})^{1/2}\mathbf{b} + \mathbf{w}, \quad (\text{IV.2.1})$$

where $\mathbf{w} = \mathbf{\Lambda}^{-1}(\mathbf{v} + \mathbf{i})$ is the interference+noise vector. The signal $\tilde{\mathbf{y}}$ is then processed by a bank of matched filters (MF) which yields a decision variable

$$\begin{aligned} \hat{b}_m &= (\mathbf{s}_m^{(\text{MF})})^H \tilde{\mathbf{y}} \\ &= \underbrace{(\mathcal{P}_m^{(\text{MF})})^{1/2} b_m}_{\text{desired signal}} + \overbrace{(\mathbf{s}_m^{(\text{MF})})^H \left(\sum_{k=1, k \neq m}^M \mathbf{s}_k^{(\text{MF})} (\mathcal{P}_k^{(\text{MF})})^{1/2} b_k + \mathbf{w} \right)}^{\text{noise+interference}}, \end{aligned} \quad (\text{IV.2.2})$$

where $(\cdot)^H$ denotes the Hermitian operator (transpose and complex conjugate) such that for a given symbol m the SINR expression at the output of its corresponding MF is

$$\begin{aligned} \gamma_m^{(\text{MF})} &= \frac{p_m^{(\text{MF})}}{l_m^{(\text{MF})}} \\ &= \frac{p_m^{(\text{MF})}}{\underbrace{(\mathbf{s}_m^{(\text{MF})})^H \left(\sum_{k=1, k \neq m}^M \mathbf{s}_k^{(\text{MF})} p_k^{(\text{MF})} (\mathbf{s}_k^{(\text{MF})})^H + \mathbf{W} \right) \mathbf{s}_m^{(\text{MF})}}_{\mathbf{R}_m^{(\text{MF})}}}_{l_m^{(\text{MF})}} \\ &= \frac{p_m^{(\text{MF})}}{(\mathbf{s}_m^{(\text{MF})})^H \mathbf{R}_m^{(\text{MF})} \mathbf{s}_m^{(\text{MF})}}, \end{aligned} \quad (\text{IV.2.3})$$

where $p_m^{(\text{MF})}$ represents its corresponding power in $\mathbf{P}^{(\text{MF})}$,

$$l_m^{(\text{MF})} = (\mathbf{s}_m^{(\text{MF})})^H \mathbf{R}_m^{(\text{MF})} \mathbf{s}_m^{(\text{MF})}, \quad (\text{IV.2.4})$$

is the effective interference corrupting the m -th decision variable \hat{b}_m in $\hat{\mathbf{b}}$ expressed in terms of the interference+noise correlation matrix $\mathbf{R}_m^{(\text{MF})}$ corrupting \hat{b}_m and the m -th column $\mathbf{s}_m^{(\text{MF})}$ of the precoder matrix $\mathbf{S}^{(\text{MF})}$, and $\mathbf{W} = E[\mathbf{w}\mathbf{w}^H]$ is the correlation matrix of interference+noise after channel equalization. We note that the matrix \mathbf{W} is related to the original interference and noise correlation matrices by

$$\mathbf{W} = \mathbf{\Lambda}^{-1}(\mathbf{R}_i + \mathbf{R}_v)\mathbf{\Lambda}^{-H}. \quad (\text{IV.2.5})$$

Matrix $\mathbf{R}_m^{(\text{MF})}$ is obtained by subtracting the contribution corresponding to symbol m from the correlation matrix of the equalized signal $\mathbf{R}_{\tilde{\mathbf{y}}}^{(\text{MF})}$ and is expressed as

$$\mathbf{R}_m^{(\text{MF})} = \mathbf{R}_{\tilde{\mathbf{y}}}^{(\text{MF})} - p_m^{(\text{MF})}\mathbf{s}_m^{(\text{MF})}(\mathbf{s}_m^{(\text{MF})})^H, \quad (\text{IV.2.6})$$

where $\mathbf{R}_{\tilde{\mathbf{y}}}^{(\text{MF})}$ is

$$\mathbf{R}_{\tilde{\mathbf{y}}}^{(\text{MF})} = E[\tilde{\mathbf{y}}\tilde{\mathbf{y}}^H] = \mathbf{S}^{(\text{MF})}\mathbf{P}^{(\text{MF})}(\mathbf{S}^{(\text{MF})})^H + \mathbf{W}. \quad (\text{IV.2.7})$$

It is worth noting that the target SINR is implied by the QoS requirements of the application that must be supported by the CR system and should satisfy the following admissibility condition [98]

$$\frac{\gamma^*}{1 + \gamma^*} < \frac{N}{M}. \quad (\text{IV.2.8})$$

Once the SU nulled out the spectrum used by the PU, the SU can access the remaining RF spectrum with joint adaptation of the precoder and power matrices to satisfy the QoS constraints specified in terms of SINR with minimum possible total transmitted power. For joint adaptation of precoder $\mathbf{S}^{(\text{MF})}$ and power $\mathbf{P}^{(\text{MF})}$ matrices the cost function is defined as:

$$u^{(\text{MF})} = \sum_{m=1}^M p_m^{(\text{MF})} i_m^{(\text{MF})} = \sum_{m=1}^M p_m^{(\text{MF})} (\mathbf{s}_m^{(\text{MF})})^H \mathbf{R}_m^{(\text{MF})} \mathbf{s}_m^{(\text{MF})}. \quad (\text{IV.2.9})$$

For given target SINR γ^* with minimum possible total transmitted power, the optimization problem is formally written as

$$\begin{aligned} \min_{\substack{\mathbf{s}_m^{(\text{MF})} \in \mathcal{S}_m \\ p_m^{(\text{MF})} \in \mathcal{P}_m}} u^{(\text{MF})} &= \min_{\substack{\mathbf{s}_m^{(\text{MF})} \in \mathcal{S}_m \\ p_m^{(\text{MF})} \in \mathcal{P}_m}} \left(\sum_{m=1}^M p_m^{(\text{MF})} (\mathbf{s}_m^{(\text{MF})})^H \mathbf{R}_m^{(\text{MF})} \mathbf{s}_m^{(\text{MF})} \right) \\ \text{subject to} & \\ g_1^{(\text{MF})} : (\mathbf{s}_m^{(\text{MF})})^H \mathbf{s}_m^{(\text{MF})} - 1 &= 0 \quad \forall m = 1, \dots, M \\ g_2^{(\text{MF})} : p_m^{(\text{MF})} - \gamma^* (\mathbf{s}_m^{(\text{MF})})^H \mathbf{R}_m^{(\text{MF})} \mathbf{s}_m^{(\text{MF})} &= 0 \quad \forall m = 1, \dots, M \\ h_1^{(\text{MF})} : \sum_{m=1}^M p_m^{(\text{MF})} - P_{Tmax} &\leq 0 \end{aligned} \quad (\text{IV.2.10})$$

with $\mathcal{S}_m = \{\mathbf{s}_m^{(\text{MF})} | \mathbf{s}_m^{(\text{MF})} \in \mathbb{R}^N, \|\mathbf{s}_m^{(\text{MF})}\| = 1\}$ and $\mathcal{P}_m = \{p_m^{(\text{MF})} | p_m^{(\text{MF})} \in (0, P_{Tmax}]\}$, where \mathcal{S}_m is the N -dimensional sphere with radius 1.

The cost function $u^{(\text{MF})}$ is optimized using the classical Lagrangian method for which the Lagrangian function is

$$\begin{aligned} \mathcal{L}^{(\text{MF})} &= \sum_{m=1}^M p_m^{(\text{MF})} (\mathbf{s}_m^{(\text{MF})})^H \mathbf{R}_m^{(\text{MF})} \mathbf{s}_m^{(\text{MF})} + \sum_{m=1}^M \alpha_m^{(\text{MF})} ((\mathbf{s}_m^{(\text{MF})})^H \mathbf{s}_m^{(\text{MF})} - 1) \\ &+ \sum_{m=1}^M \chi_m^{(\text{MF})} (p_m^{(\text{MF})} - \gamma^* (\mathbf{s}_m^{(\text{MF})})^H \mathbf{R}_m^{(\text{MF})} \mathbf{s}_m^{(\text{MF})}) + \eta^{(\text{MF})} \left(\sum_{m=1}^M p_m^{(\text{MF})} - P_{Tmax} \right), \end{aligned} \quad (\text{IV.2.11})$$

where $\alpha_m^{(\text{MF})}$, $\chi_m^{(\text{MF})}$, $m = 1, \dots, M$, and $\eta^{(\text{MF})}$ are the Lagrangian multipliers. The necessary or first order conditions for minimizing the Lagrangian in (IV.2.11) are obtained by partially differentiating (IV.2.11) with respect to $\mathbf{s}_m^{(\text{MF})}$, $p_m^{(\text{MF})}$, $\alpha_m^{(\text{MF})}$, $\chi_m^{(\text{MF})}$, $m = 1, \dots, M$, and $\eta^{(\text{MF})}$ and equating each result equal to zero, that is,

$$\frac{\partial \mathcal{L}^{(\text{MF})}}{\partial \mathbf{s}_m^{(\text{MF})}} = 0 \quad \forall m = 1, \dots, M, \quad (\text{IV.2.12})$$

$$\frac{\partial \mathcal{L}^{(\text{MF})}}{\partial p_m^{(\text{MF})}} = 0 \quad \forall m = 1, \dots, M, \quad (\text{IV.2.13})$$

$$\frac{\partial \mathcal{L}^{(\text{MF})}}{\partial \alpha_m^{(\text{MF})}} = 0 \quad \forall m = 1, \dots, M, \quad (\text{IV.2.14})$$

$$\frac{\partial \mathcal{L}^{(\text{MF})}}{\partial \chi_m^{(\text{MF})}} = 0 \quad \forall m = 1, \dots, M, \quad (\text{IV.2.15})$$

$$\frac{\partial \mathcal{L}^{(\text{MF})}}{\partial \eta^{(\text{MF})}} \geq 0, \quad (\text{IV.2.16})$$

$$\eta^{(\text{MF})} \left(\sum_{m=1}^M p_m^{(\text{MF})} - P_{Tmax} \right) = 0, \quad \eta^{(\text{MF})} \geq 0. \quad (\text{IV.2.17})$$

The (IV.2.17) represents the complementary slackness conditions for $h_1^{(\text{MF})}$ inequality constraint. The optimum values of $\mathbf{s}_m^{(\text{MF})}$ and $p_m^{(\text{MF})}$ must satisfy the necessary conditions (IV.2.12)–(IV.2.17) simultaneously and (IV.2.12) leads to the eigenvalue/eigenvector equation,

$$\frac{\partial \mathcal{L}^{(\text{MF})}}{\partial \mathbf{s}_m^{(\text{MF})}} = 0 \Rightarrow \mathbf{R}_m^{(\text{MF})} \mathbf{s}_m^{(\text{MF})} = \lambda_m^{(\text{MF})} \mathbf{s}_m^{(\text{MF})} \quad \forall m = 1, \dots, M \quad (\text{IV.2.18})$$

where $\lambda_m^{(\text{MF})}$ is the eigenvalue of the $\mathbf{R}_m^{(\text{MF})}$ and can be represented in terms of Lagrangian multipliers $\alpha_m^{(\text{MF})}$, $\chi_m^{(\text{MF})}$, and $p_m^{(\text{MF})}$. Similarly, (IV.2.15) implies that,

$$\frac{\partial \mathcal{L}^{(\text{MF})}}{\partial \chi_m^{(\text{MF})}} = 0 \Rightarrow p_m^{(\text{MF})} = \gamma^* \lambda_m^{(\text{MF})}. \quad (\text{IV.2.19})$$

The two equations (IV.2.18) and (IV.2.19) implied by the necessary conditions of the optimization problem (IV.2.10) indicate that, at the optimal point, the following necessary conditions are satisfied for symbol m precoder and power matrices:

- Any column of a precoder matrix, $\mathbf{s}_m^{(\text{MF})}$, is an eigenvector of corresponding $\mathbf{R}_m^{(\text{MF})}$ matrix.
- For the given $\mathbf{s}_m^{(\text{MF})}$ the power value, $p_m^{(\text{MF})}$, corresponding to symbol m matches the specified target SINR γ^* .

In order to meet the specified value for the target SINR of symbol m with minimum transmit power, the corresponding precoder column must be chosen to be

the eigenvector corresponding to the minimum eigenvalue, $(\lambda_m^{(\text{MF})})^*$, of matrix $\mathbf{R}_m^{(\text{MF})}$. This is also referred to as the minimum eigenvector of $\mathbf{R}_m^{(\text{MF})}$. After the update, the Karush-Kuhn-Tucker (KKT) necessary condition (IV.2.18) gives the optimal value of the optimization problem of (IV.2.11). From (IV.2.3) when $\mathbf{s}_m^{(\text{MF})}$ is replaced by the minimum eigenvector of $\mathbf{R}_m^{(\text{MF})}$, the interference to the symbol m is minimum [99]. From (IV.2.3) and (IV.2.18), it is noted that at the critical point the minimum power,

$$(p_m^{(\text{MF})})^* = \gamma^* (\lambda_m^{(\text{MF})})^* \quad \forall m = 1, \dots, M \quad (\text{IV.2.20})$$

is achieved because $(\lambda_m^{(\text{MF})})^*$ is the minimum value obtained from (IV.2.18).

Using equations (IV.2.6) and (IV.2.18) along with the SINR expression in terms of $\mathbf{R}_y^{(\text{MF})}$ in equation (IV.2.3), the minimum eigenvector of $\mathbf{R}_m^{(\text{MF})}$ matrix is also an eigenvector of the $(\mathbf{R}_y^{(\text{MF})})$ matrix satisfying

$$\mathbf{R}_y^{(\text{MF})} \mathbf{r}_m^{(\text{MF})} = (p_m^{(\text{MF})})^* \left(1 + \frac{1}{\gamma^*} \right) \mathbf{r}_m^{(\text{MF})} \quad \forall m = 1, \dots, M \quad (\text{IV.2.21})$$

The power value $(p_m^{(\text{MF})})^*$ is the minimum power to match the specified target SINR γ^* which also implies that $\mathbf{r}_m^{(\text{MF})}$ corresponds actually to the minimum eigenvalue $(\vartheta_m^{(\text{MF})})^*$ of matrix $\mathbf{R}_y^{(\text{MF})}$. As a consequence, an ensemble where all the columns of a given symbol precoder $\mathbf{s}_m^{(\text{MF})}$ are minimum eigenvectors of their corresponding matrices $\mathbf{R}_m^{(\text{MF})}$ (with $(\vartheta_m^{(\text{MF})})^*$ being the minimum eigenvalue of matrix $\mathbf{R}_y^{(\text{MF})}$) satisfies the necessary conditions (IV.2.18) and (IV.2.19) and is a stationary point of the constrained optimization problem (IV.2.10). At the critical point, the value of the cost function is

$$(u^{(\text{MF})})^* = \sum_{m=1}^M (\lambda_m^{(\text{MF})})^*. \quad (\text{IV.2.22})$$

The second order, or the sufficient KKT condition, is used to investigate whether the minimum eigenvector strategy is also optimal with respect to the constrained minimization of the given cost function. We use the approach in [100, Ch. 5], which involves the calculation of the bordered Hessian matrix. For the Lagrangian expression in (IV.2.11), the bordered Hessian matrix is expressed as

$$\mathbf{H}_B^{(MF)} = \left[\begin{array}{c|c} \mathbf{0}_{(2M+1) \times (2M+1)} & \mathbf{B}_{(2M+1) \times M(N+1)}^{(MF)} \\ \hline (\mathbf{B}^{(MF)})^H_{M(N+1) \times (2M+1)} & \mathbf{H}_{M(N+1) \times M(N+1)}^{(MF)} \end{array} \right] \quad (\text{IV.2.23})$$

where

$$\mathbf{B}^{(MF)} = \left[\begin{array}{ccc|ccc} 2(\mathbf{s}_1^{(MF)})^{*H} & \dots & 0 & 0 & \dots & 0 \\ \vdots & \ddots & \vdots & \vdots & \ddots & \vdots \\ 0 & \dots & 2(\mathbf{s}_M^{(MF)})^{*H} & 0 & \dots & 0 \\ \hline -2(p_1^{(MF)})^* (\mathbf{s}_1^{(MF)})^{*H} & \dots & 0 & 1 & \dots & 0 \\ \vdots & \ddots & \vdots & \vdots & \ddots & \vdots \\ 0 & \dots & -2(p_M^{(MF)})^* (\mathbf{s}_M^{(MF)})^{*H} & 0 & \dots & 1 \\ \hline & & 0 & \dots & 0 & 1 \dots 1 \end{array} \right], \quad (\text{IV.2.24})$$

$$\mathbf{H}^{(MF)} = \left[\begin{array}{ccc|ccc} -4 \frac{(p_1^{(MF)})^{*2}}{\gamma^*} & \dots & 0 & \frac{(p_1^{(MF)})^*}{\gamma^*} (\mathbf{s}_1^{(MF)})^{*H} & \dots & 0 \\ \vdots & \ddots & \vdots & \vdots & \ddots & \vdots \\ 0 & \dots & -4 \frac{(p_M^{(MF)})^{*2}}{\gamma^*} & 0 & \dots & \frac{(p_1^{(MF)})^*}{\gamma^*} (\mathbf{s}_1^{(MF)})^{*H} \\ \hline \frac{(p_1^{(MF)})^*}{\gamma^*} (\mathbf{s}_1^{(MF)})^* & \dots & 0 & & & 0 \dots 0 \\ \vdots & \ddots & \vdots & & & \vdots \dots \vdots \\ 0 & \dots & \frac{(p_M^{(MF)})^*}{\gamma^*} (\mathbf{s}_M^{(MF)})^* & & & 0 \dots 0 \end{array} \right] \quad (\text{IV.2.25})$$

Thus, following KKT sufficient condition should be satisfied at the optimal point

$$(-1)^{(2M+1)} |\mathbf{H}_{B,l}^{(MF)}| > 0 \quad \forall l = 4M+3, 4M+4, \dots, M(N+3)+1 \quad (\text{IV.2.26})$$

where $|\mathbf{H}_{B,l}^{(MF)}|$ is the l -th principal determinant of the bordered Hessian matrix $\mathbf{H}_B^{(MF)}$. In this context, the MF-based transmitter adaptation algorithm is formally presented in the following section:

IV.2.1 MF-BASED CR SYSTEMS ADAPTATION ALGORITHM

The proposed approach for MF-based transmitter adaptation is based on joint adaptation of the precoder $\mathbf{S}^{(MF)}$ and power $\mathbf{P}^{(MF)}$ matrices through a distributed incremental algorithm that adjusts the columns of the precoder matrix to minimize the interference function corresponding to each symbol followed by incremental adaptation of its power to meet the specified target SINR. The optimal equilibrium of the precoder matrix adaptation is formally defined as:

Definition 2: Equilibrium for precoder Matrix Adaptation. *The precoder ensemble $\{(\mathbf{s}_1^{(MF)})^*, \dots, (\mathbf{s}_m^{(MF)})^*, \dots, (\mathbf{s}_M^{(MF)})^*\}$ is an optimal equilibrium of precoder adaptation if*

$$\begin{aligned} u^{(MF)}((\mathbf{s}_1^{(MF)})^*, \dots, (\mathbf{s}_m^{(MF)})^*, \dots, (\mathbf{s}_M^{(MF)})^*) &\leq \\ u^{(MF)}(\mathbf{s}_1^{(MF)}, \dots, \mathbf{s}_m^{(MF)}, \dots, \mathbf{s}_M^{(MF)}) \quad \forall (\mathbf{s}_m^{(MF)})^* &\in \mathcal{S}_m. \end{aligned} \quad (\text{IV.2.27})$$

Definition 3: Equilibrium of Power Adaptation. *The optimum power $(p_m^{(MF)})^*$ is the minimum possible power that can be used to transmit the symbol m to satisfy the target SINR. The sum of the transmitted power at the equilibrium point is always less or equal to the sum of power at other points, that is,*

$$\sum_{m=1}^M (p_m^{(MF)})^* \leq \sum_{m=1}^M p_m^{(MF)} \leq P_{Tmax}. \quad (\text{IV.2.28})$$

It is worth noting that the updates implied by (IV.2.18) and (IV.2.19) may result in

abrupt changes of $\mathbf{s}_m^{(\text{MF})}$ and/or $p_m^{(\text{MF})}$ which are not desirable in practical implementations. The proposed algorithm uses incremental updates. The idea of the incremental update method is to design a step size sequence to update in the incremental direction towards the optimal value. The algorithm uses the following incremental updates:

- At step j of the algorithm, one column m of the precoder matrix is updated to

$$\mathbf{s}_m^{(\text{MF})}(j+1) = \frac{\mathbf{s}_m^{(\text{MF})}(j) + z(j)\beta\mathbf{r}_m^{(\text{MF})}(j)}{\|\mathbf{s}_m^{(\text{MF})}(j) + z(j)\beta\mathbf{r}_m^{(\text{MF})}(j)\|}, \quad (\text{IV.2.29})$$

where $\mathbf{r}_m^{(\text{MF})}(j)$ is the minimum eigenvector of interference+noise correlation matrix $\mathbf{R}_m^{(\text{MF})}(j)$, β is a parameter that limits the how far (in terms of Euclidean distance) the updated vector is from the previous, and

$$z(j) = \text{sgn}[(\mathbf{s}_m^{(\text{MF})})^H(j)\mathbf{r}_m^{(\text{MF})}(j)]. \quad (\text{IV.2.30})$$

- Power for symbol m at the step of j of the algorithm is updated to

$$p_m^{(\text{MF})}(j+1) = p_m^{(\text{MF})}(j) - \mu[p_m^{(\text{MF})}(j) - \gamma^*i_m^{(\text{MF})}(j)] \quad (\text{IV.2.31})$$

where $0 < \mu < 1$.

Using the incremental updates (IV.2.29)–(IV.2.31), the proposed algorithm for dynamic spectral shaping with joint precoder and power adaptation for precoded OFDM based CR is formally stated in Algorithm 3. This algorithm sequentially adapts the corresponding precoder matrix column and power for each symbol to be transmitted until a fixed point is reached. Numerically, a fixed point of the algorithm is reached when the updates result in changes of the cost function that are smaller than the specified tolerance ϵ . The KKT sufficient condition (IV.2.26) confirms the optimal

Algorithm 3 :MF-based Joint Spectral Shaping and Power Control (JSSPC) Algorithm

```

1: Input data:
    • precoder matrix  $\mathbf{S}^{(\text{MF})}$ , power matrix  $\mathbf{P}^{(\text{MF})}$ , channel matrix  $\mathbf{A}$ , and target SINR  $\gamma^*$ .
    • Spectrum sensing information: noise and PU correlation matrices  $\mathbf{R}_n$  and  $\mathbf{R}_j$ .
    • Algorithm constants  $\beta$ ,  $\mu$ , and tolerance  $\epsilon$ .

2: if there is idle licensed spectrum then
3:   GO TO Step 7.
4: else
5:   wait until spectrum becomes available.
6: end if
7: Notch out unavailable sub-carriers as described in chapter III.
8: if admissibility condition in (IV.2.8) is satisfied then
9:   GO TO Step 13.
10: else
11:   STOP, the desired target SINR is not admissible.
12: end if
13: for each symbol  $m = 1, 2, \dots, M$  do
14:   Compute corresponding  $\mathbf{R}_m^{(\text{MF})}(j)$  using equation (IV.2.6) and determine its minimum eigenvector  $\mathbf{r}_m^{(\text{MF})}(j)$  corresponding to the minimum eigenvalue  $\lambda_m^{(\text{MF})}(j)$ ,
15:   Update  $\mathbf{s}_m^{(\text{MF})}(j)$  using equation (IV.2.29).
16:   Update  $p_m^{(\text{MF})}(j)$  using equation (IV.2.31).
17: end for
18: if change in cost function is larger than  $\epsilon$  then
19:   GO TO Step 13.
20: else
21:   STOP, a fixed point has been reached.
22: end if
23: if optimality condition equation (IV.2.26) is true then
24:   STOP, an optimal equilibrium has been reached.
25: else
26:   GO TO Step 13.
27: end if

```

point and it also guarantees the convergence of the algorithm to the fixed point. The check of the optimality condition (IV.2.26) in Step 23 also ensures that the fixed point is reached and that the algorithm does not stop in a sub-optimal fixed point. The proposed algorithm was used in a distributed way where individual CRs updated precoder and power matrices using feedback from a CR receiver [101, 102].

For the fixed point, a precoder matrix ensemble is not unique and unitary transformation of a fixed point precoder matrix ensemble which preserves norms and cross-correlation will imply a new precoder matrix ensemble which is also a fixed point. The fixed point is also optimal if the determinant sufficient conditions (IV.2.26) are also satisfied. At an optimal point, all symbol precoders are minimum eigenvectors of their corresponding interference+noise correlation matrices $\mathbf{R}_m^{(\text{MF})}$, that is,

$$\mathbf{R}_m^{(\text{MF})}(\mathbf{s}_m^{(\text{MF})})^* = \lambda_m^*(\mathbf{s}_m^{(\text{MF})})^*. \quad (\text{IV.2.32})$$

At the fixed point, the eigenvalue can be written in terms of target SINR γ^* and minimum power $(p_m^{(\text{MF})})^*$ as

$$(\lambda_m^{(\text{MF})})^* = (p_m^{(\text{MF})})^* / \gamma^*. \quad (\text{IV.2.33})$$

Hence, at the optimal point the target SINR are achieved with minimum transmitted power.

IV.3 ADAPTIVE CR SYSTEMS WITH MMSE RECEIVERS

An MF receiver is an ideal receiver when the characteristics of the transmitted signal are known a priori at the receiver to detect the signal. But, for the CR, the nature of the received signal is not available a priori. A linear MMSE receiver does

not require the feature of the received signal a priori to detect the received signal. So, MMSE is the optimal linear receiver [103] for maximizing the SINR of the received signal for CR.

This section considers a precoded OFDM-based CR system with an MMSE-based decoder at the receiver side and formulates the constrained optimization problem for joint frequency allocation and power control subject to a target SINR. The solution of the optimization problem with necessary and sufficient conditions for optimal assignment of OFDM sub-carriers and transmitted power control for the symbol to transmit the subject to the specified target SINR will be derived, and an algorithm will be presented which adjusts the sub-carrier assignment and power distribution until a fixed point is reached where the specified target SINR is achieved with minimum power.

In MMSE receiver processing (see Fig. 15 (a) and (c)), in order to obtain the expression of the SINR of m -th symbol at the output of the receiver filter (IV.1.4) can be written as:

$$\mathbf{y} = \overbrace{\Lambda_m b_m \mathbf{s}_m^{(\text{ME})} \sqrt{p_m^{(\text{ME})}}}^{\text{desired symbol}} + \underbrace{\sum_{\substack{k=1 \\ k \neq m}}^M \Lambda_k b_k \mathbf{s}_k^{(\text{ME})} \sqrt{p_k^{(\text{ME})}}}_{\mathbf{i}_m^{(\text{ME})} \text{ interference+noise}} + \mathbf{w}. \quad (\text{IV.3.1})$$

The first term in (IV.3.1) represents the desired signal corresponding to symbol m while the remaining terms represent the interference and noise, $\mathbf{i}_m^{(\text{ME})}$, corrupting it with correlation matrix

$$\mathbf{R}_m^{(\text{ME})} = E[\mathbf{i}_m^{(\text{ME})} (\mathbf{i}_m^{(\text{ME})})^H] = \mathbf{R}_y^{(\text{ME})} - \Lambda \mathbf{s}_m^{(\text{ME})} p_m^{(\text{ME})} (\mathbf{s}_m^{(\text{ME})})^H \Lambda^H, \quad (\text{IV.3.2})$$

where $\mathbf{R}_y^{(\text{ME})}$ is the received signal correlation matrix in (IV.1.4) and given by,

$$\mathbf{R}_y^{(\text{ME})} = E[\mathbf{y}\mathbf{y}^H] = \mathbf{\Lambda}\mathbf{S}^{(\text{ME})}\mathbf{P}^{(\text{ME})}(\mathbf{S}^{(\text{ME})})^H\mathbf{\Lambda}^H + \mathbf{R}_w. \quad (\text{IV.3.3})$$

At the receiver, a bank of MMSE filters \mathbf{C} is used to obtain the vector of decision variables [98]

$$\mathbf{d} = \mathbf{C}^H\mathbf{y} = \mathbf{C}^H\mathbf{\Lambda}\mathbf{S}^{(\text{ME})}(\mathbf{P}^{(\text{ME})})^{1/2}\mathbf{b} + \mathbf{C}^H\mathbf{w}. \quad (\text{IV.3.4})$$

where

$$\mathbf{C} = (\mathbf{R}_y^{(\text{ME})})^{-1}\mathbf{\Lambda}\mathbf{S}^{(\text{ME})}(\mathbf{P}^{(\text{ME})})^{1/2}. \quad (\text{IV.3.5})$$

The individual decision variable for symbol m is denoted by d_m and is given by

$$d_m = \mathbf{c}_m^H\mathbf{y} = \mathbf{c}_m^H\mathbf{\Lambda}\mathbf{S}^{(\text{ME})}(\mathbf{P}^{(\text{ME})})^{1/2}\mathbf{b} + \mathbf{c}_m^H\mathbf{w}, \quad (\text{IV.3.6})$$

where \mathbf{c}_m is the m -th column of the MMSE receiver matrix \mathbf{C} expressed as

$$\begin{aligned} \mathbf{c}_m &= (\mathbf{R}_y^{(\text{ME})})^{-1}\mathbf{\Lambda}\mathbf{s}_m^{(\text{ME})}\sqrt{p_m^{(\text{ME})}} \\ &= (\mathbf{R}_m^{(\text{ME})})^{-1}\mathbf{\Lambda}\mathbf{s}_m^{(\text{ME})}\frac{\sqrt{p_m^{(\text{ME})}}}{1 + p_m^{(\text{ME})}(\mathbf{s}_m^{(\text{ME})})^H\tilde{\mathbf{R}}_m^{(\text{ME})}\mathbf{s}_m^{(\text{ME})}} \end{aligned} \quad (\text{IV.3.7})$$

where

$$\tilde{\mathbf{R}}_m^{(\text{ME})} = \mathbf{\Lambda}^H(\mathbf{R}_m^{(\text{ME})})^{-1}\mathbf{\Lambda} \quad \forall m = 1, \dots, M. \quad (\text{IV.3.8})$$

Based on these notations, the SINR for symbol m at the output of the linear receiver is

$$\gamma_m^{(\text{ME})} = \frac{p_m^{(\text{ME})}(\mathbf{c}_m^H\mathbf{\Lambda}\mathbf{s}_m^{(\text{ME})})^2}{E[(\mathbf{c}_m^H\mathbf{i}_m^{(\text{ME})})^2]} = \frac{p_m^{(\text{ME})}(\mathbf{c}_m^H\mathbf{\Lambda}\mathbf{s}_m^{(\text{ME})})^2}{\mathbf{c}_m^H\mathbf{R}_m^{(\text{ME})}\mathbf{c}_m}, \quad (\text{IV.3.9})$$

and the corresponding error in m -th decision variable is,

$$e_m = b_m - d_m. \quad (\text{IV.3.10})$$

In order to maximize the probability of a correct decision, the mean square error should be minimized [103]

$$\varepsilon_m = E[e_m^2] = E[(b_m - d_m)^2]. \quad (\text{IV.3.11})$$

From (IV.3.7) and (IV.3.9), $\gamma_m^{(\text{ME})}$ is expressed as,

$$\begin{aligned} \gamma_m^{(\text{ME})} &= \frac{p_m^{(\text{ME})} (\mathbf{s}_m^{(\text{ME})})^H \mathbf{\Lambda}^H (\mathbf{R}_y^{(\text{ME})})^{-1} \mathbf{\Lambda} \mathbf{s}_m^{(\text{ME})}}{1 - p_m^{(\text{ME})} (\mathbf{s}_m^{(\text{ME})})^H \mathbf{\Lambda}^H (\mathbf{R}_y^{(\text{ME})})^{-1} \mathbf{\Lambda} \mathbf{s}_m^{(\text{ME})}} \\ &= p_m^{(\text{ME})} (\mathbf{s}_m^{(\text{ME})})^H \tilde{\mathbf{R}}_m^{(\text{ME})} \mathbf{s}_m^{(\text{ME})}. \end{aligned} \quad (\text{IV.3.12})$$

The decision error and SINR for the MMSE receiver are related by the expression [98, 104]

$$\begin{aligned} \varepsilon_m &= \frac{1}{1 + \gamma_m^{(\text{ME})}} = 1 - p_m^{(\text{ME})} (\mathbf{s}_m^{(\text{ME})})^H \mathbf{\Lambda}^H (\mathbf{R}_y^{(\text{ME})})^{-1} \mathbf{\Lambda} \mathbf{s}_m^{(\text{ME})} \\ &= \frac{1}{1 + p_m^{(\text{ME})} (\mathbf{s}_m^{(\text{ME})})^H \tilde{\mathbf{R}}_m^{(\text{ME})} \mathbf{s}_m^{(\text{ME})}}. \end{aligned} \quad (\text{IV.3.13})$$

In this setup, the joint spectrum shaping and power control as a constrained optimization problem for a precoded OFDM-based CR with the specified constraints on the transmitted power at a CR transmitter and target SINR γ^* at the MMSE receiver that satisfies the admissibility condition (IV.2.8) will be derived. A novel algorithm for joint adaptation of the precoder and power matrices for a precoded OFDM-based CR transmitter will also be formally presented.

After the SU notches out the PU spectrum, the SU can access the remaining RF spectrum with the joint adaptation of precoder and power matrices to satisfy the QoS constraints specified in terms of target SINR with minimum total transmitted power. For joint adaptation of precoder $\mathbf{S}^{(\text{ME})}$ and power $\mathbf{P}^{(\text{ME})}$ matrices, the following cost function is proposed in which the sum of MMSE at the cognitive radio receiver

is minimized,

$$u^{(\text{ME})} = \sum_{m=1}^M \varepsilon_m = \sum_{m=1}^M \frac{1}{1 + p_m^{(\text{ME})} (\mathbf{s}_m^{(\text{ME})})^H \tilde{\mathbf{R}}_m^{(\text{ME})} \mathbf{s}_m^{(\text{ME})}} \quad (\text{IV.3.14})$$

subject to the specific constraints implied by the system model discussed in Section IV.3. Formally, the optimization problem is written as

$$\begin{aligned} \min_{\substack{\mathbf{s}_m^{(\text{ME})} \in \mathcal{S}_m \\ p_m^{(\text{ME})} \in \mathcal{P}_m}} u^{(\text{ME})} &= \min_{\substack{\mathbf{s}_m^{(\text{ME})} \in \mathcal{S} \\ p_m^{(\text{ME})} \in \mathcal{P}}} \left(\sum_{m=1}^M \frac{1}{1 + p_m^{(\text{ME})} (\mathbf{s}_m^{(\text{ME})})^H \tilde{\mathbf{R}}_m^{(\text{ME})} \mathbf{s}_m^{(\text{ME})}} \right) \\ \text{subject to} & \\ g_1^{(\text{ME})} : (\mathbf{s}_m^{(\text{ME})})^H \mathbf{s}_m^{(\text{ME})} - 1 &= 0 \quad \forall m = 1, \dots, M \\ g_2^{(\text{ME})} : p_m^{(\text{ME})} (\mathbf{s}_m^{(\text{ME})})^H \tilde{\mathbf{R}}_m^{(\text{ME})} \mathbf{s}_m^{(\text{ME})} - \gamma^* &= 0 \quad \forall m = 1, \dots, M \\ h_1^{(\text{ME})} : \sum_{m=1}^M p_m^{(\text{ME})} - P_{T,\max} &\leq 0, \end{aligned} \quad (\text{IV.3.15})$$

with $\mathcal{S}_m = \{\mathbf{s}_m^{(\text{ME})} | \mathbf{s}_m^{(\text{ME})} \in \mathbb{R}^N, \|\mathbf{s}_m^{(\text{ME})}\| = 1\}$ being the N -dimensional sphere with radius 1 and $\mathcal{P}_m = \{p_m | p_m \in (0, P_{T,\max}]\}$.

The cost function $u^{(\text{ME})}$ is optimized using the classical Lagrangian multiplier method and the corresponding Lagrangian function is

$$\begin{aligned} \mathcal{L}^{(\text{ME})} &= \sum_{m=1}^M \frac{1}{1 + p_m^{(\text{ME})} (\mathbf{s}_m^{(\text{ME})})^H \tilde{\mathbf{R}}_m^{(\text{ME})} \mathbf{s}_m^{(\text{ME})}} + \sum_{m=1}^M \alpha_m^{(\text{ME})} \left((\mathbf{s}_m^{(\text{ME})})^H \mathbf{s}_m^{(\text{ME})} - 1 \right) \\ &+ \sum_{m=1}^M \chi_m^{(\text{ME})} \left(p_m^{(\text{ME})} (\mathbf{s}_m^{(\text{ME})})^H \tilde{\mathbf{R}}_m^{(\text{ME})} \mathbf{s}_m^{(\text{ME})} - \gamma^* \right) + \eta^{(\text{ME})} \left(\sum_{m=1}^M p_m^{(\text{ME})} - P_{T,\max} \right), \end{aligned} \quad (\text{IV.3.16})$$

where $\alpha_m^{(\text{ME})}$, $\chi_m^{(\text{ME})}$, and $\eta^{(\text{ME})}$ are the Lagrangian multipliers. The necessary or first order conditions for minimizing the Lagrangian in (IV.3.16) are obtained by partially differentiating (IV.3.16) with respect to $\mathbf{s}_m^{(\text{ME})}$, $p_m^{(\text{ME})}$, $\alpha_m^{(\text{ME})}$, $\chi_m^{(\text{ME})}$, $m = 1, \dots, M$, and $\eta^{(\text{ME})}$, and then equating each result to zero, that is,

$$\frac{\partial \mathcal{L}^{(\text{ME})}}{\partial \mathbf{s}_m^{(\text{ME})}} = 0 \quad \forall m = 1, \dots, M, \quad (\text{IV.3.17})$$

$$\frac{\partial \mathcal{L}^{(\text{ME})}}{\partial p_m^{(\text{ME})}} = 0 \quad \forall m = 1, \dots, M, \quad (\text{IV.3.18})$$

$$\frac{\partial \mathcal{L}^{(\text{ME})}}{\partial \alpha_m^{(\text{ME})}} = 0 \quad \forall m = 1, \dots, M, \quad (\text{IV.3.19})$$

$$\frac{\partial \mathcal{L}^{(\text{ME})}}{\partial \chi_m^{(\text{ME})}} = 0 \quad \forall m = 1, \dots, M, \quad (\text{IV.3.20})$$

$$\frac{\partial \mathcal{L}^{(\text{ME})}}{\partial \eta^{(\text{ME})}} \geq 0, \quad (\text{IV.3.21})$$

$$\eta^{(\text{ME})} \left(\sum_{m=1}^M p_m^{(\text{ME})} - P_{T,\max} \right) = 0, \quad \eta^{(\text{ME})} \geq 0. \quad (\text{IV.3.22})$$

Condition (IV.3.22) represents the complementary slackness condition implied by the inequality constraint $h_1^{(\text{ME})}$ that ensures that Lagrangian and the original cost function have the same value at the optimum point.

The optimum values of $\mathbf{s}_m^{(\text{ME})}$ and $p_m^{(\text{ME})}$ must satisfy the necessary conditions (IV.3.17)–(IV.3.22) simultaneously and (IV.3.17) leads to the eigenvalue/eigenvector equation,

$$\frac{\partial \mathcal{L}^{(\text{ME})}}{\partial \mathbf{s}_m^{(\text{ME})}} = 0 \Rightarrow \tilde{\mathbf{R}}_m^{(\text{ME})} \mathbf{s}_m^{(\text{ME})} = \lambda_m^{(\text{ME})} \mathbf{s}_m^{(\text{ME})} \quad \forall m = 1, \dots, M, \quad (\text{IV.3.23})$$

where $\lambda_m^{(\text{ME})}$ is an eigenvalue of the $\tilde{\mathbf{R}}_m^{(\text{ME})}$ which can be written in terms of the Lagrangian multipliers, $\alpha_m^{(\text{ME})}$, $\chi_m^{(\text{ME})}$, and the user power $p_m^{(\text{ME})}$.

Similarly, (IV.3.20) implies that,

$$\frac{\partial \mathcal{L}^{(\text{ME})}}{\partial \chi_m^{(\text{ME})}} = 0 \Rightarrow p_m^{(\text{ME})} = \frac{\gamma^*}{(\mathbf{s}_m^{(\text{ME})})^H \tilde{\mathbf{R}}_m^{(\text{ME})} \mathbf{s}_m^{(\text{ME})}} \quad \forall m = 1, \dots, M, \quad (\text{IV.3.24})$$

The two equations (IV.3.23) and (IV.3.24) implied by the necessary conditions of the optimization problem (IV.3.15) indicate that, at the optimal point the following necessary conditions are satisfied for the symbol m precoder and power matrices:

- Any column of a precoder matrix, $\mathbf{s}_m^{(\text{ME})}$, is an eigenvector of corresponding $\tilde{\mathbf{R}}_m^{(\text{ME})}$ matrix.
- For the given $\mathbf{s}_m^{(\text{ME})}$ the power, $p_m^{(\text{ME})}$, value corresponding to symbol m matches the specified target SINR γ^* .

In order to meet the specified value for the target SINR of symbol m with minimum transmit power, the corresponding precoder column must be chosen to be the eigenvector corresponding to the maximum eigenvalue, $(\lambda_m^{(\text{ME})})^*$, of matrix $\tilde{\mathbf{R}}_m^{(\text{ME})}$. This is also referred to as the maximum eigenvector of $\tilde{\mathbf{R}}_m^{(\text{ME})}$. After the update, the KKT necessary condition (IV.3.23) gives the optimal value of the optimization problem of (IV.3.15). From (IV.3.13) when $\mathbf{s}_m^{(\text{ME})}$ is replaced by the maximum eigenvector of $\tilde{\mathbf{R}}_m^{(\text{ME})}$, the MMSE on decoding symbol m is minimum. From (IV.3.12) and (IV.3.23), it is noted that at the critical point the minimum power,

$$(p_m^{(\text{ME})})^* = \frac{\gamma^*}{(\lambda_m^{(\text{ME})})^*} \quad \forall m = 1, \dots, M \quad (\text{IV.3.25})$$

is achieved because $(\lambda_m^{(\text{ME})})^*$ is the maximum value obtained from (IV.3.23).

It is also noted that using equation (IV.3.2) along with the SINR expression in terms of $(\mathbf{R}_y^{(\text{ME})})^{-1}$ in equation (IV.3.12), the maximum eigenvector of $\tilde{\mathbf{R}}_m^{(\text{ME})}$ matrix is also an eigenvector of the $\mathbf{\Lambda}^H (\mathbf{R}_y^{(\text{ME})})^{-1} \mathbf{\Lambda}$ matrix satisfying

$$\mathbf{\Lambda}^H (\mathbf{R}_y^{(\text{ME})})^{-1} \mathbf{\Lambda} \mathbf{r}_m^{(\text{ME})} = \frac{1}{p_m^{(\text{ME})^*}} \frac{\gamma^*}{1 + \gamma^*} \mathbf{r}_m^{(\text{ME})} \quad \forall m = 1, \dots, M \quad (\text{IV.3.26})$$

The power value $(p_m^{(\text{ME})})^*$ is the minimum power needed to match the specified target SINR γ^* which also implies that $\mathbf{r}_m^{(\text{ME})}$ corresponds actually to the maximum eigenvalue $(\vartheta_m^{(\text{ME})})^*$ of matrix $\mathbf{\Lambda}^H (\mathbf{R}_y^{(\text{ME})})^{-1} \mathbf{\Lambda}$. As a consequence, an ensemble where all

the columns of a given symbol precoder $\mathbf{s}_m^{(\text{ME})}$ are maximum eigenvectors of their corresponding matrices $\tilde{\mathbf{R}}_m^{(\text{ME})}$, with $(\vartheta_m^{(\text{ME})})^*$ being the maximum eigenvalue of matrix $\mathbf{\Lambda}^H (\mathbf{R}_y^{(\text{ME})})^{-1} \mathbf{\Lambda}$, satisfies the necessary conditions (IV.3.23) and (IV.3.24) and is a stationary point of the constrained optimization problem (IV.3.15). At the critical point, the MMSE value for a symbol m is equal to

$$(\varepsilon_m^{(\text{ME})})^* = \frac{1}{1 + \gamma^*} \quad \forall m = 1, \dots, M \quad (\text{IV.3.27})$$

which in turn gives the minimum value of the cost function

$$(u^{(\text{ME})})^* = \frac{M}{1 + \gamma^*}. \quad (\text{IV.3.28})$$

The second order, or the sufficient KKT condition, is used to investigate whether the maximum eigenvector strategy is also optimal with respect to the constrained minimization of the given cost function. We use the approach in [100, Ch. 5], which involves the calculation of the bordered Hessian matrix at the critical point. For the Lagrangian expression in (IV.3.16), the bordered Hessian matrix is expressed as [100, Ch. 5]

$$\mathbf{H}_B^{(\text{ME})} = \left[\begin{array}{c|c} \mathbf{0}_{(2M+1) \times (2M+1)} & \mathbf{B}_{(2M+1) \times M(N+1)}^{(\text{ME})} \\ \hline \mathbf{B}_{M(N+1) \times (2M+1)}^{(\text{ME})H} & \mathbf{H}_{M(N+1) \times M(N+1)}^{(\text{ME})} \end{array} \right] \quad (\text{IV.3.29})$$

where

$$\mathbf{B}^{(\text{ME})} = \left[\begin{array}{ccc|ccc} 2(\mathbf{s}_1^{(\text{ME})})^*H & \dots & 0 & 0 & \dots & 0 \\ \vdots & \ddots & \vdots & \vdots & \ddots & \vdots \\ 0 & \dots & 2(\mathbf{s}_M^{(\text{ME})})^*H & 0 & \dots & 0 \\ \hline 2\gamma^*(\mathbf{s}_1^{(\text{ME})})^*H & \dots & 0 & \frac{\gamma^*}{(p_1^{(\text{ME})})^*} & \dots & 0 \\ \vdots & \ddots & \vdots & \vdots & \ddots & \vdots \\ 0 & \dots & 2\gamma^*(\mathbf{s}_M^{(\text{ME})})^*H & 0 & \dots & \frac{\gamma^*}{(p_M^{(\text{ME})})^*} \\ \hline 0 & \dots & 0 & 1 & \dots & 1 \end{array} \right], \quad (\text{IV.3.30})$$

$$\mathbf{H}^{(ME)} = \left[\begin{array}{ccc|ccc} 2a(\mathbf{s}_1^{(ME)})^*(\mathbf{s}_1^{(ME)})^{*H} & \dots & 0 & \frac{a}{(p_1^{(ME)})^*}(\mathbf{s}_1^{(ME)})^* & \dots & 0 \\ \vdots & \ddots & \vdots & \vdots & \ddots & \vdots \\ 0 & \dots & 2a(\mathbf{s}_M^{(ME)})^*(\mathbf{s}_M^{(ME)})^{*H} & 0 & \dots & \frac{a}{(p_M^{(ME)})^*}(\mathbf{s}_M^{(ME)})^* \\ \hline \frac{a}{(p_1^{(ME)})^*}(\mathbf{s}_1^{(ME)})^{*H} & \dots & 0 & \frac{a}{2(p_1^{(ME)})^*2} & \dots & 0 \\ \vdots & \ddots & \vdots & \vdots & \ddots & \vdots \\ 0 & \dots & \frac{a}{(p_M^{(ME)})^*}(\mathbf{s}_M^{(ME)})^{*H} & 0 & \dots & \frac{a}{2(p_M^{(ME)})^*2} \end{array} \right], \quad (\text{IV.3.31})$$

where $a = \frac{4\gamma^{*2}}{(1+\gamma^*)^3}$. Thus, the following KKT sufficient condition should be satisfied at the optimal point

$$(-1)^{(2M+1)} |\mathbf{H}_{B,l}^{(ME)}| > 0 \quad \forall l = 4M+3, 4M+4, \dots, M(N+3)+1 \quad (\text{IV.3.32})$$

where $|\mathbf{H}_{B,l}^{(ME)}|$ is the l -th principal determinant of the bordered Hessian matrix $\mathbf{H}_B^{(ME)}$.

Based on the above discussion, the optimal point of precoder and power adaptation as formally defined as follows:

Definition 4: Optimal Point of Precoder Adaptation. *The precoder ensemble $\{(\mathbf{s}_1^{(ME)})^*, \dots, (\mathbf{s}_m^{(ME)})^*, \dots, (\mathbf{s}_M^{(ME)})^*\}$ is an optimal equilibrium of the precoder adaptation if*

$$\begin{aligned} u^{(ME)}((\mathbf{s}_1^{(ME)})^*, \dots, (\mathbf{s}_m^{(ME)})^*, \dots, (\mathbf{s}_M^{(ME)})^*) &\leq \\ u^{(ME)}(\mathbf{s}_1^{(ME)}, \dots, \mathbf{s}_m^{(ME)}, \dots, \mathbf{s}_M^{(ME)}) \quad \forall (\mathbf{s}_m^{(ME)})^* \in \mathcal{S}_m. \end{aligned} \quad (\text{IV.3.33})$$

Similarly, the optimal equilibrium point of the power adaptation is defined as:

Definition 5: Optimal Point of Power Adaptation. *The optimum power $(p_m^{(ME)})^*$ is the minimum possible power that can be used to transmit the symbol m to satisfy*

the target SINR. The sum of the transmitted power at the equilibrium point is always less or equal to the sum of power at other points, that is,

$$\sum_{m=1}^M (p_m^{(ME)})^* \leq \sum_{m=1}^M p_m^{(ME)}. \quad (\text{IV.3.34})$$

In this context, the MMSE-based CR systems adaptation algorithm is formally presented in the following section:

IV.3.1 MMSE-BASED CR SYSTEMS ADAPTATION ALGORITHM

The proposed approach for joint spectral shaping and power control algorithm is based on joint adaptation of the precoder $\mathbf{S}^{(ME)}$ and power $\mathbf{P}^{(ME)}$ matrices through a distributed incremental algorithm that adjusts the columns of the precoder matrix and power to minimize the sum of the MMSE function to meet the specified target SINR. It is worth noting that the updates implied by (IV.3.23) and (IV.3.24) may result in abrupt changes of $\mathbf{s}_m^{(ME)}$ and/or $p_m^{(ME)}$ which are not desirable in practical implementations. The proposed algorithm uses the incremental updates. The idea of the incremental update method is to design a step size sequence to update in the incremental direction towards the optimal value. The algorithm is formally stated in Algorithm 4 and uses the following incremental updates:

- At step j of the algorithm, column m of the precoding matrix $\mathbf{S}^{(ME)}$ is updated to:

$$\mathbf{s}_m^{(ME)}(j+1) = \frac{\mathbf{s}_m^{(ME)}(j) + z(j)\beta\mathbf{r}_m^{(ME)}(j)}{\|\mathbf{s}_m^{(ME)}(j) + z(j)\beta\mathbf{r}_m^{(ME)}(j)\|}, \quad (\text{IV.3.35})$$

where $\mathbf{r}_m^{(ME)}(j)$ is the maximum eigenvector of the matrix $\tilde{\mathbf{R}}_m^{(ME)}(j)$, β is a parameter that limits how far (in terms of Euclidean distance) the updated vector

is from the previous, and

$$z(j) = \text{sgn}[(\mathbf{s}_m^{(\text{ME})})^H(j)\mathbf{r}_m^{(\text{ME})}(j)]. \quad (\text{IV.3.36})$$

- Power for symbol m at step of j of the algorithm is updated to:

$$p_m^{(\text{ME})}(j+1) = p_m^{(\text{ME})}(j) + \mu[\tilde{p}_m^{(\text{ME})}(j) - p_m^{(\text{ME})}(j)], \quad (\text{IV.3.37})$$

where

$$\tilde{p}_m^{(\text{ME})}(j) = \frac{\gamma^*}{((\mathbf{s}_m^{(\text{ME})})^H(j+1)\tilde{\mathbf{R}}_m^{(\text{ME})}(j)\mathbf{s}_m^{(\text{ME})}(j+1))}, \quad (\text{IV.3.38})$$

and $0 < \mu < 1$ which define the proper value of the power increment.

This algorithm jointly adapts the corresponding precoder matrix column and power by minimizing the cost function $u^{(\text{ME})}$ until a fixed point is reached. Numerically, a fixed point of the algorithm is reached when the updates result in changes of the cost function that are smaller than the specified tolerance ϵ , and convergence to a fixed point is ensured by checking the second order determinant condition.

It is observed empirically that the increment updates implied by (IV.3.35) and (IV.3.37) result in a monotonic decrease of a cost function, that is, the difference between $u^{(\text{ME})}(j)$ before step j updates (IV.3.35) and (IV.3.37) are applied and $u^{(\text{ME})}(j+1)$ after the updates is always non-negative

$$\Delta u^{(\text{ME})} = u^{(\text{ME})}(j) - u^{(\text{ME})}(j+1) \geq 0 \quad (\text{IV.3.39})$$

Thus, the constrained minimum of $u^{(\text{ME})}$ in (IV.3.28), according to [98] $u^{(\text{ME})}$, is lower bounded by $\frac{M}{1+\gamma^*}$, that is,

$$u^{(\text{ME})} \geq \frac{M}{1+\gamma^*} \quad (\text{IV.3.40})$$

Algorithm 4 MMSE-based Joint Spectral Shaping and Power Control (JSSPC)
 Algorithm

```

1: Input data:

    • precoder matrix  $\mathbf{S}^{(\text{ME})}$ , power matrix  $\mathbf{P}^{(\text{ME})}$ , channel matrix  $\mathbf{A}$ , and target SINR  $\gamma^*$ .

    • Spectrum sensing information: noise and interference correlation matrix  $\mathbf{R}_w$ .

    • Algorithm constants  $\beta$ ,  $\mu$ , and tolerance  $\epsilon$ .

2: if there is idle licensed spectrum then
3:   GO TO Step 7.
4: else
5:   wait until spectrum becomes available.
6: end if
7: Notch out unavailable sub-carriers as described in chapter III.
8: if admissibility condition in (IV.2.8) is satisfied then
9:   GO TO Step 13.
10: else
11:   STOP, the desired target SINR is not admissible.
12: end if
13: for each symbol  $m = 1, 2, \dots, M$  do
14:   Compute corresponding  $\tilde{\mathbf{R}}_m^{(\text{ME})}$  using equation (IV.3.8) and determine its maximum eigenvector  $\mathbf{r}_m^{(\text{ME})}(j)$  corresponding to the maximum eigenvalue  $(\lambda_m^{(\text{ME})})^*(j)$ .
15:   Update  $\mathbf{s}_m^{(\text{ME})}(j)$  using equation (IV.3.35).
16:   Update  $p_m^{(\text{ME})}(j)$  using equation (IV.3.37).
17: end for
18: if change in cost function is larger than  $\epsilon$  then
19:   GO TO Step 13.
20: else
21:   STOP, a fixed point has been reached.
22: end if
23: if optimality condition equation (IV.3.32) is true then
24:   STOP, an optimal equilibrium has been reached.
25: else
26:   GO TO Step 13.
27: end if

```

which implies that iterative application of the precoder and power updates (IV.3.35) and (IV.3.37) is guaranteed to converge to a fixed point.

It is worth noting that testing the KKT sufficient condition (IV.3.32) in Line 23 of Algorithm 4 guarantees that iterations will not stop in a suboptimal point and will reach the optimal point discussed in the previous section. It is also worth noting that the proposed algorithm requires knowledge of the noise and interference matrix \mathbf{R}_w at the receiver which may be obtained through a feedback channel [97].

The precoder matrix yielded by the algorithm is not unique and a unitary transformation of this matrix which preserves vector norms and cross-correlations will imply a new precoder matrix ensemble which also satisfies the necessary and sufficient conditions discussed in Section IV.3.

IV.4 SIMULATION RESULTS

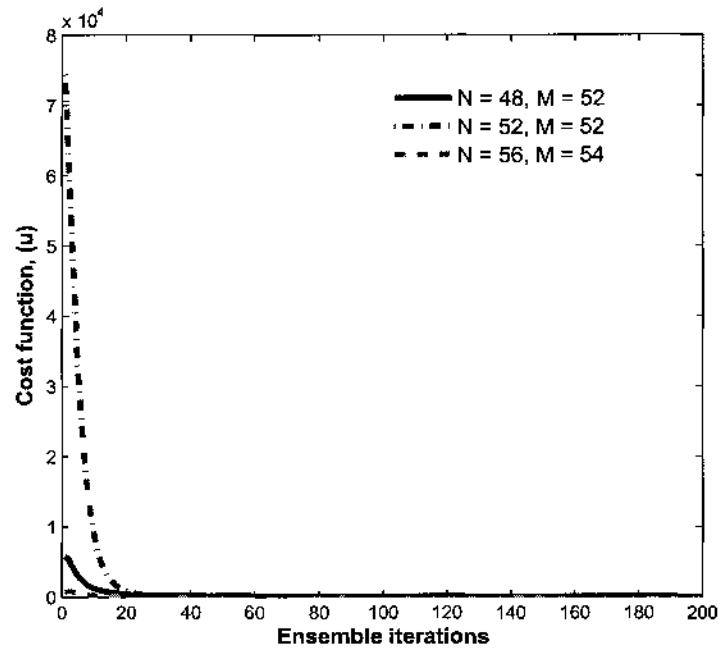
Extensive simulations are performed to evaluate the proposed algorithms for spectrum shaping, cost function convergence, precoder and power matrices adaptation, and dependency of the algorithm convergence with algorithm constants μ , β , algorithm tolerance ϵ , and with number of subcarriers N used for the transmission. The proposed algorithms are applied to notch out the spectrum used by the PUs based on the information obtained from the spectrum sensing stage and obtain the optimal precoder and power matrices that allow the CR system to operate alongside the PU without interfering with them.

The parameters of the simulation setup were chosen similar to IEEE 802.11a [105]

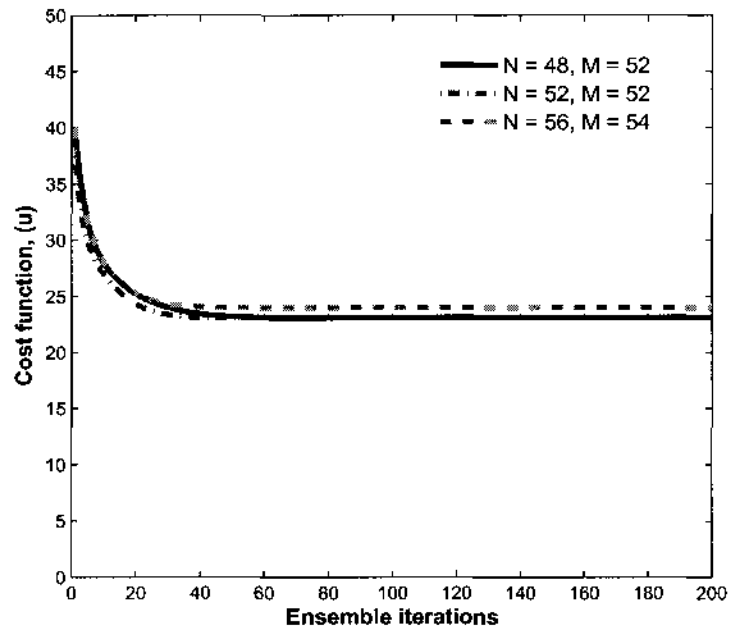
and these are summarized in Table 2. A system that uses a variable number of orthogonal sub-carriers with a variable number of transmitted symbols per frame to enable flexible data rate is considered. Each sub-carrier occupies a bandwidth of 312.5 kHz, resulting in an adjustable bandwidth and ensuring flexible spectrum availability for the SU transmission. QPSK modulation is used to map data bits to digital symbols and, depending upon the rate requirements of different applications, the unlicensed system may transmit different rates by changing the number of digital symbols M in a frame through adaptation of the number of columns of the precoder matrix. A non-ideal channel is considered between transmitter and receiver. The values of the channel coefficients are randomly generated between 0 and 1. The proposed algorithms are tested to find optimal precoder and power matrices considering MF and MMSE based receiver processing to decode the transmitted symbols.

TABLE 2: Simulation parameters chosen as a reference of 802.11a

Parameter	Value
FFT size	64
Number of used sub-carriers.	48, 52, 56
FFT sampling frequency	20MHz
Sub-carrier spacing	312.5kHz
Cyclic prefix duration	$0.8\mu s$
Data symbol duration	$3.2\mu s$
Total symbol duration	$4\mu s$
Data Sub-carrier Modulation	QPSK
Target SINR γ^*	1.25
Algorithm constant μ	0.15
Algorithm constant β	0.15
Algorithm tolerance ϵ	0.001
P_{Tmax}	5



(a) MI-based receiver processing



(b) MMSE-based receiver processing

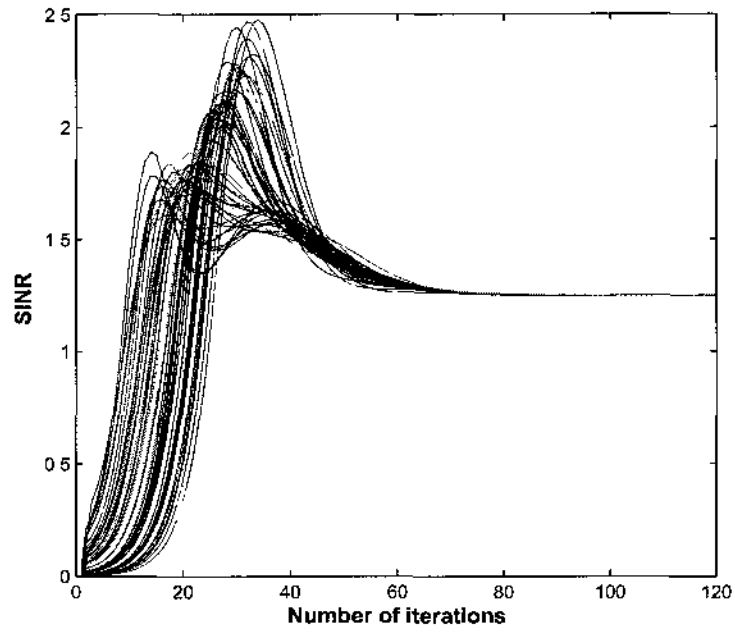
FIG. 16: Cost function convergence for varying number of sub-carriers N and number of data symbols M for a CR system.

EXPERIMENT I: COST FUNCTION CONVERGENCE

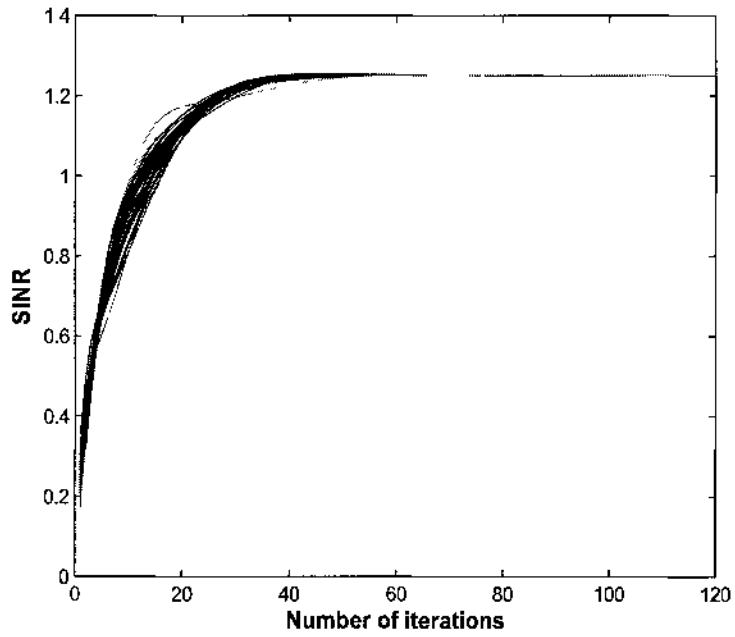
Extensive simulations are performed starting from the random initialization to show the convergence of the proposed algorithms to a fixed point. Figs. 16 (a) and (b) show the convergence of MF and MMSE based algorithms respectively. The convergence of the proposed algorithm does not depend upon the initial values of the \mathbf{S} and \mathbf{P} , that is, the proposed algorithm convergence is independent to the initial values of the \mathbf{S} and \mathbf{P} matrices.

EXPERIMENT II: SINR AND POWER ADAPTATION

Once the CR nulls out the PU sub-carriers, it adapts for specified target SINR with the minimum possible transmitted power. The proposed algorithm is applied to obtain the precoder and power matrices that allow the CR system to operate alongside the PU without interfering with them. The number of sub-carriers N and number of symbols M used in this experiment are 52. Figs. 17 (a) and (b) show the SINR adaptation of the symbols of the CR with MF- and MMSE-based receiver processing, respectively. From Fig. 17, it is noted that the SINRs corresponding to all symbols vary until the desired target value is reached. When the system configuration changes, the SINRs changes, but the proposed algorithm adapts the CR transmission to the new available spectrum such that, when the fixed point is reached, the desired target SINR value continues to be maintained. Figs. 18 (a) and (b) show a similar behavior for the power values of all symbols. It is noted that while initial power values might be high, the algorithm ensures that the desired target SINRs are achieved with minimum transmitted power. It is also noted that

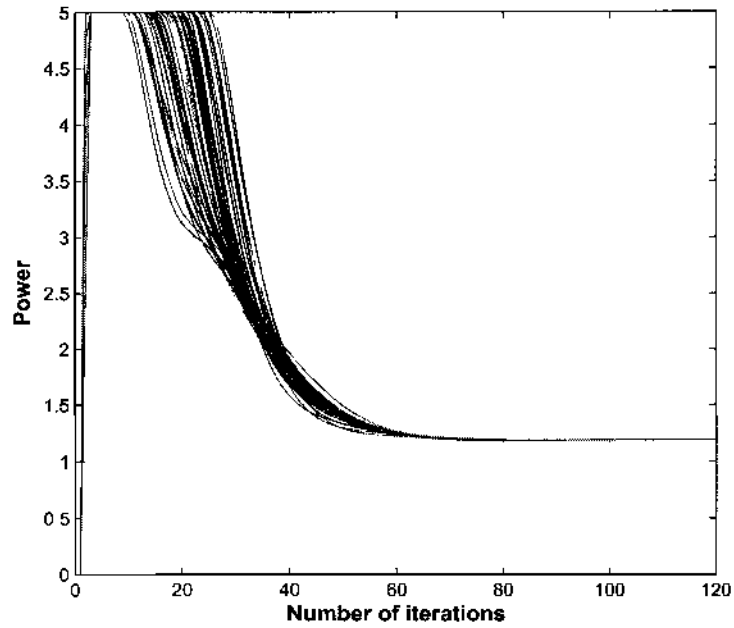


(a) MF-based

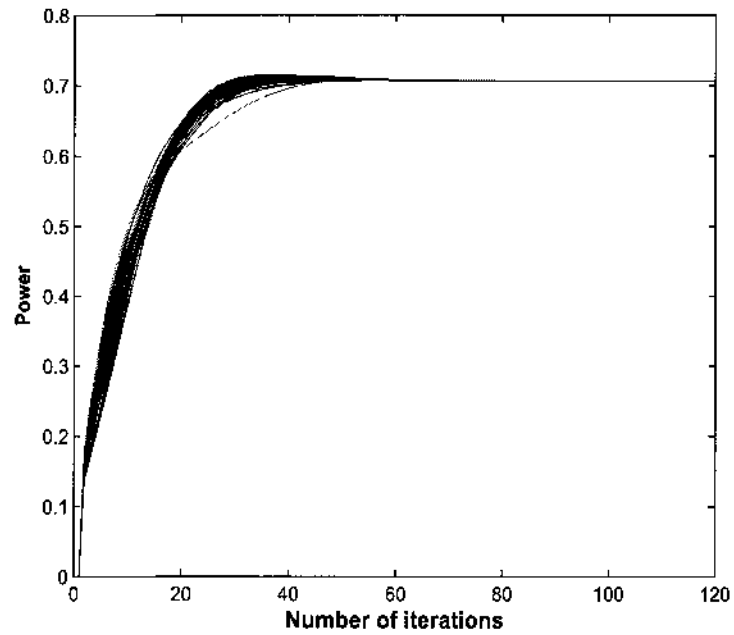


(b) MMSE-based

FIG. 17: SINR adaptation for numbers of sub-carrier $N=52$ and $M=52$ for a pre-coded OFDM-based CR system.



(a) MF-based receiver processing



(b) MMSE-based receiver processing

FIG. 18: Power adaptation for numbers of sub-carrier $N=52$ and $M=52$ for a pre-coded OFDM-based CR system.

power values may increase when a change in the system configuration occurs and the available spectrum changes, but they return to minimal values upon successful adaptation by the proposed algorithms.

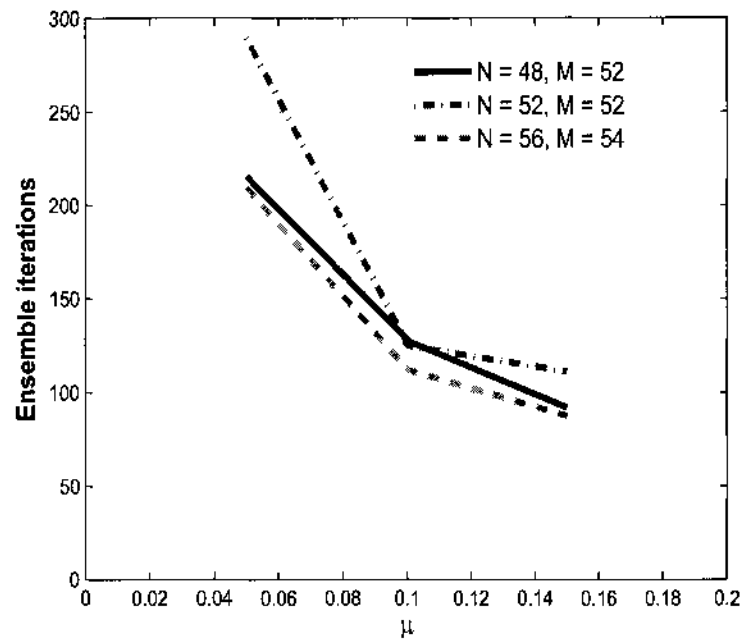
EXPERIMENT III: ALGORITHM CONVERGENCE SPEED

The proposed algorithms are the case of incremental algorithms, the convergence speed of the algorithm depends on the values of the corresponding increments specified by the algorithm constants μ , β , and algorithm tolerance ϵ . Extensive simulations for the proposed algorithms are performed to study convergence speed dependency with the algorithm constants μ , β , and algorithm tolerance ϵ .

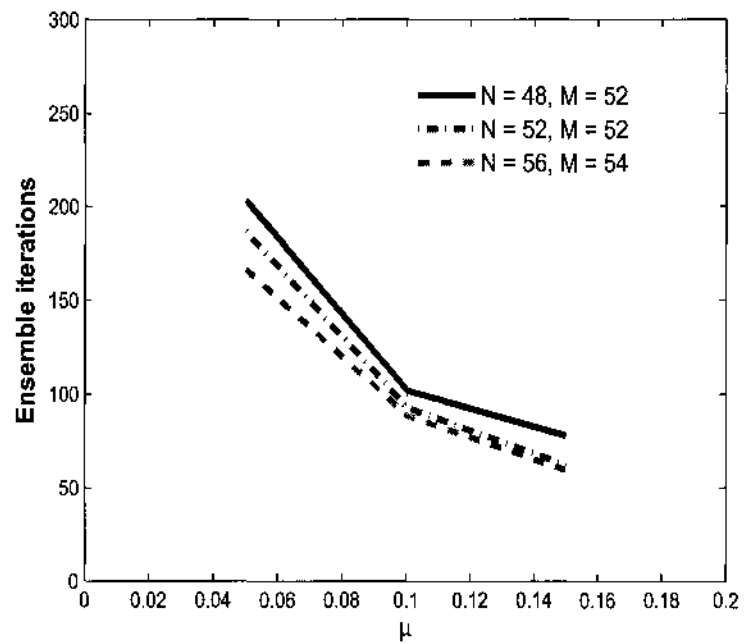
In this experiment, the dependence of convergence speed on the algorithm constants μ , β , and algorithm tolerance ϵ for fixed values of N and M is studied. The number of ensemble iterations for varying μ , β , and ϵ for MF- and MMSE-based receiver processing are plotted.

- **Dependency on algorithm constant μ :**

In this experiment, the dependence of convergence speed on μ for fixed values of N , M , β , and ϵ is studied. The random experiment is run 100 times and the convergence behavior with the algorithm constants μ is analyzed. The number of ensemble iterations for varying μ for MF- and MMSE-based receiver processing are plotted in Fig. 19 (a) and (b) respectively, from where it is noted that the convergence to the pre-specified SINR do not depend significantly on the values of μ . It is also noted that, MF-based processing took more time (approximately 125) iterations than the MMSE based processing (approximately 75 iterations) to reach an optimal equilibrium point for all the experiments.

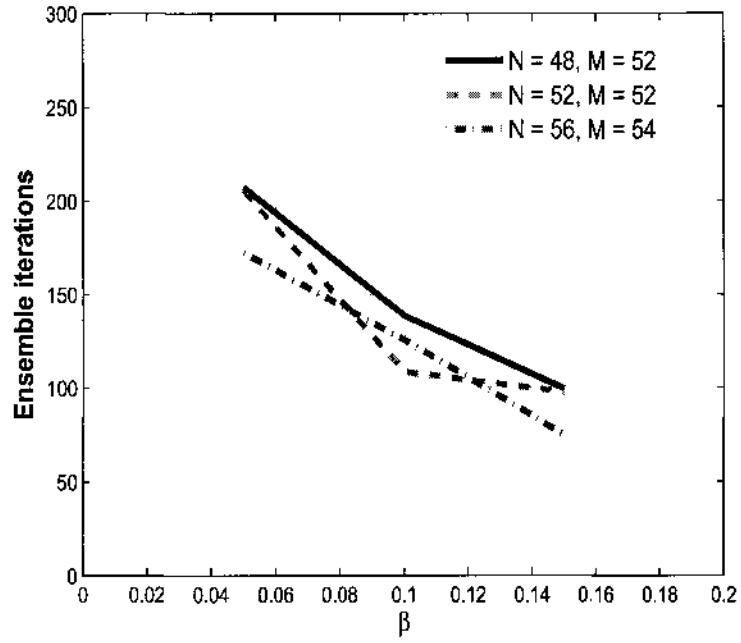


(a) MF-based receiver processing

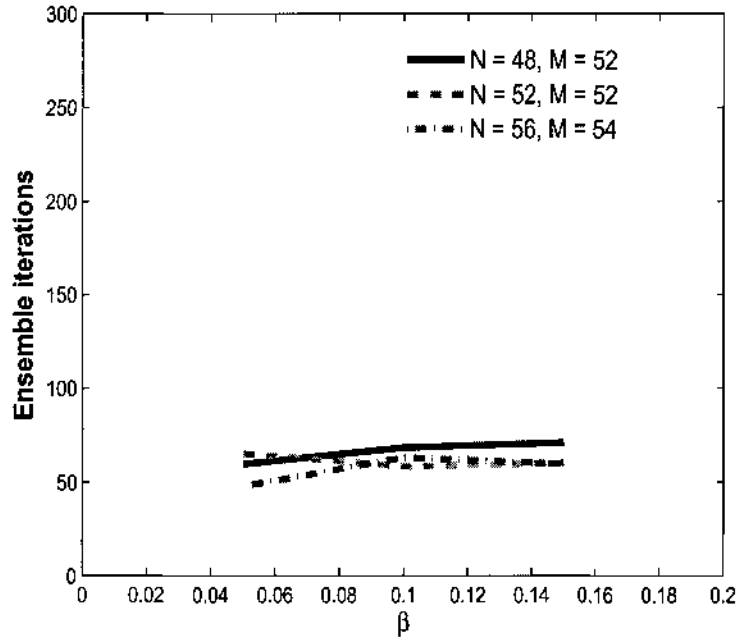


(b) MMSE-based receiver processing

FIG. 19: Average number of ensemble iterations for convergence to a fixed point for different number of sub-carriers, N and M , for varying μ and fixed $\beta=0.15$ and $\epsilon = 0.001$.



(a) MF-based receiver processing



(b) MMSE-based receiver processing

FIG. 20: Average number of ensemble iterations for convergence to a fixed point for different number of sub-carriers, N and M , for varying β and fixed $\mu=0.15$ and $\epsilon = 0.001$.

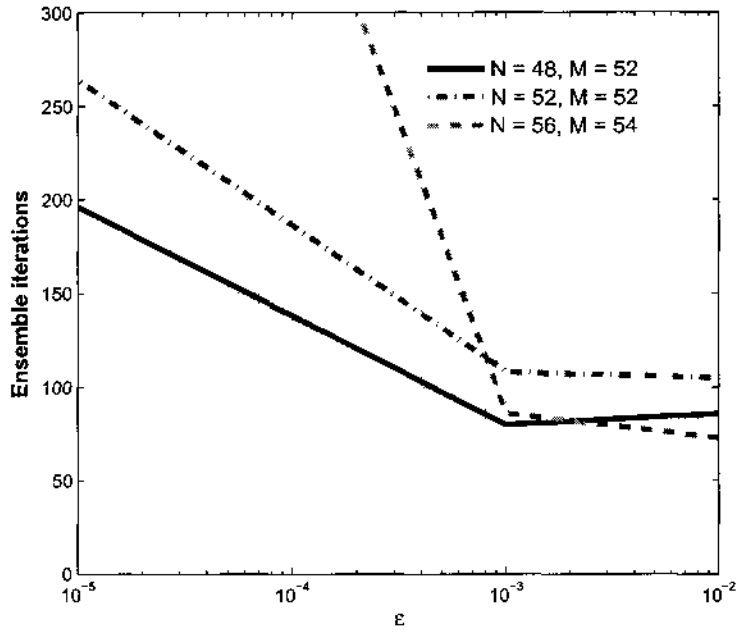
- **Dependency on algorithm constant β :**

In this experiment, the dependence of convergence speed on fixed values of N and M with varying β is studied. The random experiment is run 100 times and the convergence behavior with the algorithm constants β is analyzed. The number of ensemble iterations for varying β for MF- and MMSE-based receiver processing is plotted in Figs. 20 (a) and (b) respectively, from where it is noted that the convergence to the pre-specified SINR do not depend significantly on the value of β . It is also noted that MF-based processing took more time (approximately 100 iterations) than the MMSE based processing (approximately 75 iterations) to reach the optimal equilibrium point for all the experiments.

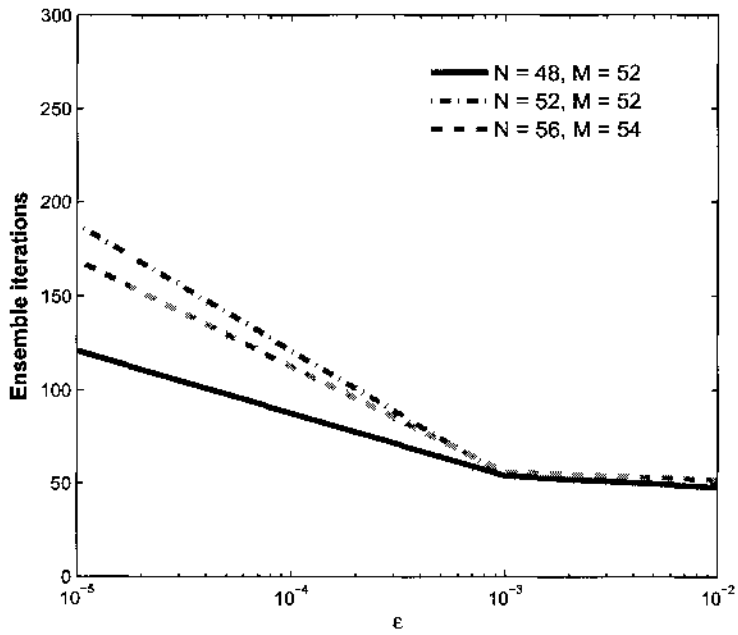
- **Dependency on algorithm tolerance ϵ :**

In this experiment, the dependence of convergence speed for fixed values of N , M , μ , and β with varying algorithm tolerance ϵ is studied. The random experiment is run 100 times and the convergence behavior with the algorithm tolerance ϵ is analyzed. The number of ensemble iterations for varying tolerance ϵ for MF- and MMSE-based receiver processing is plotted in Figs. 21 (a) and (b) respectively, from where it is noted that the convergence to the pre-specified SINR depends on the value of ϵ . It is also noted that MF-based processing took more time than the MMSE based processing to reach the optimal equilibrium for all the experiments. From Figs 21, it is also noted that the lower the value of ϵ the higher the precision of the result, with more time required to get the optimal point.

- **Dependency on N :**



(a) MF-based receiver processing



(b) MMSE-based receiver processing

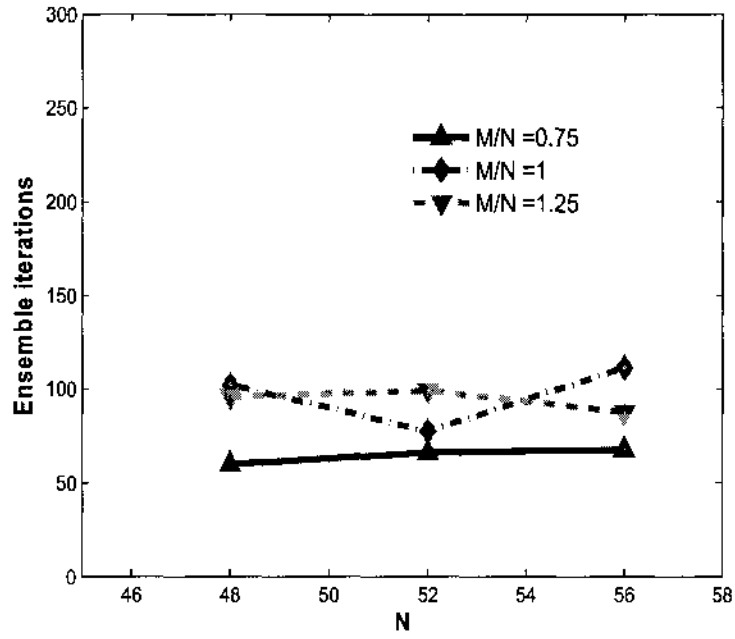
FIG. 21: Average number of ensemble iterations for convergence to a fixed point for different number of sub-carriers, N and M , for varying tolerance ϵ and fixed $\mu=0.15$ and $\beta = 0.15$.

In this experiment, the dependence of convergence speed on values of N with the fixed ratio M/N is studied. 100 trials of the algorithms ran for $\epsilon = 0.001$, algorithm constants $\mu = 0.15$, and $\beta = 0.15$ and the number of ensemble iterations needed are recorded and plotted in Figs. 22 (a) and (b) for MF- and MMSE-based receiver processing respectively, from where it is noted that the average number of ensemble iterations to reach an optimal point does not significantly change with increasing the values of N and M .

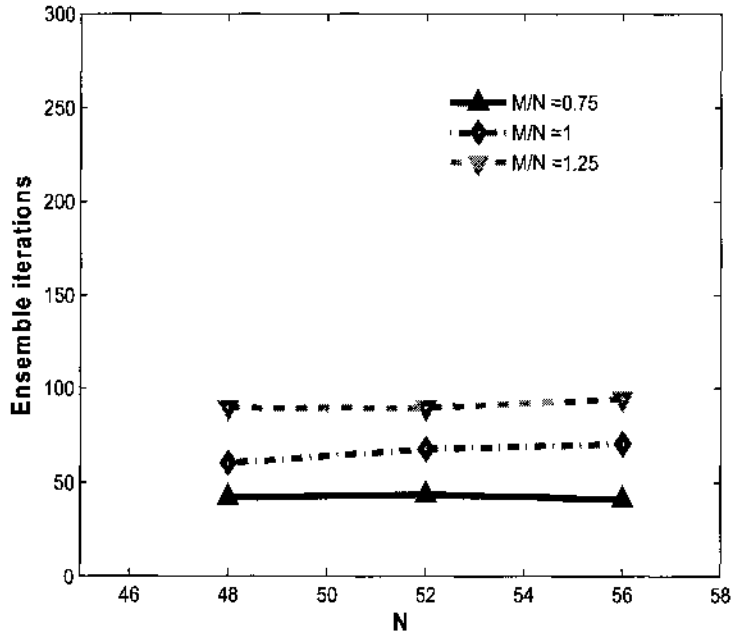
All of these experiments conclude that the algorithm desirable for dynamic cognitive systems with number of sub-carriers available for transmission are increased/decreased with respect to time and have the variable SINR requirements.

EXPERIMENT IV: BER PERFORMANCE ANALYSIS

To illustrate the rate of flexibility of the proposed system, the complete precoded OFDM-based CR system is simulated. The random experiments are performed by varying the number of symbols and keeping the number of sub-carriers constant. An analytical BER curve is plotted using $P_{b,QPSK} = \frac{1}{2}erfc(\sqrt{\frac{E_b}{N_0}})$ [106]. From Figs. 23 (a) and (b), it is observed that when the number of transmitted symbols is less than or equal to the number of sub-carriers, the precoded OFDM and the conventional OFDM system have the same BER performances. This is because of the orthogonality among symbols' sub-carrier frequencies. However, when the number of transmitted symbols is greater than the available number of sub-carriers, the BER performance of the system deteriorates as the transmission rate is increased. It is

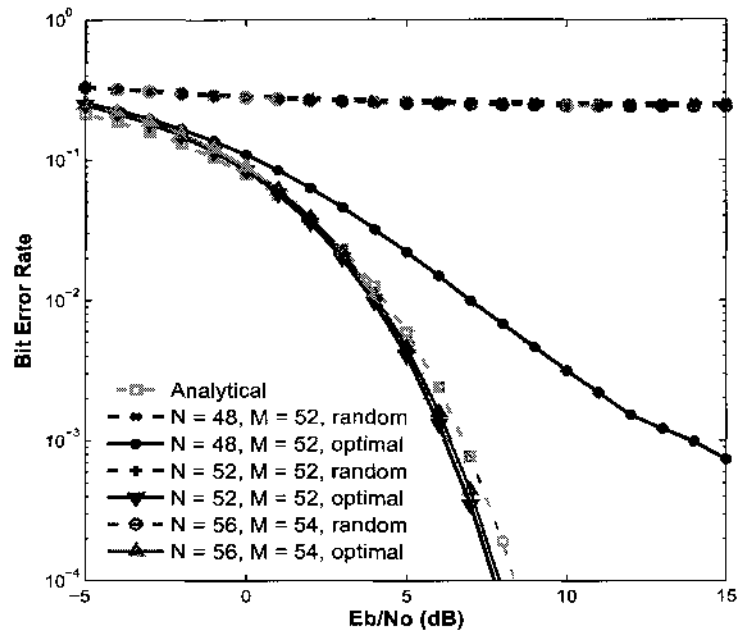


(a) MF-based receiver processing

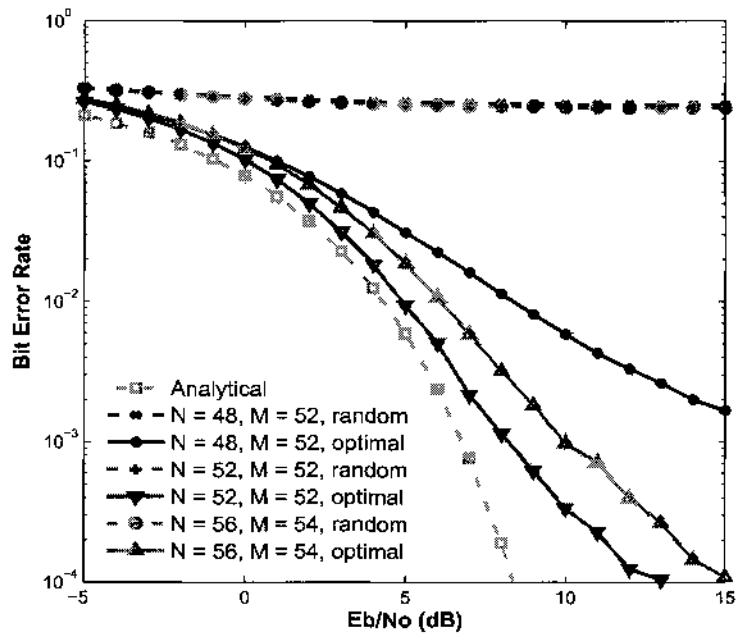


(b) MMSE-based receiver processing

FIG. 22: Average number of ensemble iterations for convergence to a fixed point for different number of sub-carriers, N and M , and fixed $\mu=0.15$ and $\beta = 0.15$ and increasing N and M for tolerance $\epsilon = 0.001$.



(a) MF-based receiver processing



(b) MMSE-based receiver processing

FIG. 23: A BER comparison for a precoded OFDM-based CR system receiver with varying N and M .

also noted that the precoded OFDM-based CR system has the ability to accommodate higher rates than that of the conventional OFDM systems. The result is also compared with the random precoder. It is also observed that for the same power the BER for random precoder is very high compared to the optimal precoder obtained from the proposed algorithm (see Fig. 23).

IV.5 CHAPTER SUMMARY

This chapter proposed the new decentralized dynamic transmitter adaptation algorithms for linearly precoded OFDM-based CR system. Two different types of receiver processing techniques, MF- and MMSE-based, are analyzed in detail. The constrained optimization problem for joint frequency allocation and power control in a precoded OFDM-based CR system, that operate subject to target SINR requirements, are formulated. The solution of the optimization problems with necessary and sufficient condition are also derived. The simulation results are also discussed in this chapter.

Chapter V

ADJACENT BAND INTERFERENCE SUPPRESSION

When it is required to adapt the spectrum of a transmitted signal to meet specific emission masks [107], OFDM provides straightforward spectral shaping abilities through nulling and windowing [25,26,108]. The OFDM can be utilized to transmit on the white spectrum band because of the possibility of the non-contiguous OFDM (NC-OFDM) transmission. But the drawbacks of the NC-OFDM based CR system is out of band radiation due to high sidelobe energy which might cause the interference to the PU. A number of methods have been proposed in the literature for OFDM spectral shaping, which belong to either time domain or frequency domain approach. In the time domain approach, windowing the transmitted signal [25] and adaptive symbol transition techniques [109] are used. Insertion of the guard bands [25], cancellation carrier [110], subcarrier weighting [111], constellation expansion [112,113], multiple choice sequences [114], and the adaptive symbol method [115] are some of the examples of the frequency domain sidelobe suppression approach. Recently, Ghassemi et. al. discussed about the joint sidelobe and peak power reduction in [116].

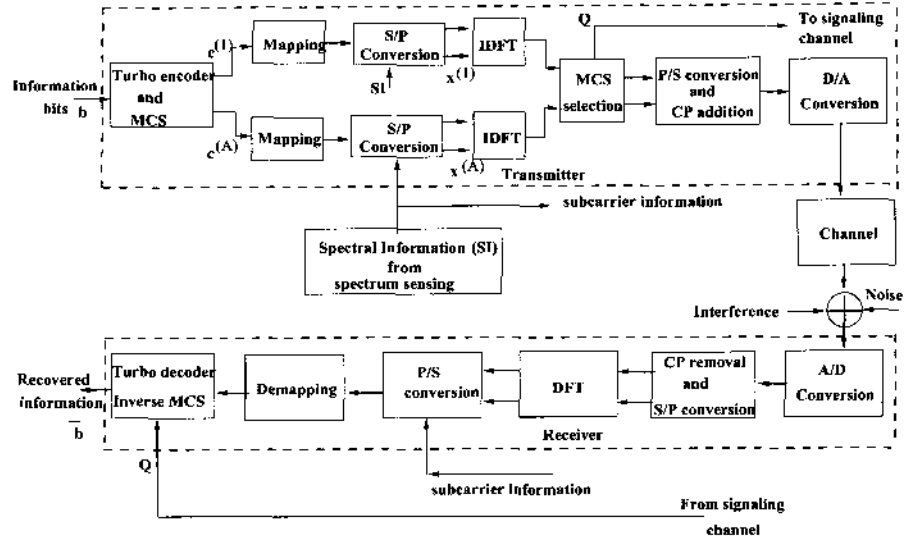
In this chapter, the spectral shaping algorithms for a turbo-coded OFDM-based CR system is proposed. Multiple choice sequences for the signal to be transmitted are generated by using different pseudo random bit sequences, diverse interleaver, or a combination of both. The average sidelobe power for all is calculated, and the sequence with the least average sidelobe power is transmitted along with sequence index number. The rest of the chapter is organized as follows: In Section V.1 the

system model is introduced and the problem of spectral shaping by suppressing the sidelobe energy is formally stated. In Section V.2, the proposed spectral shaping algorithms for a turbo coded OFDM-based CR system is presented. Section V.3 contains the simulation results that illustrate the proposed algorithms. Finally, Section V.4 summarizes the chapter.

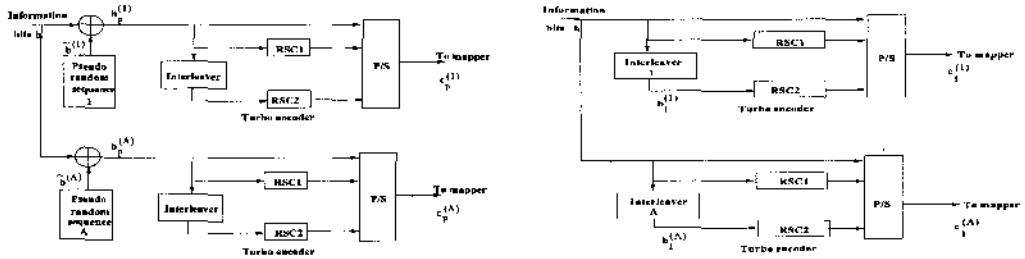
V.1 TURBO-CODED OFDM-BASED CR SYSTEMS

A block diagram of the turbo-coded OFDM-based CR is sketched in Fig. 24, which employs a turbo encoder at the transmitter and turbo decoder at the receiver [117, 118]. However, when compared to the conventional system, the MCS mapping block is added, which provides the best spectral shaping, or, in other words, the least sidelobe energy. The MCS are generated using different pseudo random bit sequences or diverse interleavers, or a combination of both. In pseudo random-based MCS generation, information carrying data stream \mathbf{b} is added with the pseudo random sequence stored at the transmitter and each sequence is passed through the turbo encoder block. The details of the generation of pseudo random-based MCS are shown in Fig. 24 (b). In the turbo encoder two Recursive Systematic Convolutional (RSC) encoder are used in which input for one of the encoders is interleaved. Different types of interleaver can be implemented in the turbo encoder [119]. The pseudo random interleaver is considered in this chapter. Interleaver based MCS are generated using diverse interleaver depth. The details of the generation of interleaver-based MCS are shown in Fig. 24 (c).

The output of the turbo encoder is digitally mapped to get the digital symbols.



(a) General block diagram



(b) Pseudo random based MCS generation. (c) Interleaver based MCS generation.

FIG. 24: Block diagram of the turbo-coded OFDM-based CR system.

Thus, obtained symbols are converted to the parallel and given to the IFFT. There might not be the continuous frequency bands available for the CR system so, the CR system can transmit the information in the non-continuous frequency band. This can be feasible in a turbo-coded OFDM transceiver by deactivating the PU sub-carriers.

The frequency domain data symbol vector $\mathbf{x} = [x_0, x_1, \dots, x_{N-1}]^T$, where $[-]^T$ denotes the transpose operation, are transmitted on N orthogonal sub-carriers. Each sub-carrier is carrying the PSK or QAM signal. The output of the inverse discrete

Fourier transform (IDFT) is,

$$x[n] = \frac{1}{N} \sum_{k=0}^{N-1} x_k \exp(j2\pi nk/N). \quad (\text{V.1.1})$$

In practice, oversamples are taken and FFT is used to calculate the IDFT.

The output of the mapping block is the MCS of data symbols. A set of $\{\mathcal{A} > 1\}$ multiple sequences

$$\mathbf{x}^{(i)} = [x_1^{(i)}, x_2^{(i)}, \dots, x_{N-1}^{(i)}], \quad i = 1, 2, \dots, \mathcal{A} \quad (\text{V.1.2})$$

can be generated from the original sequence. A rectangular pulse-shape is used for the k -th sub-carrier of the transmitted signal (V.1.1), so the average sidelobe power in the legacy user frequency band for sequence $\{i\}$ is [114],

$$P^{(i)} = \frac{1}{M} \sum_{m=1}^M \left| \sum_{k=1}^N x_k^{(i)} S(g_m - f_k) \right|^2, \quad i = 1, 2, \dots, \mathcal{A} \quad (\text{V.1.3})$$

where $S(x)$ is the individual sub-carrier spectrum, $f_k, k = 1, 2, \dots, N$ are the normalized sub-carrier frequencies, and $g_m, m = 1, 2, \dots, M$ are the normalized frequency samples within the frequency range called the optimization range which is spanning several sidelobes of the OFDM symbol. The spectrum $S(x)$ depends on the type of the window function, e.g., for a time domain rectangular window the spectrum is a sinc function. Other types of the time domain windowing functions such as raised-cosine, Gaussian, etc, can also be used for better result. The index Q of the sequence with minimum sidelobe power is given by

$$Q = \min_i P^{(i)}, \quad i = 1, 2, \dots, \mathcal{A} \quad (\text{V.1.4})$$

Hence Q -th sequence

$$\mathbf{x}^{(Q)} = [x_1^{(Q)}, x_2^{(Q)}, \dots, x_{N-1}^{(Q)}]^T \quad (\text{V.1.5})$$

is provided by the MCS selection block.

The proposed approach for sidelobe power suppression by MCS is shown in Fig. 25, which shows the normalized PSD of the OFDM signals averaged over a set of possible data sequences before and after the application of the MCS method. The advantages of the proposed method in reducing the sidelobe power is clearly seen in this figure. A number of predetermined pseudo random sequences with their

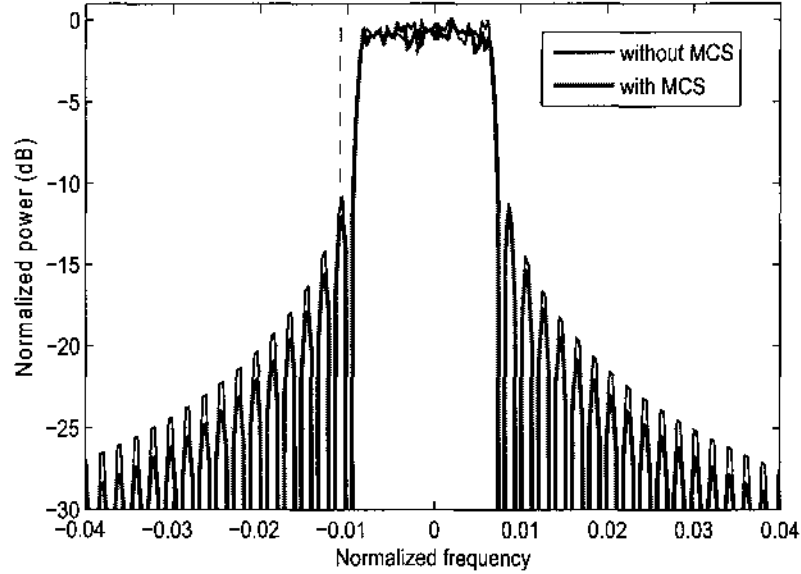


FIG. 25: Exampe of power spectral density for the original and MCS sequences

index, interleaver with interleaver depth, or a combination of both should be known to both the transmitter and the receiver. The indexes that are used for the transmitted signal must be sent to the receiver. Thus, there are certain overheads to be transmitted through the control channel with the OFDM symbol. The overhead is based on the number of sequence i.e. $\{\log_2 \mathcal{A}\}$. The overhead needed for the signaling information is [114]

$$\frac{\lceil \log_2(\mathcal{A}) \rceil}{N \cdot \log_2(M) + \lceil \log_2(\mathcal{A}) \rceil}, \quad (\text{V.1.6})$$

where $\lceil x \rceil$ returns the smallest integer greater than or equal to x . The index Q is coded in bits, and transmitted along with the information bit through the signaling channel.

At the receiver, the cyclic prefix is removed, DFT is performed and an estimate of the transmitted sequence $\bar{\mathbf{b}}$ is obtained by the turbo decoder. The receiver can identify the demapping sequence based on the value of the Q . Hence, overall throughput might be compromised. But, it is important that the CR system keep the interference to the PU below pre-specified threshold as it's using the spectrum opportunistically on the basis that it will not harmfully interfere with the legacy user.

V.2 MCS GENERATION AND SELECTION ALGORITHMS

The objective of the proposed algorithms is to avoid or reduce the interference to the PU by choosing the OFDM signal having least sidelobe energy from the possible MCS. It is worth to note that the OFDM signal has a significant amount of sidelobe energy which can interfere the PU when the CR transmitted the OFDM

signal through the opportunistically detected white hole. It is well known that the different sequences have different sidelobe power so, at the CR transmitter the MCS are generated at the bit level. The average sidelobe power for all set of the MCS is calculated and the sequence having the least sidelobe power is selected to transmit from the transmitter.

V.2.1 PSEUDO RANDOM BASED MCS GENERATION

The information bit sequence to be transmitted is mapped to a new sequences using pseudo random sequences to generate the multiple choice sequences. As shown in Fig. 24 (a), the output of the pseudo random based MCS block is

$$\mathbf{b}_p^{(i)} = \left(\mathbf{b} \oplus \tilde{\mathbf{b}}^{(i)} \right), \quad i = 1, 2, \dots, \mathcal{A} \quad (\text{V.2.1})$$

where $\{\tilde{\mathbf{b}}^{(i)}, \quad i = 1, 2, \dots, \mathcal{A}\}$ are the pseudo random sequence stored at the CR transmitter. The output of the MCS is a new sequence different from the original sequence. The average energy in the sidelobe for each sequence is calculated and the sequence with the least sidelobe energy is transmitted. The index of the selected sequence Q is also transmitted with an OFDM symbol which is used to demap the sequence to the original sequence at the receiver. The pseudo code for this method is outlined in Algorithm 5.

V.2.2 INTERLEAVER BASED MCS GENERATION

In this approach, an interleaver having different interleaver depths is utilized to get the multiple choice sequences. A pseudo random interleaver is used that produces $\{\mathcal{A}\}$, multiple choice sequences permuting the input sequence in pseudo

Algorithm 5 :Pseudo Random MCS-based Spectral Shaping Algorithm

1: **Input:**

- input information bit sequence.
- $\{\mathcal{A}\}$ pseudo random sequences.

2: **for** each Pseudo random sequence $\{i = 1, 2, \dots, \mathcal{A}\}$ **do**

3: add information bit sequence and pseudo random sequences,

4: use turbo encoder and map resulting sequence to the digital symbol.

5: calculate average sidelobe power for each sequence

6: **end for**

7: choose the sequence Q having least sidelobe energy.

8: **Output:**

- transmit the Q -th sequence with sequence index number.
-

random order. As shown in Fig. 24 (b), the output of the i -th interleaver is expressed as [114],

$$\mathbf{b}_j^{(i)} = \pi^{(i)} \mathbf{b}, \quad i = 1, 2, \dots, \mathcal{A} \quad (\text{V.2.2})$$

where $\pi^{(i)}$ is the i -th permutation matrix used for interleaving the information. The bit sequence of the interleaver-based MCS is the same but the position of the bits in the new sequence is interleaved according to the interleaver depth. The average sidelobe energy for each interleaved sequence is calculated and the sequence having least sidelobe energy is selected. Thus, the selected sequence with index number Q is transmitted from the CR transmitter. The pseudo code for this approach is outlined in Algorithm 6.

Algorithm 6 :Interleaver-based Spectral Shaping Algorithm

1: **Input data:**

- input information bit sequence.

2: generate $\{\mathcal{A}\}$ sequences from interleaver with different interleaver depth.3: **for** each interleaved sequences $\{i = 1, 2, \dots, \mathcal{A}\}$ **do**

4: map sequence to the digital symbol.

5: calculate average sidelobe power for each sequence

6: **end for**7: choose the sequence Q having least sidelobe energy.8: **Output:**

- transmit the Q -th sequence with sequence index number.
-

Algorithm 7 :Combined Spectral Shaping Algorithm

1: **Input:**

- input information bit sequence.

- $\{\mathcal{A}\}$ pseudo random sequences.

2: **for** each pseudo random sequences $\{i = 1, 2, \dots, \mathcal{A}\}$ **do**

3: add information bit sequence and pseudo random sequences,

4: interleave the sequence with different interleaver depth.

5: map to digital symbol, convert the symbol serial to parallel, and perform IDFT.

6: calculate average power for each sequence

7: choose the sequence Q having least sidelobe energy.8: **end for**9: **output:**

- transmit the sequence Q with sequence index number Q .
-

V.2.3 COMBINED MCS GENERATION

This method is a combination of the above two methods. First the binary information data sequence is mapped to the new sequence using the pseudo random sequence. Then, this sequence is interleaved for different depth and finds the optimal sequence with least sidelobe energy. The pseudo code for this method is presented in Algorithm 7.

V.3 SIMULATION RESULTS

Extensive simulations were performed to evaluate the proposed algorithms in a turbo coded OFDM system. The proposed algorithms are applied to find the signal with the least sidelobe energy.

Simulation Parameters

A turbo-coded OFDM system is considered that uses the proposed algorithms to find the transmitted OFDM signal with the least sidelobe energy. The pseudo random interleaver is used in the turbo encoder. QPSK modulation is used to map data bits to digital symbols. The proposed algorithm is applied to find the optimal sequence to transmit from the turbo-coded OFDM transmitter. The parameters of the simulation setup were chosen similar to IEEE 802.11a [105].

Simulation Results

Fig. 26 shows the result of the sidelobe suppression results averaged over all possible data symbol sequences for different sizes of the MCS set $\{\mathcal{A}\}$ and different MCS

techniques. The average sidelobe suppression is calculated relative to the standard OFDM without MCS block. The optimization range consists of five sidelobes at each side of the spectrum. It can be seen that the combined method of generating MCS outperforms the other techniques. However, in this approach, indexes of both the pseudo random and interleaver sequences have to send, resulting in a reduced transmission rate. From Fig. 26, we also note that in all considered MCS approaches, an increase in the size of the MCS set $\{\mathcal{A}\}$ improves sidelobe suppression. However, as $\{\mathcal{A}\}$ increases the number of bits required for the side information also grows decreasing the overall throughput. Thus, there is trade off between the additional sidelobe reduction and the MCS set size $\{\mathcal{A}\}$. In Fig. 27, the probability that the

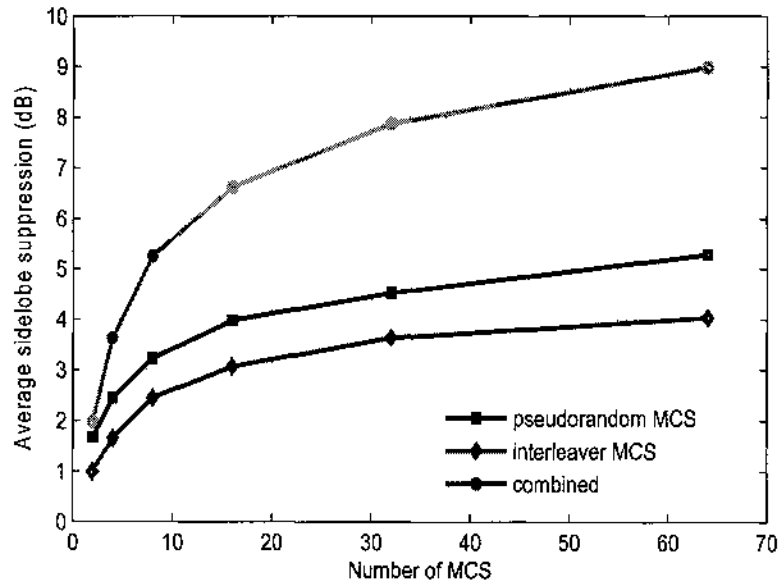


FIG. 26: Sidelobe suppression with respect to the length of the MCS set $\{\mathcal{A}\}$ and for different MCS methods; QPSK; $N = 48$

sidelobes of the chosen MCS exceeds the threshold β is presented. Simulation results

are given for $\{\mathcal{A} = 4\}$ and $\{\mathcal{A} = 16\}$ with different MCS algorithms. For reference purposes, the corresponding probability for standard OFDM without the MCS block is also presented in Fig. 27. We note that the combined MCS with $\{\mathcal{A} = 16\}$ outperforms the other techniques. For $\{\mathcal{A} = 4\}$ there is almost similar performance between the pseudo random- and interleaver-based approaches. It is also noted that for $\{\mathcal{A} = 16\}$ the performance of the pseudo random MCS technique is better than the interleaver-based technique. The proposed algorithms are simulated for QPSK

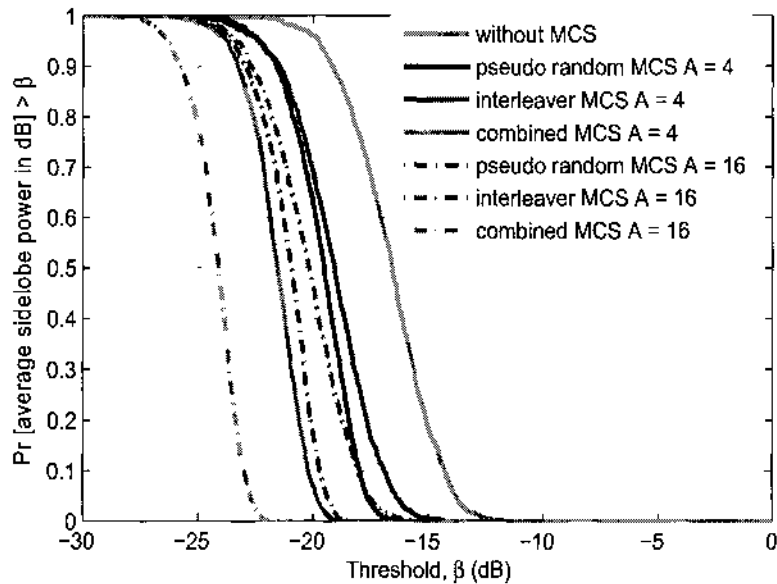


FIG. 27: Probability that average sidelobe power of the chosen MCS exceeds the threshold β ; QPSK; $N = 48$

modulation system. However, the proposed algorithms can easily be adapted to sub-carriers with other modulation schemes such as 8QAM, 16QAM, and 64QAM. The overhead to be transmitted in the proposed algorithms remains the same irrespective, of the modulation level, because only the index number is transmitted through the

control channel. Hence, proposed algorithms can be even more efficient for higher order modulation levels such as 64QAM.

V.4 CHAPTER SUMMARY

In this chapter, spectral shaping for adjacent band interference suppression algorithms for a turbo-coded OFDM-based CR system is proposed. The MCS techniques are implemented to reduce the sidelobe energy. Different types of the MCS generating algorithms, i.e. pseudo random bit sequences, diverse interleave, or a combination of both, are presented. The combined method outperformed the other methods. However, the overall throughput is also decreased in the combined method as the index of both pseudo random sequence and interleave depth have to be transmitted along with the information bits. Though there is some overhead to be paid on transmitting MCS index number and computation, proposed algorithms are useful for dynamic spectrum access, as avoiding the adjacent band interference to the PU is important in such scenarios. The performance of all three methods was illustrated with numerical results obtained from simulations.

Chapter VI

CONCLUSIONS AND FUTURE RESEARCH

This chapter summarizes the contributions of this dissertation and discusses possible directions for future work.

VI.1 RESEARCH CONTRIBUTION

RF spectrum is a scarce natural resource. Due to the traditional types of spectrum assignment policy, there is an artificial scarcity of the spectrum for new and existing communications systems. Innovative CR systems can exploit uses of the RF spectrum.

In this dissertation, a number of contributions have been made in the area of the physical layer design of CR systems. Spectrum sensing, spectrum shaping, and rate/power adaptation are the important functionalities of CR systems. The contribution of this dissertation are summarized as follows:

- Spectrum sensing is the most important task of CR systems in finding the spectrum opportunities as well as avoiding the currently used spectrum by the PU. There are two types of spectrum sensing errors, false alarm and missed detection, which are functions of the threshold in energy detector based spectrum sensing. A threshold adaptation for energy detector to minimize the spectrum sensing errors is presented.
- Extension of the threshold adaptation for wide band signal using filter bank approach is studied.

- Spectrum shaping using a linear transformation matrix for LTE-A CR systems is investigated.
- The concept of “Carrier aggregation” in LTE-A is analyzed.
- Decentralized algorithms for dynamic transmitter adaptation with QoS constraints specified in terms of target SINR for LT-OFDM based CR systems are investigated. The non-ideal channel between transmitter and receiver is considered for the analysis. The algorithm can be combined with any wide band spectrum sensing systems to allow the fully operational CR systems to utilize the scarce RF spectrum effectively and efficiently. This dissertation presented a solution of the constrained optimization problem for power control with specified SINR constraints for LT-OFDM based CR. It also contains the novel algorithms for joint spectrum shaping and power control for LT-OFDM based CR systems that operate in non-ideal channels under specified target SINR at the receiver. The proposed algorithms can be used for dynamic spectral shaping to avoid frequency bands that are actively used by licensed transmitters.
- Adjacent band interference suppression techniques using MCS in turbo-coded OFDM-based CR systems are also analyzed. MCS can be generated utilizing different methods, however, in this dissertation MCS are generated using different pseudo random bit sequences, diverse interleaver, or a combination of both. Three algorithms with simulation results are also analyzed.

VI.2 FUTURE WORK

The topics covered in this dissertation can be extended towards other research directions. Below are listed some important open questions derived from the research carried during this dissertation.

- The threshold adaptation in energy detector spectrum sensing in CR systems is proposed in Chapter II. It is a very fruitful future direction to perform comparative studies with other sensing methods such as feature detector, compressed spectrum sensing, and cooperative spectrum sensing in terms of computational complexities, sensing times, and reliabilities. It is also a very good future direction to study FBMC as a physical layer technology and to do comparative studies between OFDM and FBMC for a physical layer technology for CR systems.
- This dissertation presents the results on dynamic transmitter adaptation for LT-OFDM-based CR, for which many issues remain yet to be addressed and are worth further investigating. It is shown by simulation that a spectrum used by the PU can be masked using the LT matrix. But it is not proven that the attenuation in the side lobe is sufficient in all cases.
- Application of the proposed algorithm presented in Chapter 3 in the context of non-contiguous component carrier aggregation and femtocells would also be an interesting future direction.
- Designing a hardware prototype to test spectrum sensing, shaping, and rate/power adaptation would also be a very good future research direction.

BIBLIOGRAPHY

- [1] UMTS Forum, <http://www.umts-forum.org/>.
- [2] International Telecommunication Union, <http://www.itu.int/ITU-R/>.
- [3] Federal Communications Commission, "Spectrum Policy Task Force Report ET Docket No. 02-135", November 2002.
- [4] Shared Spectrum Company, "NSF Spectrum Occupancy Measurements Project Summary", <http://www.sharespectrum.com/>.
- [5] Shared Spectrum Company, "Spectrum Occupancy Measurements: Dublin, Ireland April 16-18, 2008", <http://www.sharespectrum.com/>.
- [6] J. Mitola and G. Q. Maguire, "Cognitive radio: Making Software Radios More Personal," *IEEE Personal Communications magazine*, vol. 6, no. 6, pp. 13–182, August 1999.
- [7] S. Haykin, "Cognitive Radio: Brain-Empowered Wireless Communications," *IEEE Journal on Selected Areas in Communications*, vol. 23, no. 2, pp. 201–220, February 2005.
- [8] I. F. Akyildiz, W. Y. Lee, M. C. Vuran, and S. Mohanty, "NoXt generation/dynamic spectrum access/cognitive radio wireless networks: A survey," *Computer Networks*, vol. 50, no. 13, pp. 2127–2159, September 2006.
- [9] J. Wang, M. Ghosh, and K. Challapali, "Emerging cognitive radio applications: A survey," *IEEE Communications Magazine*, vol. 49, no. 3, pp. 74–81, March 2011.

- [10] P. Amini, P. Kempter, R. R. Chen, and L. Lin, "Filter bank multitone: a physical layer candidate for cognitive radios," in *Proceedings of the SDR Forum technical Conference*, November 2005, pp. 14–18.
- [11] R. Rajbanshi, A. M. Wyglinsky, and G. J. Minden, "An Efficient Implementation of NC-OFDM Transceivers for Cognitive Radios," in *Proceedings International Conference on Cognitive Radio Oriented Wireless Networks and Communications (CrownCom'06)*, Mykonos Island, Greece, June 2006.
- [12] M. G. Bellanger, "Specification and design of a prototype filter for filter bank based multicarrier transmission," in *Proceedings IEEE International Conference on Acoustics, Speech, and Signal Processing (ICASSP'01)*, vol. 4, 2001, pp. 2417–2420.
- [13] P. Siohan, C. Siclet, and N. Lacaille, "Analysis and design of OFDM/OQAM systems based on filterbank theory," *IEEE Transactions on Signal Processing*, vol. 50, no. 5, pp. 1170–1183, 2002.
- [14] M. G. Bellanger, "Filter banks and OFDM-OQAM for high throughput wireless LAN," in *Proceedings International Symposium on Communications, Control, and Signal Processing (ISCCSP'08)*, vol. 4, March 2008, pp. 758–761.
- [15] B. Farhang-Boroujeny and R. Kempter, "Multicarrier Communication Techniques for Spectrum Sensing and Communication in Cognitive Radios," *IEEE Communications Magazine*, vol. 46, no. 12, pp. 80–85, April 2008.
- [16] B. Farhang-Boroujeny, "Filter bank spectrum sensing for cognitive radios," *IEEE Transactions on Signal Processing*, vol. 56, no. 5, pp. 1801–1811, 2008.

- [17] H. Zhang, D. L. Ruyet, and M. Terre, "Spectral efficiency comparison between OFDM/OQAM and OFDM-based CR networks," *Wireless Communications and Mobile Computing*, vol. 9, no. 11, pp. 1487–1501, 2009.
- [18] T. Ihalainen, T. H. Stitz, A. Viholainen, and M. Renfors, "Performance comparison of LDPC-coded FBMC and CP-OFDM in beyond 3G context," in *Proceedings International Symposium on Circuits and Systems (ISCAS'06)*, pp. 2049–2052.
- [19] D. S. Waldhauser, L. G. Baltar, and J. A. Nossek, "Comparison of filter bank based multicarrier systems with OFDM," in *Proceedings IEEE Asia Pacific Conference on Circuits and Systems (APCCS'06)*, December 2006, pp. 976–979.
- [20] C. S. Lee and K. Y. Yoo, "Polyphase filter-based OFDM transmission system," in *Proceedings IEEE Vehicular Technology Conference (VTC'04)*, vol. 1, September 2004, pp. 525–528.
- [21] D. Lacroix, N. Goudard, and M. Alard, "OFDM with guard interval versus OFDM/OffsetQAM for high data rate UMTS downlink transmission," in *Proceedings IEEE Vehicular Technology Conference (VTC'01)*, vol. 4, 2001, pp. 2682–2686.
- [22] W. Rhee, J. C. Chuang, and L. J. C. Jr., "Performance comparison of OFDM and multitone with polyphase filter bank for wireless communications," in *Proceedings IEEE Vehicular Technology Conference (VTC'98)*, May 1998, pp. 768–772.

- [23] H. A. Mahmoud, T. Yucek, and H. Arslan, "OFDM for Cognitive Radio: Merits and Challenges," *IEEE Wireless Communications*, pp. 6–14, April 2009.
- [24] D. Cabric and R. W. Brodersen, "Physical Layer Design Issues Unique to Cognitive Radio Systems," in *Proceedings of IEEE Personal, Indoor and Mobile Radio Communications Symposium (PIMRC'05)*, Berlin, Germany, September 2005, pp. 759–763.
- [25] T. A. Weiss and F. K. Jondral, "Spectrum Pooling: An Innovative Strategy for the Enhancement of Spectrum Efficiency," *IEEE Communications Magazine*, vol. 42, no. 3, pp. S8–S14, March 2004.
- [26] T. C. Clancy and B. D. Walker, "Spectrum Shaping for Interference Management in Cognitive Radio Networks," in *Proceedings Software Defined Radio Technical Conference, Orlando, FL* available online at <http://www.sdrforum.org/pages/sdr06/sdr06-papers/3.6/3.6-4.pdf>, November 2006, pp. 724–736.
- [27] H. Sari, G. Karam, and I. Jeanclaude, "Transmission techniques for digital terrestrial TV broadcasting," *IEEE Communications Magazine*, vol. 33, no. 2, pp. 100–109, February 1995.
- [28] W. Zou and W. Yiyang, "COFDM: an overview," *IEEE Transactions on Broadcasting*, vol. 41, no. 1, pp. 1–8, March 1995.
- [29] IEEE Std. 802.11 TM-2007, part11:Wireless LAN Medium Access Control (MAC) and Physical (PHY) layer specification, New York, USA, June 12, 2007.

- [30] IEEE 802.16TM-2004/Cor1-2005 (Amendment and Corrigendum to IEEE 802.16-2004), Part 16: Air Interface for Fixed Broadband Wireless Access Systems; Amendment 2: Physical and Medium Access Control Layers for Combined Fixed and Mobile Operation in Licensed Bands and Corrigendum 1, IEEE, New York, USA, February 2006.
- [31] ETSI EN 300 401 V1.3.3. European Standard for Radio Broadcasting Systems. Digital Audio Broadcasting (DAB) to mobile, portable and fixed receivers, May 2001.
- [32] ETSI EN 300 744 V1.4.1. European Standard for Digital Video Broadcasting (DVB). Framing structure, channel coding and modulation for digital terrestrial television, January 2001.
- [33] Assymetrical Digital subscriber Line (ADSL) transmission, ITU-T Recommendation G.992.1, June 1999.
- [34] Third Generation Partnership Project- Long Term Evolution (3gpp-LTE), <http://www.3gpp.org/lte>.
- [35] S. Weinstein and P. Ebert, "Data Transmission by Frequency-division multiplexing using the discrete Fourier transform," *IEEE Transactions on Communication Technology*, vol. 19, pp. 628–635, October 1971.
- [36] S. Hara and R. Prasad, *Multicarrier techniques for 4G Mobile Communications*. Artech House, USA, 2003.

- [37] D. Katselis, E. Kofidis, A. Rontogiannis, and S. Theodoridis, "Preamble-based channel estimation for CP-OFDM and OFDM/OQAM systems: A comparative study," *IEEE Transactions on Signal Processing*, vol. 58, no. 5, pp. 2911–2916, May 2010.
- [38] H. Zhang, D. L. Ruyet, and D. Roviras, "Spectral Efficiency Comparison of OFDM/FBMC for Uplink Cognitive Radio Networks," *EURASIP Journal on Advanced Signal Processing*, vol. 2010, 2010.
- [39] H. Zhang, D. L. Ruyet, and M. Terre, "Spectral Correlation of Multicarrier Modulated Signals and its Application for Signal Detection," *EURASIP Journal on Advanced Signal Processing*, vol. 2010, 2010.
- [40] M. Shaat and F. Bader, "Computationally Efficient Power Allocation Algorithm in Multicarrier Based Cognitive Radio Networks: OFDM and FBMC systems," *EURASIP Journal on Advanced Signal Processing*, vol. 2010, March 2010.
- [41] M. Payaro, A. Pascual-Iserte, and M. Najar, "Performance Comparison between FBMC and OFDM in MIMO Systems under Channel Uncertainty," in *Proceedings European Wireless 2010*, Lucca, Italy, April 2010.
- [42] Q. Bai, N. Passas, and J. Nohsek, "Scheduling and resource allocation on OFDM and FBMC systems: an interactive approach and performance comparison," in *Proceedings European Wireless 2010*, Lucca, Italy, April 2010.

- [43] M. Shaat and F. Bader, "A Two-Step Resource Allocation Algorithm in Multicarrier Based Cognitive Radio Systems," in *Proceedings Wireless Communications and Networking Conference (WCNC'2010)*, Sydney, Australia, April 2010.
- [44] M. Shaat and F. Bader, "An Uplink Resource Allocation Algorithm for OFDM and FBMC Based Cognitive Radio Systems," in *Proceedings International Conference on Cognitive Radio Oriented Wireless Networks and Communications (CrownCom'10)*, Cannes, France, June 2010.
- [45] T. Ihalainen, A. Viholainen, T. H. Stitz, and M. Renfors, "Reappearing primary user detection in FBMC/OQAM cognitive radios," in *Proceedings International Conference on Cognitive Radio Oriented Wireless Networks and Communications (CrownCom'10)*, Cannes, France, June 2010.
- [46] H. Z. abd D. LeRuyet, D. Roviras, and H. Sun, "Capacity analysis of OFDM/FBMC based cognitive radio," in *International Conference on Cognitive Radio Oriented Wireless Networks and Communications (CrownCom'10)*, Cannes, France, June 2010.
- [47] I. Estella, M. Payaró, and A. Pascual-Iserte, "OFDM and FBMC performance comparison for multistream MIMO systems," in *Proceedings Future Network & Mobile Summit (FNMS'10)*, Florence, Italy, June 2010.
- [48] M. Renfors, "Spectrum monitoring schemes for FBMC cognitive radios," in *Proceedings Future Network & Mobile Summit (FNMS'10)*, Florence, Italy, June 2010.

- [49] V. Ringset, H. Rustad, F. Schaich, J. Vandermot, and M. Najar, "Performance of a FilterBank MultiCarrier (FBMC) Physical Layer in the WiMAX Context," in *Proceedings Future Network & Mobile Summit (FNMS'10)*, Florence, Italy, June 2010.
- [50] M. Shaat and F. Bader, "Fair and Efficient Resource Allocation Algorithm for Uplink Multicarrier Based Cognitive Networks," in *Proceedings of IEEE Personal, Indoor and Mobile Radio Communications Symposium (PIMRC'10)*, Istanbul, Turkey, September 2010.
- [51] P. P. Vaidyanathan, *Multirate Systems and Filter Banks*. Prentice Hall Signal Processing Series, 1993.
- [52] Y. Zeng, Y. Liang, A. T. Hoang, and R. Zhang, "A Review on Spectrum Sensing for Cognitive Radio: Challenges and Solutions," *EURASIP Journal on Advanced Signal Processing*, vol. 2010, 2010.
- [53] D. Ariananda, M. Lakshmanan, and H. Nikoo, "A survey on spectrum sensing techniques for Cognitive Radio," in *Second International Workshop on Cognitive Radio and Advanced Spectrum Management*, May 2009.
- [54] T. Yucek and H. Arslan, "A survey of spectrum sensing algorithms for cognitive radio applications," *IEEE Communications Surveys & Tutorials*, vol. 11, March 2009.
- [55] A. Ghasemi and E. S. Sousa, "Spectrum sensing in cognitive radio networks: requirements, challenges and design trade-offs," *IEEE Communications Magazine*, vol. 46, no. 4, pp. 32–39, April 2008.

- [56] S. Haykin, D. J. Thomson, and J. H. Reed, "Spectrum Sensing for Cognitive Radio," *Proceedings IEEE*, vol. 97, no. 5, pp. 849–877, May 2009.
- [57] D. Cabric, "Cognitive Radios: System Design Perspective," Ph.D. dissertation, University of California, Berkeley, 2007.
- [58] O. A. Dobre, S. Rajan, and R. Inkol, "Joint Signal Detection and Classification based on First-Order Cyclostationarity for Cognitive Radios," *EURASIP Journal on Advances Signal Processing*, July 2009.
- [59] F. J. Harris, C. Dick, and M. Rice, "Digital Receivers and Transmitters Using Polyphase Filter Banks For Wireless Communications," *IEEE Transactions on Microwave Theory And Techniques*, vol. 51, no. 4, pp. 1395–1412, April 2003.
- [60] H. Urkowitz, "Energy Detection of Unknown Deterministic Signals," *IEEE Proceedings*, vol. 55, pp. 523–531, April 1967.
- [61] W. A. Gardner, Ed., *Cyclostationarity in Communications and Signal Processing*. IEEE Press Marketing, Piscataway, NJ, USA, 1994.
- [62] W. A. Gardner, "Spectral Correlation of Modulated Signals: Part i -Analog Modulation," *Communications, IEEE Transactions on [legacy, pre 1988]*, vol. 35, no. 6, pp. 584–594, 1987.
- [63] A. Al-Habashna, O. A. Dobre, R. Venkatesan, and D. C. Popescu., "Cyclostationarity-Based Detection of LTE OFDM Signals for Cognitive Radio Systems," in *Proceedings IEEE Global Telecommunications Conference (GLOBECOM'10)*, Miami, FL, December 2010.

- [64] Z. Quan, S. Cui, A. H. Sayed, and H. V. Poor, "Wideband spectrum sensing in cognitive radio networks," in *Proceedings IEEE International Conference on Communications (ICC'08)*, Beijing, China, May 2008, pp. 901–906.
- [65] R. Lopez-Valcarce and G. Vazquez-Vilar, "Wideband spectrum sensing in cognitive radio: Joint estimation of noise variance and multiple signal levels," in *Proceedings IEEE Signal Processing Advances in Wireless Communications (SPAWC'09)*, Perugia, June 2009, pp. 96–100.
- [66] Z. Tian and G. B. Giannakis, "Compressed sensing for wideband cognitive radios," in *Proceedings IEEE International Conference on Acoustics, Speech and Signal Processing (ICASSP'07)*, vol. 4, Honolulu, HI, April 2007, pp. 1357–1360.
- [67] Y. L. Polo, Y. Wang, A. Pandharipande, and G. Leus, "Compressive wide-band spectrum sensing," in *Proceedings IEEE International Conference on Acoustics, Speech and Signal Processing (ICASSP'09)*, vol. 4, Taipei, April 2009, pp. 2337–2340.
- [68] S. V. V. Havary-Nassab, S. Hassan, "Compressive Detection for Wide-Band Spectrum Sensing," in *Proceedings IEEE International Conference on Acoustics, Speech and Signal Processing (ICASSP'10)*, Dallas, Tx, USA, 2010.
- [69] E. J. Candes and M. B. Wakin, "An introduction to compressive sampling," *IEEE Signal Processing Magazine*, vol. 25, no. 2, pp. 21–30, March 2008.

- [70] G. Bansal, M. J. Hossain, and V. K. Bhargava, "Adaptive power loading for OFDM-based cognitive radio systems," in *Proceedings IEEE International Communications Conference (ICC'07)*, June 2007, pp. 5137–5142.
- [71] P. Wang, M. Zhao, L. Xiao, S. Zhou, and J. Wang, "Power allocation in OFDM-based cognitive radio systems," in *Proceedings IEEE Global Telecommunications Conference (GLOBECOM'07)*, November 2007, pp. 4061–4065.
- [72] T. Qin and C. Leung, "Fair adaptive resource allocation for multiuser OFDM cognitive radio systems," in *Proceedings of the 2nd International Conference on Communications and Networking in China (CHINACOM'07)*, 2007, pp. 115–119.
- [73] D. R. Joshi, D. C. Popescu, and O. A. Dobre, "Dynamic Threshold Adaptation for Spectrum Sensing in Cognitive radio Systems," in *Proceedings IEEE Radio and Wireless Symposium (RWS'10)*, New Orleans, LA, USA, January 2010, pp. 468–471.
- [74] D. R. Joshi, D. C. Popescu, and O. A. Dobre, "Adaptive Spectrum Sensing with Noise Variance Estimation for Dynamic Cognitive Radio Systems," in *Proceedings 44th Information Sciences and Systems (CISS'10)*, Princeton, NJ, USA, March 2010.
- [75] D. R. Joshi, D. C. Popescu, and O. A. Dobre, "GradientBased Threshold Adaptation for Energy Detector in Cognitive Radio Systems," *IEEE Communications Letters*, vol. 15, no. 1, pp. 19–21, January 2011.

- [76] D. R. Joshi, D. C. Popescu, and O. A. Dobre, "Dynamic Spectral Shaping in Cognitive Radios With Quality of Service Constraints," in *Proceedings Annual Asilomar Conference on Signals, Systems, and Computers (Asilomar'09)*, Pacific Grove, California, USA, November 2009.
- [77] D. C. Popescu, D. R. Joshi, and O. A. Dobre, "Spectrum Allocation and Power Control in OFDM-based Cognitive Radios with Target SINR Constraints," in *Proceedings Annual Asilomar Conference on Signals, Systems, and Computers (Asilomar'10)*, Pacific Grove, California, USA, November 2010.
- [78] D. R. Joshi, D. C. Popescu, O. A. Dobre, and K. E. Baddour, "Spectral Shaping for Adjacent Band Interference Suppression in Cognitive Radio Systems," in *Proceedings IEEE Global Telecommunications Conference (GLOBECOM'11)*, Houston, TX, USA, December 2011, to appear.
- [79] K. K. Paliwal, "Estimation of Noise Variance from the Noisy AR Signal and Its Application in Speech Enhancement," in *Proceedings IEEE International Conference on Acoustics, Speech, and Signal Processing (ICASSP'87)*, vol. 12, 1987, pp. 297–300.
- [80] J. A. Cadzow, "Spectral estimation: An overdetermined rational model equation approach," *Proceedings IEEE*, vol. 70, no. 9, pp. 907–939, September 1982.
- [81] M. Abramowitz and I. A. Stegun, Eds., *Handbook of Mathematical Functions with Formulas, Graphs, and Mathematical Tables*. Dover Publication, Inc., 180 Varick Street, New York, N.W. 10014, 1972.

- [82] S. B. Weinstein and P. M. Ebert, "Data Transmission by Frequency Division Multiplexing Using the Discrete Fourier Transform," *IEEE Transactions on Communications*, vol. 19, no. 5, pp. 628–634, 1971.
- [83] J. A. C. Bingham, "Multicarrier Modulation for Data Transmission: An Idea Whose Time Has Come," *IEEE Communications Magazine*, vol. 28, no. 5, pp. 5–14, May 1990.
- [84] J. D. Poston and W. D. Horne, "Discontiguous OFDM considerations for Dynamic Spectrum Access in Idle TV Channels," in *Proceedings First IEEE International Symposium on New Frontiers in Dynamic Spectrum Access Networks – DySPAN 2005*, Baltimore, MD, 2005, pp. 607–610.
- [85] T. A. Weiss and F. K. Jondral, "Spectrum Pooling: An Innovative Strategy for the Enhancement of Spectrum Efficiency," *IEEE Communications Magazine*, vol. 42, no. 3, pp. S8–S14, Mar. 2004.
- [86] "3GPP TR 36.913, Requirements for Further Advancements for Evolved Universal Terrestrial Radio Access (E-UTRA) (LTE-Advanced)," 3GPP, Tech. Rep. v. 10.0.0, Mar. 2011, <http://www.3gpp.org> Accessed on January 01, 2011.
- [87] Y. Wu, C. K. Ho, and S. Sun, "On Some Properties of Walsh-Hadamard Transformed OFDM," vol. 3, pp. 2096–2100, September 2002.
- [88] C.-D. Chung, "Spectral Precoding for Constant-Envelope OFDM," *IEEE Transactions on Wireless Communications*, vol. 58, no. 2, pp. 555–567, February 2010.

- [89] L. Akter and B. Natarajan, "QoS Constrained Resource Allocation to Secondary Users in Cognitive Radio Networks," *Computer Communications*, vol. 32, pp. 1923–1930, 2009.
- [90] A. Attar, O. Holland, M. R. Nakhai, and A. H. Aghvami, "Interference-limited resource allocation for cognitive radio in orthogonal frequency division multiplexing networks," *IET Communications*, vol. 2, no. 6, pp. 806–814, March 2008.
- [91] Q. Qu, L. B. Milstein, and D. R. Vaman, "Cognitive Radio Based Multi-User Resource Allocation in Mobile Ad Hoc Networking Using Multi-Carrier CDMA Modulation," *IEEE Journal on Selected Areas in Communications*, vol. 26, no. 1, pp. 70–82, January 2008.
- [92] Y. Zhang and C. Leung, "Resource Allocation in an OFDM-Based Cognitive Radio System," *IEEE Transactions on Communications*, vol. 27, no. 7, pp. 1928–1931, July 2009.
- [93] R. Etkin, A. Parekh, and D. Tse, "Spectrum Sharing for Unlicensed Bands," *IEEE Journal on Selected Areas in Communications*, vol. 25, no. 3, pp. 517–528, April 2007.
- [94] W. Ren, Q. Zhao, and A. Swami, "Power Control in Cognitive Radio Networks: How to Cross a Multi-Lane Highway," *IEEE Journal on Selected Areas in Communications*, vol. 27, no. 7, pp. 1283–1296, September 2009.
- [95] M. J. Rahman, X. Wang, and S. L. Primak, "Efficient Mutual Interference Minimization and Power Allocation for OFDM-based Cognitive Radio," in

Proceedings IEEE Global Telecommunications Conference (GLOBECOM'09), Honolulu, HA, December 2009, pp. 4050–4054.

- [96] A. T. Hoang, Y. Liang, and M. H. Islam, “Power Control and Channel Allocation in Cognitive Radio Networks with Primary users’ Cooperation,” *IEEE Transactions on Mobile Computing*, vol. 9, no. 3, pp. 348–360, March 2010.
- [97] R. W. Heath Jr., D. J. Love, V. K. N. Lau, D. Gesbert, B. D. Rao, and M. Andrews, “Guest editorial - exploiting limited feedback in tomorrow’s wireless communication networks,” *IEEE Journal on Selected Areas in Communications*, vol. 26, no. 8, pp. 1337–1340, October 2008.
- [98] D. C. Popescu, O. Popescu, and O. A. Dobre, “User Admissibility in Uplink Wireless Systems with Multipath and Target SINR Requirements,” *IEEE Communications Letter*, vol. 14, no. 2, pp. 106–108, February 2010.
- [99] D. C. Popescu and C. Rose, *Interference Avoidance Methods for Wireless Systems*. New York, NY: Kluwer Academic Publishers, 2004.
- [100] R. K. Sundaram, *A First Course in Optimization Theory*. New York, NY: Cambridge University Press, 1996.
- [101] W. Santipac and M. L. Honig, “Signature Optimization for CDMA with Limited Feedback,” *IEEE Transactions on Information Theory*, vol. 51, no. 10, pp. 3475–3492, October 2005.

- [102] D. J. Love, R. W. Heath Jr., W. Santipach, and M. L. Honig, "What Is the Value of Limited Feedback for MIMO Channels," *IEEE Communications Magazine*, vol. 42, no. 10, pp. 54–59, October 2004.
- [103] P. Viswanath, V. Anantharam, and D. Tse, "Optimal Sequences, Power Control, and User Capacity of Synchronous CDMA Systems with Linear MMSE Multiuser Receivers," *IEEE Transactions on Information Theory*, vol. 45, no. 6, pp. 1968–1983, September 1999.
- [104] U. Madhow and M. L. Honig, "MMSE Interference Suppression for Direct-Sequence Spread-Spectrum CDMA," *IEEE Transactions on Communications*, vol. 42, no. 12, pp. 3178–3188, December 1994.
- [105] IEEE 802.11 working group on wireless regional area networks, Available online at: <http://www.ieee802.org/11/>.
- [106] J. G. Proakis, *Digital Communications*, 4th ed. Boston, MA: McGraw Hill, 2000.
- [107] T. K. Forde, L. E. Doyle, and B. Ozgul, "Dynamic block-edge masks (BEMs) for dynamic spectrum emission masks (SEMs)," in *Proceedings IEEE International Symposium on New Frontiers in Dynamic Spectrum Access Networks (DySPAN'10)*, Singapur, April 2010, pp. 1–10.
- [108] D. C. Popescu and P. Yaddanapudi, "Narrowband Interference Avoidance in OFDM-Based UWB Communication Systems," *IEEE Transactions on Communications*, vol. 55, no. 9, pp. 1667–1673, September 2007.

- [109] H. A. Mahmoud and A. Arslan, "Sidelobe suppression in OFDM-based spectrum sharing systems using adaptive symbol transition," *IEEE Communication Letter*, vol. 12, no. 2, pp. 133–135, February 2008.
- [110] S. Brandes, I. Cosovic, and M. Schnell, "Reduction of out-of-band radiation in OFDM systems by insertion of cancellation carriers," *IEEE Communication Letter*, vol. 10, no. 6, pp. 420–422, June 2006.
- [111] I. Cosovic, S. Brandes, and M. Schnell, "Subcarrier weighting: a method for sidelobe suppression in OFDM systems," *IEEE Communication Letter*, vol. 10, no. 6, pp. 444–446, June 2006.
- [112] S. Pagadarai, R. Rajbanshi, A. M. Wyglinski, and G. J. Minden, "Sidelobe suppression for OFDM-based cognitive radios using constellation expansion," in *Proceedings IEEE Wireless Communications and Networking Conference (WCNC'08)*, Las Vegas, NV USA, April 2008, pp. 88–93.
- [113] D. Li, D. Xianhua, and H. Zhang, "Sidelobe Suppression in NC-OFDM Systems using Constellation Adjustment," *IEEE Communication Letter*, vol. 13, no. 5, pp. 327–329, May 2009.
- [114] I. Cosovic and T. Mazzon, "suppression of sidelobes in OFDM systems by multiple-choice sequence," *European Transactions on Telecommunications*, pp. 623–630, June 2006.
- [115] I. Cosovic and T. Mazzoni, "Suppression of sideobes in OFDM spectrum sharing systems via adaptive symbol method," in *Proceedings IEEE Vehicular Technology Conference (VTC'07)*, Dublin, Ireland, April 2007, pp. 2692–2696.

- [116] A. Ghassemi, L. L. Attar, and T. A. Gulliver, "Joint sidelobe and peak power reduction in OFDM-based cognitive radio," in *Proceedings IEEE Vehicular Technology Conference Fall (VTC'10)*, Ottawa, ON Canada, September 2010, pp. 1–5.
- [117] Y. Tsai, S. Deng, K. Chen, and M. Lin, "Turbo coded OFDM for reducing PAPR and error rates," *IEEE Transactions on wireless Communications*, vol. 7, no. 1, pp. 84–89, January 2008.
- [118] M. Lin, K. Chen, and S. Li, "Turbo Coded OFDM system with peak power reduction," in *Proceedings IEEE Vehicular Technology Conference*, October 2003, pp. 2282–2286.
- [119] O. Y. Takeshita and D. J. Costello, Jr., "New deterministic interleaver designs for turbo codes," *IEEE Transactions on Information Theory*, vol. 46, no. 6, pp. 1988–2006, September 2000.

VITA

Deepak R. Joshi
 Department of Electrical and Computer Engineering
 Old Dominion University
 Norfolk, VA 23529

EDUCATION

- M. Sc. Information & Communication Engineering, 2007, Tribhuvan University
- B. E. Electronics Engineering, 2000, Tribhuvan University

PUBLICATIONS

- Deepak R. Joshi, Dimitrie C. Popescu, and Octavia A. Dobre, “Gradient-Based Threshold Adaptation for Energy Detector in Cognitive Radio Systems”, *IEEE Commun. Let.*, vol. 15, no. 1, pp. 19-21, Jan. 2011.
- Deepak R. Joshi, Dimitrie C. Popescu, Octavia A. Dobre, and Kareem E. Baddour “Spectral Shaping for Adjacent Band Interference Suppression in Cognitive Radio Systems”, *Proc. IEEE Globecom-2011*, to appear
- Dimitrie C. Popescu, Deepak R. Joshi, and Octavia A. Dobre, “Spectrum Allocation and Power Control in OFDM-based Cognitive Radios with Target SINR Constraints”, *Proc. IEEE Asilomar Conference*, Nov. 2010, Pacific Grove, CA
- Deepak R. Joshi, Dimitrie C. Popescu, and Octavia A. Dobre, “Adaptive Spectrum Sensing with Noise Variance Estimation for Dynamic Cognitive Radio Systems”, *Proc. IEEE CISS*, Mar. 2010, Princeton, NJ
- Deepak R. Joshi, Dimitrie C. Popescu, and Octavia A. Dobre, “Dynamic Threshold Adaptation for Spectrum Sensing in Cognitive radio Systems”, *Proc. IEEE RWS*, pp 468-471, Jan. 2010, New Orleans, LA
- Deepak R. Joshi, Dimitrie C. Popescu, and Octavia A. Dobre, “Dynamic Spectral Shaping in Cognitive radios with Quality of Service Constraints”, *Proc. IEEE Asilomar Conference*, pp 539-543, Nov. 2009, Pacific Grove, CA

Typeset using L^AT_EX.